HIGH-PRESSURE COAL INJECTION IN THE ZINC SLAG FUMING PROCESS

by

STEVEN LEE COCKCROFT

B.Sc., University of British Columbia, 1980

B.A.Sc., University of British Columbia, 1984

A THESIS SUBMITTED IN PARTIAL FULFILMENT OF

THE REQUIREMENTS FOR THE DEGREE OF

MASTER OF APPLIED SCIENCE

in

THE FACULTY OF GRADUATE STUDIES

(Department of Metallurgical Engineering)

We accept this thesis as conforming

to the required standard

THE UNIVERSITY OF BRITISH COLUMBIA
December 1986

In presenting this thesis in partial fulfilment of the requirements for an advanced degree at the University of British Columbia, I agree that the Library shall make it freely available for reference and study. I further agree that permission for extensive copying of this thesis for scholarly purposes may be granted by the head of my department or by his or her representatives. It is understood that copying or publication of this thesis for financial gain shall not be allowed without my written permission.

Department of METALLURGICAL ENGINEERING

The University of British Columbia
1956 Main Mall
Vancouver, Canada
V6T 1Y3

Date April 10/87

ABSTRACT

Zinc slag fuming is a kinetically controlled process based on the direct reduction of slag by entrained coal. The kinetics of the process are governed primarily by two factors:

(1) the fraction of coal entrained in the slag, and

(2) the rate of ferrous iron oxidation.

A series of high-pressure coal injection trials have been completed at Cominco's lead smelter in Trail, British Columbia in order to facilitate increased coal entrainment. Fuming rates were increased substantially and over-all efficiencies were improved. These results are in direct contradiction to the predictions of models based on equilibrium.

The kinetics based mathematical model of the zinc slag - fuming process originally developed by Richards and Brimacombe[1a] has been modified to include the reduction and removal of lead from the furnace. A lead " prill " - slag reaction model has been formulated to account for the behaviour of liquid metallic lead. Analyses of the trial data with the modified model indicates that significant improvements in entrainment were achieved with high-pressure coal injection.

TABLE OF CONTENTS

LIST OF TABLES

LIST OF FIGURES

LIST OF SYMBOLS

A_b	Surface area of secondary bubble	m^2
A_O^B	Boudouard Reaction Rate pre-exponential constant	k Pa^{-1} s^{-1}
A_o^s	Char-Steam Reaction Rate pre-exponential contant	k Pa^{-1} s^{-1}
$\dot{B}_r$	Boudouard Reaction Rate	k Pa^{-1} s^{-1}
a_j	Activity of Species j	k Pa^{-1} s^{-1}
C_j^b	Concentration of Species j in secondary bubble	kg mole m^{-3}
C_j^{sl}	Concentration of species j in slag	kg mole m^{-3}
C_j^i	Concentration of species j at bubble slag interface	kg mole m^{-3}
D_j	Diffusivity of species j	m^2 s^{-1}
D_{1-5}	Constants	
E_a^B	Activation energy Boudouard Reaction	kJ kg $mole^{-1}$
E_o^S	Activation energy Char-Steam	kJ kg $mole^{-1}$
F_{LPCE}	Fraction of low-pressure coal entrained	
F_{HPCE}	Fraction of high-pressure coal entrained	
F_{LPCC}	Fraction of low-pressure coal combusted	

F_{HPCC}	Fraction of high-pressure coal combusted	
F_{oxy}	Fraction of unconsumed oxygen which oxidizes ferrous iron	
F_{PBL}	Initial fraction of Pb as metallic lead in charge	
g	gravitational acceleration	ms^{-2}
I_{PWT}	initial coal particle weight	
k_j	mass-transfer coefficient of species j	
K_j	equilibrium constant reaction j	
M_c^C	kg mole of contained carbon	
M_l^{Pb}	kg mole of metallic lead	
$\dot{n}_j$	Molar mass-transfer rate of species	j
Pe_j	Peclet Number of species j	
P_j	Partial pressure of species j	k Pa
p_j	density of species j	kg m^{-3}
p_g^m	Molar gas density	kg mole m^{-3}
r_b	Radius of secondary bubble	m
r_p	Radius of char particle	m

$\dot{r}$	rate of reaction	
Sh_j	Sherwood Number os species j	
$\dot{S}_r$	Rate of Char-Steam Reaction	k Pa^{-1} s^{-1}
u	Slag velocity	m s^{-1}
$_j$	Activity coefficient of species j	

ACKNOWLEDGEMENTS

I would like to express my sincere indebtedness to Dr. Greg Richards for his untiring support and friendship throughout this project. I would also like to thank Dr. G. W. Toop, E. T. DeGroot and G. Heney for their guidance and assistance during my stay at Cominco. The co-operation and financial support of Cominco Ltd., Trail, B.C., was greatly appreciated. The financial support of the Science Council of B.C. also was greatly appreciated.

Many thanks are also in order to Dr. Keith Brimacombe for his encouragement throughout the entire project and his very helpful editorial suggestions during the writing of this thesis.

It is impossible to assess the contribution that the "boys" in the office have made. Many thanks to Dave Tripp, Bob Adamic, and Barry Wiskel.

Finally, I would like to express my deepest thanks to my wife, Susan, for the many sacrifices she has made and the support she has given me throughout this project.

CHAPTER 1

INTRODUCTION: SLAGS AND SLAG PROCESSING

Slags play a vital role in pyrometallurgical processes. The functions of slags include: the thermal insulation of melts, chemical insulation of melts from the surrounding atmosphere, resistive heat sources in melting processes, and the refining of metals through both the chemical and physical absorption of unwanted liquid and solid components and the supply of desired components. Yet in spite of their importance in the processing of metals, they remain poorly understood theoretically and not exploited to their full potential in industry.

This situation can be attributed to three main factors: firstly, the circumstances under which slags form in industrial processes; secondly, the complexity of industrial slag systems, and thirdly, the prevailing economics. The role these factors have played in determining the technological state of slag metallurgy is interesting and worthy of further discussion.

With regard to the first factor, slags generally form in pyrometallurgical processes through contributions from three main sources. These are: gangue material, which is introduced with the concentrate or ore; flux additions, which are deliberately made during the smelting stage; and oxidation of the metal or

matte. A fourth and more minor contribution is made through the chemical and/or mechanical erosion of refractories where present. Of these four only one, the flux addition, is the result of a deliberate addition made in an attempt to optimize the physiochemical properties of a slag which in the majority of cases already exists via other contributions. Historically, therefore, slags have been present as a consequence of the process, not through deliberate efforts. Optimization has been by trial and error which has promoted the practice of slag metallurgy through tradition rather than science.

The second factor, slag complexity, has acted to further perpetuate the traditional unimaginate approach. This complexity is a consequence of several factors which include: slag behaviour which ranges from that of ionic melts to that of polymeric or network forming melts; the fact that slags are solutions not dominated by any one species; and the realties of the industrial environment - such as the natural variation in gangue material, and the availability and changing economics of fluxes. These factors have all hindered slag investigation. Not surprisingly, therefore, there has been little experimental work done resulting in a profound lack of fundamental thermodynamic, physiochemical and reaction kinetic data on metallurgical slags.

The two factors discussed so far have helped to keep slag metallurgy in a relatively unenlightened state. The third and

debateably most important contributor to this trend is economics. Not surprisingly, if there is little obvious monetary gain to be made through the exploitation of slags the driving force for their study is limited. A classic example of this is the electro-slag remelting process (ESR) which produces expensive specialty tool steels. Due to this interest there is considerably more physiochemical data available on the CaF_2-Al_2O_3 - CaO ternary on which ESR slags are based than on industrially more prevalent slag systems. It is these three factors which have acted, and continue to act, to slow the exploitation of slags in the industrial work place. Recently, however, signs of interest have been shown both on the academic and industrial fronts in the slag cleaning process.

1.1 Slag Processing

An inherent problem associated with slags in pyrometallurgical processes is that they unavoidably contain metal values at the end of the process. The metal appears in the slag in two forms: one, as solution or chemical losses in which the metal is dissolved into the slag as a result of an existing chemical potential; and second, as physical losses due to mechanical entrainment. In many cases, these metal values are discarded with the slag and lost, or stock piled, with the slag to await an economic means of recovery. The driving force for the development of an economic means of recovery may arise from

several sources: for example, an increase in the price of the contained metal brought about by an increase in demand and/or a decrease in the grade of ore bodies, or the development of a new technology requiring slag treatment as an integral part of the process. A good example of the latter are the Q.S.L. and flash smelting processes for the treatment of lead concentrates. These processes use continuous multi-stage single-vessel reactors and therefore require improved methods of slag treatment. The same can be said for developments in the smelting of tin, copper and nickel.

1.1.1 Slag Cleaning

Historically, slag processing, when practiced, has been a secondary step outside the primary flow chart of the smelter and mainly consists of slag cleaning. The term slag cleaning refers to those processes concerned with the removal of metals from slags. To date there have been three main approaches to this problem. The most predominant of these, pyrometallurgical reductive processes, involve the treatment of slag with a reducing agent, such as coal, natural gas or pyrites. Metal values are then recovered in metallic form or as sulphides. For example, in the zinc slag fuming process, coal is injected into molten lead blast furnace slag to produce a metallic vapour which is then oxidized and collected for subsequent treatment.

The second cleaning technique 'settling' employs gravity to facilitate separation based on density differences. This method is particularly effective in those instances where the slag contains a large amount of mechanically entrained metal, for example, for the removal of copper droplets in copper slags. This technique is often used in conjunction with reductive treatment of the slag. In fact, a combination of settling and reductive treatment were applied in the developmental stage for the Kivcet process for the treatment of lead concentrates. In this process zinc and lead bearing slags are reacted in a relatively quiescent electric arc furnace with coke to permit both settling and reduction.

The third cleaning process is milling and floatation. This involves grinding the cold slag followed by separation of any metallic or sulphide particles in a standard rougher-cleaner circuit. There are both advantages and disadvantages to this process in comparison to the pyrometallurgical routes depending on the particular application. These will not be discussed further as they are beyond the scope of this thesis.

The potential for improvement in the area of slag cleaning appears to be considerable. The factors alluded to previously have contributed to create a technology which is in a relatively backward state and yet is poised to play a critical role in the

newer non-ferrous processes. A good example of this is the zinc slag fuming process which is only just beginning to be understood mechanistically. Thermodynamic data, physiochemical data and a knowledge of process kinetics have been brought to bear to describe the process in detail for the first time.[1a,b] The results of this analysis could potentially have a great influence on slag processing in general.

The application of high-pressure coal injection to the zinc slag fuming process, the focus of this thesis, follows as a direct result of the "kinetic" conception of the process. However, before proceeding, it is both necessary and illustrative to review the zinc slag fuming process in general, its history, and its potential role in the future of slag processing.

1.2 The Zinc Slag Fuming Process

In the zinc slag fuming process, molten slag is treated reductively in order to recover contained zinc and lead. Zinc, the more prevalent metal, is present dissolved in the slag in oxidic form, whereas lead usually appears in both oxidic and metallic forms. The process is carried out on a batch basis in rectangular water-jacketed furnaces that are, on average, 6m long by 2.5m wide; see the schematic diagram in Fig. 1.1. The charge may be made up entirely of liquid slag or a combination of liquid and solid materials. Typically batches containing 50 tonnes are

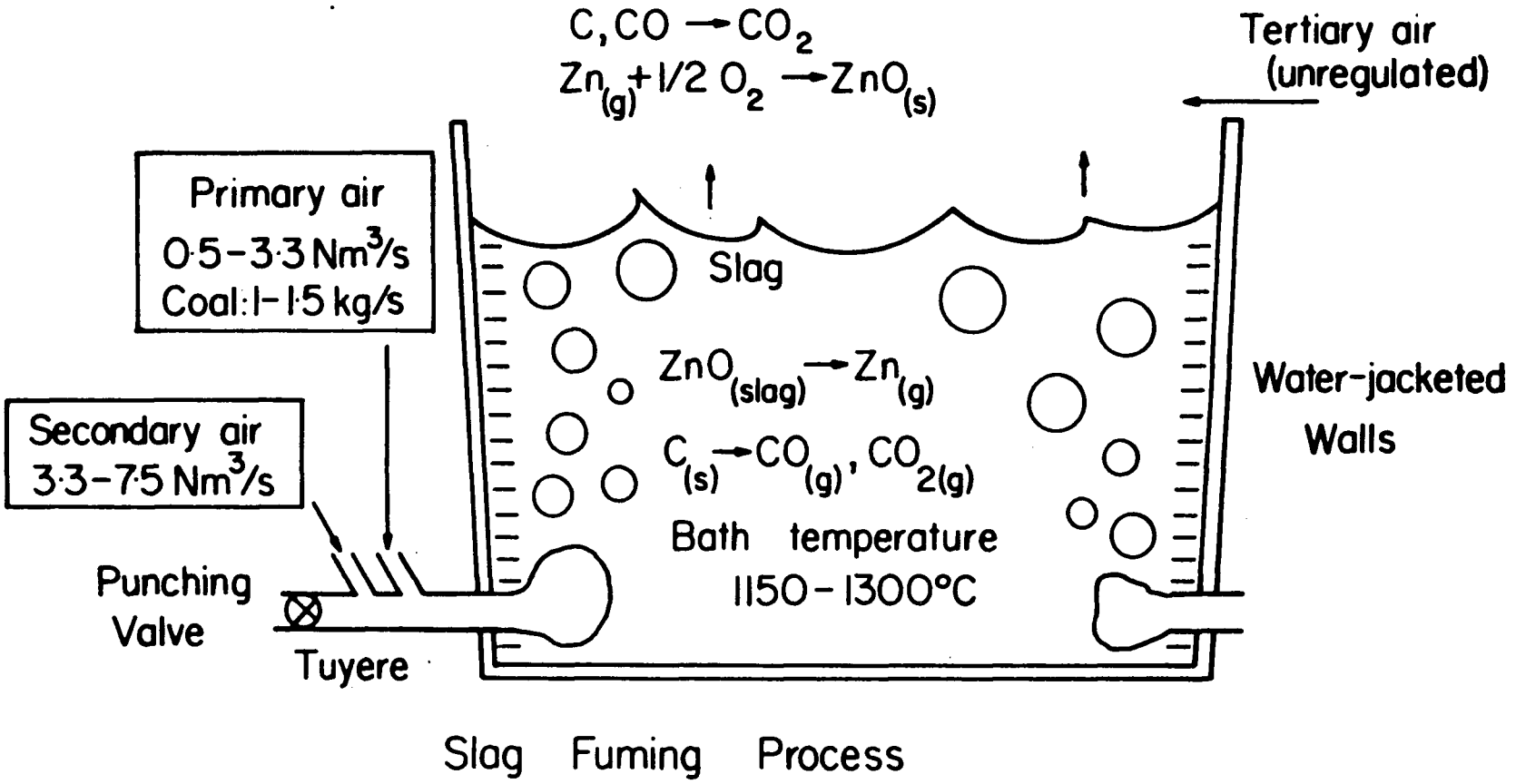

Slag Fuming Process

Figure 1.1 Schematic diagram showing the furnace in cross-section and the chemical reactions occurring in the process

processed at a time. A reductant, usually coal, pulverized to approximately 80%-200 mesh (B.S.S.), is injected into the furnace through a row of tuyeres located near the bottom of each of the two long sides. The coal is injected into the tuyeres at overall rates ranging from 50 - 75 kg/min. conveyed by "primary air" at typical overall rates of approximately 30 Nm^3/min. The main or "secondary blast" enters the tuyeres behind the coal/air mixture at overall rates ranging from 300 - 400 Nm^3 /min usually at ambient temperature. In some operations however, there are variations in furnace geometry and operating practice. For example, primary and secondary blast flow rates may be equal at about 200 Nm^3 /min and secondary blast preheats of up to 700^oC have been used.

Removal of zinc from the bath is effected through reduction of dissolved zinc oxide to metallic zinc vapour which then exits via the surface of the bath. However, the vapour form in which lead exits the bath, be it as metal, oxide or sulphide is less clear as these compounds are present predominantly as liquids at slag fuming temperatures. The characterization of lead removal from the bath is an important aspect of this thesis and will be discussed in the sections that follow.

After exiting the surface of the bath the metallic zinc vapour and any lead bearing species are then reoxidized by "tertiary" or leakage air. This mixture of metal oxides (fume),

combusted coal and tertiary air is then drawn up through a flue and the fume is collected in a baghouse for subsequent processing. The exothermic nature of these oxidation reactions results in extremely hot off-gases. An attempt is made to recoupe some of this sensible heat by passing the gases through a steam boiler prior to entering the baghouse.

Slag fuming is normally used to treat lead blast furnace slags. At some operations, however, it has been applied successfully to the treatment of copper reverberatory slags. The only significant difference in this case is in the initial zinc and lead concentrations: 13-18 wt% zinc and 1-3 wt% lead for the lead blast furnace slags, 8 wt% zinc and less than one weight percent lead for the copper reverberatory slags. These slags are then fumed down to between 1.5 and 2.5% zinc at which point the furnace is tapped. In both cases lead contents are typically around 0.02% at this point. Complete fuming cycles take approximately 3 hours including 30 minutes for charging and tapping. The recovery of zinc is generally 85-90% with 1-2 kg of coal required per kg of zinc fumed. In contrast, lead recoveries tend to be higher, near 100%. In addition to zinc and lead, the fume from lead blast furnace slag contains traces of volatile species such as sulphur, tin, cadmium, indium, chlorine and fluorine.

Under ideal conditions at some operations, the fuming cycle is broken down into two periods distinct from those associated with charging and tapping the furnace. These may be described as an initial "heating period" followed by a period of "proper fuming". In the heating period, the coal-to-air ratio is reduced in order to approach stoichiometric combustion of the air/coal mixture providing the highest possible heat input per unit of coal. Throughout this period, the bath temperature rises, zinc and lead fuming rates tend to be low, and the bath ferric iron concentration increases reflecting the oxidizing conditions prevailing in the furnace. There are several reasons for having an initial heating period. These may include: the build up of a reserve of sensible heat which is later consumed throughout the fuming period and/or, the ability to process solid crushed slag or ladle skull. The heating period is generally terminated when the bath temperature approaches approximately 1325 ^{o}C . The onset of the fuming period is initiated by an increasing in the coal-to-air ratio causing conditions in the furnace to become reducing. This period is characterized by a steady decline in bath temperature, high zinc and lead fuming rates, and a decrease in the bath concentration of ferric iron.

At other operations however, this two-stage fuming cycle is not practiced. The entire fuming cycle is run at a constant coal-to-air ratio. At still other operations, a significantly different approach is taken. Instead of a batch type operation,

slag fuming is carried out on a continuous basis in a geometrically smaller furnace using fuel oil as the reductant.

1.2.1 History

The development of the zinc slag fuming process is rooted in the development of the sinter-lead blast furnace process for the smelting of lead sulphide ores in the 1870's. The presence of significant amounts of zinc sulphide in association with the lead sulphide in the concentrate meant that the process had to effect separation between the two. This was achieved by taking advantage of the difference in stability between lead oxide and zinc oxide. By controlling the oxygen potential in the blast furnace it is possible to produce lead while holding the majority of the zinc as oxide in the slag phase. Initially, this slag was stock piled and smelters the world over began to accumulate slag dumps containing up to 20% zinc. This provided the industrial setting for the emergence of a process that could recover this zinc. What was still required, was the economic incentive and technical expertise.

The economic incentive was provided by a sharp increase in the demand for zinc which followed the outbreak of World War I, and continued through the 1920's as the industrial potential of zinc was realized. The technical development began almost immediately.

Some of the earliest work on the extraction of zinc from lead blast furnace slags was carried out by the Sulphide Corporation at Cockle Creek between 1906 and 1916. The initial experiments in 1906 involved blowing compressed air through molten slag. This resulted in some fuming and rapid freezing of the slag. A second set of experiments was carried out using a coal-air mixture and proved to be successful enough to warrant patenting. The patent was issued to F.H. Evans and P.A. McKay in 1908. Other experiments included: the reverberatory furnace treatment of slag by firing with coke and limestone, and a blast furnace type treatment of slag briquettes and nodules. The only result of any significance was that water-jacketed furnaces appeared to be necessary in any industrial application.

In the 1920's, investigation into the commercial application of the process lead to the first furnace being blown in at the Anaconda Copper Mining Company at East Helena, Mont.[3], and to the installation of the second furnace by the Consolidated Mining and Smelting Company, Trail, B.C. in 1930. These two furnaces were slightly different. The East Helena furnace was 2.44m (8ft) by 3.66m (12ft) and used a tuyere design borrowed from the burners in coal-fired reverberatory furnaces, whereas the Trail furnace was slightly wider at 3.5m (10ft), significantly longer at 7.9m (20ft), used newer double-inlet tuyeres, and incorporated a waste-heat boiler. Apart from these differences, the furnaces were essentially the same and were both used in the treatment of

solid and liquid material in order to recover zinc from slag dumps. As the dump supply of zinc was exhausted, they were shifted to the treatment of liquid lead blast furnace slag.

Since the 1930's, there have been little or no significant changes in the process despite its adoption in virtually every lead smelter throughout the world. Individual modifications have included: the adoption of secondary blast preheat at the Broken Hill Associated Smelters of Port Pirie in 1967[4]; continuous fuming in Bulgaria utilizing fuel oil instead of coal[5]; and the use of natural gas as a reductant in a Russian process.[6]

As mentioned previously, the newer technologies for the smelting of lead concentrates require improved methods of slag treatment. These technologies all employ continuous smelting processes incorporating reductive slag cleaning stages within the main stream of the process. In the pilot QSL process for example, natural gas is injected through submerged tuyeres in a reductive zone. In the Kivcet process, coke additions are made to the slag surface in a relatively quiescent electric arc holding furnace. Both of these processes require a fundamental understanding of the kinetics of oxidic zinc and lead reduction, and metallic lead removal from these slags in order for them to be economically successful processes. The role played by the zinc slag fuming process in the near future of the non-ferrous metals industry must be that of a testing arena. It must be used

to investigate kinetic phenomena essential to the success of the newer smelting technologies.

In reflection, the lack of consistency in zinc fuming practice, the non-universal adoption of process improvements, such as blast preheat and continuous operation, and the fact that the process remains essentially unchanged since the 1930's, all point to a traditional optimization approach to process improvement. The proposed slag cleaning stages in the newer smelting technologies also suggest the continuation of this trend in thinking. In both the QSL and Kivcet processes, the approaches taken suggest a lack of understanding of slag reduction kinetic phenomena. The economic incentive for the elucidation of these phenomena now exists as they are paramount to the success of these processes. High-pressure coal injection follows from an understanding of kinetics and could prove to be of considerable benefit to slag treatment technology. Taken one step further, the phenomena described elsewhere[1a,b] and built upon in this thesis help forge the way to the use of slags as active tools in metals extraction.

CHAPTER II

LITERATURE REVIEW

This thesis deals with the application of high-pressure coal injection to the industrial zinc slag fuming process. In order to outline some of the options available for coal injection systems, experimental techniques and data analysis, it is necessary to review the literature. The results of these reviews are presented in this chapter.

2.1 Pulverized Coal Transport

A general review of the literature[7-10] indicates that there are several precautions which must be observed when handling and transporting pulverized coal. Firstly, because in certain concentrations coal dust suspended in air constitutes a highly explosive mixture, extreme caution must be exercised in its handling, ensuring that work areas are well vented and clean. The second precaution is directly concerned with the transport of coal and therefore of direct applicability to this project. There is strong evidence to suggest that under certain conditions, such as during pneumatic transport in plastic pipes with little or no moisture present, a significant static charge can be generated. The random uncontrolled grounding of this charge can result in ignition of the coal/air mixture. Since the

conditions leading to this phenomena are not well documented, metallic pipes and/or grounding must be provided for pneumatic transport as a general precaution. Finally, it is essential to maintain proper aeration to achieve fluid-like behaviour when transporting pulverized coal. Sticky solid-like behaviour can result from lack of aeration as well as from other factors: for example, high moisture contents and/or a build up of static surface charge.

2.1.1 Pneumatic Conveying of Materials

Pneumatic conveying systems have been classified historically into a broad range of categories including: gravity-feed systems, low-velocity systems, high-velocity systems, light-phase systems, dense-phase systems, vacuum systems, low-pressure systems, medium-pressure systems, high-pressure systems, etc.[7,8,9] In certain instances these terms have been used loosely by manufacturers to classify different types of equipment. In the engineering literature, a quantitative classification system has been developed. For example, dense phase systems are considered to be those with mass flow ratios of solid to gas in the hundreds; light phase or lean systems, have ratios below about one hundred, with eighty frequently being the division between the two. Additional classifications include: vacuum systems, considered to be those operating below atmospheric pressure; low-pressure systems,

between atmospheric and 82.73 kPa (12 psig); medium-pressure systems, up to 310.23 kPa (45 psig); and high-pressure systems, up to 861.75 kPa (125 psig). Unfortunately, there are no universally adopted standards for classifying these systems. It is clear, however, that for gas-solids mixtures pneumatic conveying systems essentially can be broken down into three main types[7] : material-into-air, air-mixing and air-into-material systems.

2.1.1.1 Material-Into-Air Systems

The material-into-air systems are classified as those systems in which material enters a stream of air under either negative or low pressure or, is induced into a stream by vacuum. This classification includes the vacuum systems and low-pressure systems mentioned earlier. Table 2.1 presents a summary of some of the advantages and disadvantages of this type of system.

2.1.1.2 Air-Mixing Systems

In the air-mixing systems the material to be conveyed and air are intimately mixed in a special feeder prior to entering a conveying line. These systems resemble the first type except that a denser stream, and, feeding into higher pressures are possible. These systems include the medium pressure systems. The feeders used include: rotary feeders, Fuller Kinyon pumps

TABLE 2.1

Classification of Pneumatic Conveyors

Classification	Advantages	Disadvantages
Material-into-air	1. Handles wides range of materials,including irregular shapes.	1. Uses lower material-to-air ratios than other systems. 2. Requires larger equipment than other systems-air movers, pipelines, dust filters, etc.
Positive-pressure	1. Delivers material through a single pipeline to several discharge points. 2. Uses smaller pipelines than comparable vacuum systems. 3. Air leakage is outward so that moisture can not be drawn into equipment.	1. Requires an airlock feeder and blowback vent filter at each material entry point. 2. Requires large dust filter at each material discharge point. 3. Transport unloading requires use of fixed or portable airlock feeder installation.
Negative-pressure	1. Transports easily unloaded using pickup hoppers or nozzles. 2. Material can enter a single pipeline from several sources of supply without venting 3. Material can enter line using airlock feeder, controlled-feed tank, or pickup hopper.	1. Material can be delivered only to a single discharge point. 2. Dust filter and airlock discharger required at the discharge point. 3. Moisture and outside air can be drawn into equipment. 4. Requires larger piping and equipment than positive-pressure systems, due to lower density air. 5. Air mover and receiver-filter requires location stop silos or building roof.
Negative-pressure (vacuum)with dust-return loop	1. Delivers material to several discharge points. 2. Dust is returned to a single, conveniently located dust filter for re-entry into conveying line or silo.	1. Requires a collector and an airlock discharger at each discharge point. 2. Requires diverter valves in the dust return and conveying lines at all but one discharge point.

Combination vacuum/ pressure	1. Permits pickup of material from transports by vacuum and simultaneous discharge to each of several discharge points by pressure. 2. Dust from vacuum-side receiver is delivered into conveying line.	1. See above for respective portions of system-vacuum or pressure side. 2. Requires larger-capacity and horsepower air mover than for the vacuum or positive-pressure system. 3. If air mover breaks down, two plant operations are affected - unloading and reclaiming.
Closed-loop, positive or negative pressure	1. Permits use of inert gas for conveying, with minimum make-up requirement. 2. Permits re-use of conveying air where air is dried or filtered to be free of contamination. 3. Eliminates the use of diverter valves on dust-return line at each discharge point.	1. Same as for combination vacuum-pressure system.
Air-into-material	1. Uses highest possible material-to-air ratio compared to other systems. 2. Requires smaller equipment than other systems - air movers, pipelines, dust filters. etc. 3. Low velocity, dense mixture permits handling abrasive and friable materials. 4. High-pressure units and systems permit delivery through very long pipelines. 5. Delivers material to several discharge points using a single pipeline. 6. Each batch can be weighed before being conveyed.	1. Operation is intermittent. 2. High pressure systems (over 15 psig) require ASME-Code-constructed vessels. 3. Surge hopper is reuired for rapid filling if auxiliary feed capacity is limited. 4. A dust filter is required for venting surge hopper and blow tank. 5. Material must be delivered to blow tanks at higher than pneumatic conveying rates, due to limited filling time between discharge cycles.
Free-feed blow tank	1. Bottom-discharge units can handle lumpy, non-fluidizable and fluidizable materials. 2. Bottom-discharge units can be emptied completely when handling sanitary materials.	1. Material-to-air ratio is variable - high at start and finish of each cycle. 2. Top-discharge units leave residue in bottom of tank that may cause contamination of material.

Controlled-feed blow	1. Material-to-air ratio of discharge is uniform. 2. Conveying-line velocity can be reduced to the slug flow limit. 3. Booster nozzles may be installed in the conveying line to maintain dense, low velocity flow.	1. Use is limited to fluidizable, powdered or mixed-granular materials.
Air-mixing	1. Material-to-air ratio is high, but not as high as in air-into-material systems. 2. Conveying is continuous. 3. Delivers material to several discharge points through a single pipeline. 4. High pressure permits delivery through long, small-diameter pipelines	1. Use is limited to fluidizable, powdered or mixed-granular materials. 2. Can not handle friable material. 3. Material must be delivered by metered auxiliary conveyors. 4. Feed hopper must be level-controlled and vented to dust filters. 5. Feed hoppers must be maintained full when handling abrasive material.
Feed-screw into air nozzles	1. Requires smaller auxiliary conveyors than blow tanks. 2. Requires lower headroom than blow tanks.	1. Subject to erosion and loss of capacity when handling abrasive material. 2. Requires skilled maintenance, as for high-grade machinery. 3. Must run fully loaded when handling abrasive material - wear increases when idling. 4. Requires high-prssure, sliding-vane or reciprocating air compressor. 5. Compressors require cooling vater. Oil separators must be installed ahead of air nozzles.
Air-swept, double-entry rotary feeder	1. Can be made with cutting vane to handle tacky material such as sugar or detergents.	1. Pressure limit is 20 psig. requiring low-volume, positive-displacement blowers in tandem. 2. Capacity varies with head of material in feed hopper.

and any other type of pump capable of delivering a dense material-air mixture into a pressurized air stream. The relative merits of this system are summarized in Table 2.1.

2.1.1.3 Air-Into-Material Systems

The air-into-material systems are classified as those systems in which air enters a mass of material to initiate flow. These include the high-pressure systems and dense phase systems which are more generally termed as "blow-tank" systems. The advantages and disadvantages of this type of system are described in Table 2.1.

2.1.1.4 Selection of System

The type of system selected depends on such factors as economics, application, the desired volume and mass flow rates and the type of material to be conveyed. If for example, the classification is narrowed down to include only those systems capable of conveying pulverized coal, as would be required for this project, a number of acceptable systems decreases. Unfortunately, no single best system is obvious.

2.1.2 Non-Pneumatic Transport

In addition to air, water has also been used as a conveying

medium to inject pulverized coal successfully into an iron blast furnace.[11] There are several obvious advantages to injecting coal-water slurries: reduction in explosion hazard, no gaseous oxygen injection, and the possibility of achieving higher pressures. Furthermore, this brings to light other alternatives such as coal-oil slurries and coal-steam mixtures which might find future application in the zinc slag fuming process.

2.1.3 Summary: Pneumatic Conveying

In summary, it is evident that design criterion will have to be established before the information in the literature can be applied to aid in system selection. This endeavour will be addressed in Chapter IV.

2.2 The Zinc Slag Fuming Process

The conceptual idea for high-pressure coal injection follows directly from the work of Richards.[1a] As a result, his original work[1a] and the later treatment by Richards, Brimacombe and Toop[1b] are strongly recommended as preliminary reading to this thesis.

To minimize repetition, material previously covered by Richards will only receive cursory treatment. Relevant material later than 1983 will be covered in more detail. For a more detailed review of relevant pre-1983 material the reader is

referred to Richard's work.[1a]

2.2.1 Studies and Modelling

Soon after the first furnaces were constructed two schools of thought emerged on the mechanism of reduction of zinc from slag. The first school postulated that coal entering the furnace was immediately combusted to a carbon monoxide-carbon dioxide mixture. The carbon monoxide in this gas stream then acted to reduce the dissolved zinc oxide and produce metallic zinc vapour as the reducing gas ascended through the bath.[12,13] In contrast the second school postulated that particles of coal in contact with the slag act as the sight for reduction.[14] Surprisingly, these different concepts remain the source of debate today.

2.2.1.1 Equilibrium Models

Historically, the first school of thought received substantial support in 1954 from the classical study of Bell, Turn and Peters. [15] In their investigation, a simple model based on mass balances and the assumption of internal equilibrium was developed to estimate the activity of zinc oxide in the slag for three industrial runs during which fuming rates were measured as a function of bath zinc concentration. With this data, the authors found that their model accounted quite well for the overall furnace heat balance. The model also was used to

evaluate the effect of various changes in operating practice. These included: the injection of natural gas as a reductant and preheating the blast.

Despite obvious shortcomings, such as the exclusion of the role of iron oxides and the lack of indirect experimental evidence to support the fundamental assumption of equilibrium, the model reasonably accounted for observations with only minor discrepancies. In one instance however, this was not the case. During fuming with natural gas as the reductant, fuming rates predicted by the model were significantly higher than those observed in practice. This observation is of considerable significance because it alludes to the importance of the role coal particles play in slag reduction.

Additional support for the equilibrium approach continued to build in 1956 when Kellogg conducted a "no-coal" test on No. 2 slag fuming furnace at Cominco Ltd., Trail, BC.[14] In this test the coal supply to the furnace was interrupted for a period of five minutes during which time changes in slag composition and temperature were recorded. The analysis of this data suggested that there was sufficient gas stream-slag interface for it to be the "seat of the fuming reaction".

Based on the results of this experiment and on the previous work by Bell et al, Kellogg developed a comprehensive model of

the zinc slag fuming process in 1967.[16] In this model, the thermodynamics of the iron oxides as well as that of PbO and sulphur were included. In addition, the overall furnace heat balance was improved to incorporate the melting and freezing of slag on the water cooled walls and bottom, and the reactions occurring above the bath. As a result, the rates of change of iron, lead, sulphur and temperature could be predicted in addition to that of zinc.

The model was fitted to average industrial data by adjusting slag activity coefficients and heat-transfer coefficients. This potentially could have raised concern but the resulting values of the coefficients were reported to be within expected limits.

The Kellogg[16] model represented a significant advance in the study of the zinc slag fuming process. It established conclusively that the assumption of equilibrium could be used quantitatively to account for the behaviour of zinc and qualitatively to account for the behaviour of iron, lead and bath temperature.

In the early 1970's the Kellogg model was modified by Grant and Barnett[17] at the Broken Hill Associated Smelters, Port Pirie, Australia. The heat balance in the model was upgraded to include waste heat boilers and recuperators. Some improvements also were made in the handling of input parameters, such as changing coal

rates and variations in charge with respect to hot and cold additions. As with the original Kellogg model [16], the modified model was fitted to industrial data by adjusting the activity coefficient of zinc oxide in the slag. It is interesting to note that Grant and Barnett needed a value 2.6 times greater than that used by Kellogg, and, that this increase was not substantiated by any independent thermodynamic data. This becomes a significant point because it means that the validity of the model rests on the activity of ZnO in the slag which is effectively a fitting parameter.

From a process point of view there is a fundamental problem with the assumption of equilibrium - it negates the consideration of process kinetics. In so doing, it is impossible to assess the influence of kinetic phenomena on furnace performance. For example, it could prove more efficient with respect to zinc removal to operate the process in such a manner that equilibrium is not achieved.

2.2.1.2 Empirical Models

Historically, support for the second school of thought has been less scientifically based. The empirical models of the process by Quarm[18-20], Sundstom [21] and Ivanov [22] are of little value in elucidating fundamental thermodynamic and kinetic phenomena. Even though they have been shown to reproduce

observations quite well, particularly for the furnace from which they have been derived, they lack broad applicability and therefore universal acceptance.

Nevertheless, the empirical models can be useful at least for the identification of kinetic and thermodynamic phenomena. In particular, some of the variables that have been identified by Sundstrom and Ivanov to be of critical importance to the process could be interpreted as kinetic effects. These include: the negative influence of bath weight, and the effect of the number of operating tuyeres. In the latter case, this is strong evidence that injection dynamics play a vital role in the slag fuming process. Indeed, this also has been corroborated by the findings of Glinkov et al.[30]

2.1.1.3 Industrial and Laboratory Studies

Additional support for the kinetic approach to process modelling has been received from industrial [23,24] and laboratory[25-29] studies of slag fuming. In one instance[5], engineers at the Non-Ferrous Metal Works in Plovdiv, Bulgaria departed considerably from standard practice and developed a continuous fuming furnace using fuel oil as the reductant. The furnace, which has a cross-sectional area of 5.85 m^2, received shaft smelting furnace slag via an intermediate electric arc settling furnace. Of particular interest, apart from the significance of

the approach taken, is that according to Abrashev, the fuming rate is 50% lower than that predicted by equilibrium. This statement is further corroborated by the fact that a reduction in cross-sectional area from 8.9 to 5.95 m^2 was reported to have brought about a two-fold increase in furnace capacity with oil and air rates unchanged. This is strong evidence that the furnace is limited by kinetics.

Industrial pilot-plant studies[23,24] have suggested that the coal-slag interaction may be of fundamental importance to slag reduction. Other laboratory experiments[25-29] have confirmed these findings and suggest that the reduction actually occurs via the gaseous intermediates, CO and CO_2. These studies indicate that kinetic phenomena, such as the rate of the Boudouard reaction occurring on carbon and oxide diffusion[26-29] through the slag may be rate controlling depending on the stage of reduction.

In a more recent study on the mechanisms of slag reduction by Malone, Floyd and Denholm[31], the role of carbon is less clear. Based on a series of experiments which involved coke, CO and nitrogen injection into zinc-bearing slags, with and without iron present. The authors proposed a mechanism by which ZnO is reduced from iron containing slags. Unfortunately however, there appear to be a number of difficulties in their interpretation of

the results particularly for the case where fuming was achieved with only nitrogen injection. In this experiment the Fe^{2+}/Fe^{3+} ratio was reported to have increased initially and then remained constant during fuming which is clearly inconsistent with the proposal that FeO is the source of the reductant.[31] One plausible explanation is that metallic iron was present prior to the addition of ZnO and the initiation of nitrogen injection.

Substantial proof for the zinc fuming process as a non-equilibrium process was not provided until the work of Richards[1a] in 1983. In this work, an exhaustive industrial study of the process revealed coal particles entrained in the slag negating the possibility of internal equilibrium. Analysis of tuyere injection dynamics was also used to further support these findings.

2.1.1.4 The Kinetic Model of the Process

Based on industrial findings, a mathematical model incorporating thermodynamic data, physiochemical data and kinetic phenomena was developed by Richards[1a] based on coal particles entrained in the slag as the site for reduction. Mechanistically, the model is formulated around the concept of dividing input coal into the following fractions: that entrained in the slag, that combusted in the tuyere gas column and the

balance which is assumed to pass through the furnace unconsumed.

In terms of model formulation, it follows from this coal partitioning that the furnace has effectively been separated into two reaction zones. The first of these is a reduction zone in which entrained coal reacts directly with the slag. The second then is an oxidation zone in which the tuyere gas column reacts with injected coal and the surrounding slag.

The overall furnace model can be broken down essentially into a series of heat and mass balances around the two reaction zones and the furnace as a unit. Of these balances, those associated with the reduction zone are of particular significance because they are formulated from fundamentally based kinetic concepts. They will be discussed in considerable detail.

Within the model, the heat and mass balances on the reduction zone were formulated around an elaborate coal-gas-slag reaction system which represents a cluster of several coal particles, entrained in the slag, after they have undergone pyrolysis and have become surrounded by an intermediate or "secondary bubble" containing the products of pyrolysis. This cluster or char was assumed by Richards to have an effective radius of around 80 um.

Within this system, the following reactions were considered:

$$ZnO_{(sl)} + CO_{(g)} = Zn_{(g)} + CO_{2\ (g)} \quad \ldots (2.1)$$

$$Fe_2O_{3\ (sl)} + CO_{(g)} = 2FeO_{(sl)} + CO_{2\ (g)} \quad \ldots (2.2)$$

$$C_{(s)} + CO_{2\ (g)} = 2CO_{(g)} \quad \ldots (2.3)$$

$$CO_{2\ (g)} + H_{2\ (g)} = CO_{(g)} + H_2O_{(g)} \quad \ldots (2.4)$$

Kinetic phenomena considered included: the diffusion of zinc oxide (ZnO) and hematite (Fe_2O_3) in the slag to the secondary bubble-slag interface, diffusion of wustite (FeO) from the bubble-slag interface to the bulk of the slag, and the rate of the Boudouard reaction (Eq. 2.3) on the char particle. Diffusion rates were estimated based on the dynamics of rise of the secondary bubble ascending through the slag. Mass transfer coefficients for diffusing species were calculated from an empirically based equation, taken from the literature, which is valid for rigid spheres in creeping flow. The velocity of these bubbles relative to the slag was calculated assuming Stokes law. Diffusivities for ZnO and FeO in slag systems approximating those found in slag fuming were taken from the literature. The diffusivity of Fe_2O_3 was assumed to be one tenth that of FeO.

The diffusion of zinc oxide and ferric iron to the bubble-slag interface is a consequence of the reducing conditions which

prevail in the secondary bubble. Upon arrival at the interface, zinc oxide and ferric iron were assumed to be reduced via equations 2.1 and 2.3, respectively. These reduction reactions were assumed to be rapid and therefore at equilibrium. Equilibrium was also assumed within the secondary bubble as dictated by equation 2.4.

Within the bubble, CO_2 in the gas phase, generated by the reduction reactions, reacts with the char particle according to the Boudouard reaction. The rate of the Boudouard reaction was determined by an empirically based equation taken from the literature. Mass-transfer within the gas phase was assumed to be rapid and not rate limiting.

As a result of these reactions, the partial pressure of metallic zinc vapour in the secondary bubble increases as it rises through the bath. Concurrently, ferric iron also is reduced. The rate at which these reduction reactions proceed is solely dependent on the relative rates of mass-transfer. The net result is an influx of CO_2 and H_2O, and an increase in the volume of the secondary bubble.

The tendency for the oxygen potential to rise in the secondary bubble is negated to a certain extent by the Boudouard reaction occurring on the char particles. However, because the rate of the Boudouard reaction is dependent on the amount of

carbon remaining in the char, the extent to which it can maintain an overall reduction potential decreases as reduction proceeds. Consequently, the oxygen potential of the secondary bubble increases and moves towards equilibrium with that of the slag. Within the model, reaction was assumed to cease when the char-secondary bubble reaches the surface of the bath and the contents of the secondary bubble are released to the furnace atmosphere.

Despite its inherent complexity, substantial evidence in support of this conceptualization of the process was found by Richards[1a] from electron microprobe analysis of quenched slag samples. Zinc and iron concentration profiles were observed around bubbles in these samples which is consistent with the bubbles activily reacting with the surrounding slag, and zinc oxide and ferric iron as the diffusing species. Thus the possible role of electron transfer between the Fe^{2+}/Fe^{3+} couple and oxygen diffusion in iron reduction appears to be small.

In order to complete the mathematical formulation of the reduction zone, Richards [1a] conducted a heat and mass balance on the char particle secondary bubble-slag reaction system over the residence time of the secondary bubble in the bath. The balances were constructed on the basis of a unit weight of the initial coal particle. The residence time of the particle in the bath was calculated based on a path length and an assumed slag circulation velocity. The path length of the particle, in turn,

was calculated based on estimates of the void fraction of the tuyere gas column, slag porosity and slag circulation flow patterns.

Multiplying the conservation equations by the total rate at which coal is entrained in the slag gives the instantaneous rates of change of zinc, ferric and ferrous iron concentrations, and the rate of heat consumption in the reduction zone. By holding these rates constant over a given increment of time, the heat and mass balances are determined for the period in question.

In comparison to the reduction zone, the balances associated with the tuyere gas column were formulated on a more empirical basis without invoking specific kinetic mechanisms. The heat and mass balances for this zone were determined essentially by two externally set adjustable parameters: the fraction of coal combusted, as previously described, and the fraction of oxygen consumed by ferrous iron oxidation. The latter was defined by Richards[1a] as the fraction of oxygen in the tuyere gas stream unconsumed by coal which reacts with ferrous iron. It was reasoned that ferrous iron would be oxidized to ferric iron within the tuyere gas column because the prevailing conditions generally would be oxidizing.

By specifying these two parameters, the heat and mass balances for the tuyere gas column were determined for a given

overall coal and air injection rate and temperature. The following assumptions were made:

[i] the coal is assumed to be completely combusted to CO_2 and H_2O via equations 2.5 and 2.6, respectively;

$$C + O_2 = CO_2 \quad \ldots (2.5)$$

$$H_2 + 1/2\ O_2 = H_2O \quad \ldots (2.6)$$

[ii] any ash accompanying the combusted coal is assumed to enter the bath as silica;

[iii] ferrous iron oxidation is assumed to proceed via equation 2.7;

$$2FeO + 1/2\ O_2 = Fe_2O_3 \quad \ldots (2.7)$$

and

[iv] the tuyere gas and any unburnt coal are assumed to exit the bath at the slag temperature.

In addition to these balances, the fraction of coal combusted and fraction of oxygen reacted with ferrous iron were used by Richards[1a] to predict oxygen utilization. It is with this number that the underlying kinetics of the tuyere gas column are evaluated. For example, a value less than 100% oxygen

utilization indicates a kinetic limitation to complete reaction of the input oxygen with coal and/or slag.

The third and final set of heat and mass balances were associated with the furnace walls and bottom. Similarly to Kellogg[16], Richards[1a] considered the melting and freezing of slag on the furnace walls and bottom. Heat-transfer coefficients, heat capacities and thermal conductivities were taken from the literature. Assumptions made included: a specific slag melting point based on averaged melting ranges taken from the literature, and a uniform composition through the thickness of the wall freeze layer. The composition of the freeze layer was determined by averaging a through thickness assay of actual frozen wall material taken from the wall of No. 2 furnace at Cominco.

In order to close the furnace heat balance completely, Richards assumed that the oxidation reactions occurring above the bath do not contribute to the overall slag heat balance. This is different from the approach taken in the Kellog model which considers these reactions.

The model was fitted to industrial data by adjusting the previously mentioned parameters (fraction of coal entrained, fraction of coal combusted and fraction of oxygen reacting with ferrous iron) until good agreement was obtained between measured

and predicted profiles of bath composition and temperature. Of particular significance is that this fitting procedure was carried out on a cycle-to-cycle basis, and not on averaged plant data as was the case with the Kellogg[16] model and later the Grant and Barnett model.[17] Fitted values of fraction of coal entrained, fraction of coal combusted, total furnace oxygen utilization, bath depth and non-stoichiometric factor, x, were obtained for five different furnaces and a total of eleven cycles. These results permitted a comparison to be made between cycles and furnaces so that trends could be delineated as a function of operating practice.

Despite a lack of accurate fundamental thermodynamic, kinetic and physical data, the model has been shown to predict the behaviour of zinc, ferrous and ferric iron and, at least, to approach quantitative prediction of bath temperature. The model excludes lead, however this is not a problem provided that the fuming slags under consideration have a low lead content - less than approximately 1 wt%.

Of particular significance is the consistency in the values of the fitting parameters. The overall ranges obtained for the fraction of coal entrained was 0.29 to 0.39, for fraction of coal combusted, 0.45 to 0.60, and for furnace oxygen utilization, 0.67 to 0.92. In the case of the latter, it was found that the oxygen utilization could be correlated to bath depth.

As argued by Richards[1a] , the consistency in the fraction of coal entrained is to be expected since all the furnaces have approximately the same low-pressure injection system. The lack of sensitivity of the fitting parameters to other process variables such as coal type, blast preheat, coal rate, furnace dimensions, slag composition and blast flow rate, which vary from furnace to furnace, is indicative of the general applicability of the model and supports its theoretical foundations.

Although the results of the model are self-consistent, there is cause for concern with the predictions of oxygen utilization for three furnaces, companies A, B and E, for which temperature profiles were not available. Clearly, since the only mechanisms of generating heat within the model are through either coal combustion or ferrous iron oxidation, it is anticipated that the model predictions for fraction of coal combusted and fraction of oxygen consumed in ferrous iron oxidation will be highly sensitive to bath temperature profiles. This places in question the accuracy of the model predictions with respect to these two parameters, and therefore, furnace oxygen utilization. Unfortunately, the offending cycles represent seventy percent of the oxygen utilization data.

To evaluate some of the more questionable assumptions that were necessary to formulate the model, a sensitivity analysis was

performed with respect to the effect of slag circulation velocity, coal particle cluster size, wustite stoichiometric factor, diffusivities of wustite and zinc oxide, the wustite-to-hematite diffusivity ratio, bath slag porosity, slag density, and the void fraction of the tuyere gas column on the fuming rate (%Zn/min) and fuming efficiency (kg Zn fumed/kg coal injected). Remarkably, the model was shown to be relatively insensitive to these parameters.

Finally the predictive capability of the kinetic model was compared to that of the thermodynamic models of Kellogg[16] and, Grant and Barnett.[17] For these comparisons, the entrainment factor was held constant at 0.33 (the average of the eleven cycles investigated), and the fraction of coal combusted and oxygen utilization were calculated within the model based on the correlations with bath depth. The comparison was made for the eleven cycles described earlier and shows that the kinetic model is at least as accurate as the more widely accepted thermodynamic models.

Having established the ability of the model to simulate process behaviour, Richards[1a] turned to using the model as a predictive tool. This yielded the major finding of the work- the prediction of a simultaneous increase in both fuming rate and efficiency by increasing the fraction of coal entrained. This is a particularly significant result because it implies that a

substantial improvement in furnace performance can be obtained through manipulation of injection dynamics which clearly cannot be predicted by an equilibrium based model.

2.1.1.5 Summary

In summary, the investigation of Richards[1-8] has conclusively proved that the zinc slag fuming process does not operate at internal equilibrium. In addition, a fundamentals based kinetic model of the process has been shown to predict process behaviour at least as well as the thermodynamics based models. The significance of these findings in terms of potential for process improvement and understanding slag reduction in general is profound.

CHAPTER III

OBJECTIVES AND SCOPE OF THE RESEARCH

It is clear from the literature that the zinc slag fuming process is governed by kinetic factors. The work of Richards et al[1a,b] has established conclusively that the process does not operate at internal equilibrium and that coal particles entrained in the slag are the major site for reduction.

The objective of this thesis was to study the effect of increased coal entrainment on process kinetics in an industrial furnace. This was facilitated through the use of a "high-pressure" coal stream distinct from the normal coal supply to the furnace. The data taken during the high-pressure trials was analyzed to establish the efficacy of increased coal entrainment quantitatively.

The overall project can be broken down into three phases. Phase one involves the design and acquisition of a high-pressure coal delivery/injector system which was capable of meeting specified performance criteria for a series of industrial trials. Phase two was comprised of the industrial trials with the high-pressure system. During the high-pressure runs slag composition, bath temperature, furnace operating parameters and high-pressure

coal system operating parameters were recorded in order to measure furnace performance quantitatively. Phase three focused on data analysis and involved modifying the mathematical of Richards et al[1a,b] in order to process furnace data and calculate entrained factors for the high-pressure coal.

It must be emphasized that the financial and human resources available for this project, conducted in an industrial setting, were limited. Thus the scope of the research and the number of trials undertaken were necessarily restricted to that of a preliminary investigation.

CHAPTER IV

EXPERIMENTAL EQUIPMENT AND TECHNIQUES

4.1 Industrial Equipment

The acquisition and design of the high-pressure coal delivery/injection system constituted a major part of the overall project because its successful performance was critical to achieving increased coal entrainment. The following sections present the steps taken for the acquisition and design of the system.

4.1.1 High-Pressure Coal Delivery/Injection System

Because the underlying objective of this series of trials was to increase coal entrainment in the slag significantly and to increase reduction rates, a minimal amount of carrier air was to be used to avoid oxidation of the slag. This was a basic consideration in establishing design criteria.

4.1.1.1 Design Criteria

At first glance, it would appear that the coal-slurry delivery systems would be superior to the pneumatic delivery

systems owing to a lack of gaseous oxygen in the carrier fluid. However, in order to isolate the effect of increased coal entrainment due to high-pressure injection, it was essential to maintain as much similarity as possible to the original work of Richards et al[1a,b] on conventional low-pressure air injection. Therefore considerations were restricted to pneumatic delivery systems and to minimize slag oxidation by air. This established the first overall system design criterion - maximization of coal-to-air loading. Under normal operating conditions coal-to-air loadings are about 0.15 (wt. coal/wt. air) for the No. 2 slag fuming furnace of Cominco.

Injection dynamics also figure importantly in the design. It has been established previously [1a] that in the zinc slag fuming process the gas discharges from the tuyeres as discrete bubbles. It follows then, that under conditions when a bubble is attached to the tuyere, the following events must occur in order for a coal particle exiting the tuyere to become entrained in the slag:

[i] The coal particles must traverse the bubble unconsumed.

[ii] Upon impingement with the slag, the coal particles must have sufficient momentum to overcome the surface tension at the bubble slag interface.

The probability of a coal particle surviving the traverse under

normal operating conditions has been discussed in detail by Richards[1a] and, will not be repeated here.

With respect to improving entrainment, however, it is obvious that gains could be realized through a decrease in the probability of coal particle combustion and/or an increase in the probability of coal particle entrainment. For example, one possible method would be to increase particle exit velocities which has the advantage of both decreasing traverse time and increasing particle momentum. Another approach would be to increase coal particle mass while maintaining velocity. Again this has the advantage of greater survival probabilities and higher particle momentums. As a third alternative some combination could be used.

However, due to practical constraints and the desire to avoid the introduction of an additional variable, it was decided that increasing coal particle size would not be feasible. Therefore, the only viable means of increasing coal entrainment in the study was through the use of high exit velocities. This established the second overall design criterion - maximization of tuyere exit velocity. For reference, under normal operating conditions air volume flow rates and tuyere exit diameters place coal particle exit velocities at between 40-50 m/sec in the No.2 furnace. This is calculated based on the assumption that the

coal particles are travelling 100% of the gas velocity.

Considering these system design criteria further, it is readily apparent that the desire for high stream exit velocities (high volume flow rates) is inconsistent with the desire for high stream coal-to-air loadings (low volume flow rates). The solution to this dilemma is to employ injectors having a small cross-sectional area. Qualitatively, this established the third design criterion - minimization of cross-sectional area of the injector. The standard tuyeres on the No.2 furnace have an I.D. of 38.1 mm (1.53 in.) resulting in a cross-sectional area of 11 cm^2 (1.73 in^2).

Having established the design criteria qualitatively for the injector and delivery system, it is possible to arrive at some quantitative specifications bearing in mind practical limitations of facilities and time. In the initial high-pressure trials it was decided to increase the coal entrainment rate of No.2 furnace by no more than 100%. From the analysis of the Cominco No. 2 furnace by Richards et al [1a,b], the coal entrainment rate for low-pressure injection is roughly 23 kg/min (50 lbs/min). Thus the rated maximum of the high-pressure feed system should be approximately 46 kg/min (100 lbs/min) for continuous coal delivery.

In addition, if the furnace is not well mixed, it would be

necessary to install several high-pressure injectors at different locations, eg. two on either side of the furnace. Hence the injection system had to be sufficiently flexible to facilitate this option.

Intuitively the operating pressure of the delivery system has to be high in order to overcome the large line losses associated with the high injection velocities and high coal-to-air loadings. A practical limit was 690 kN/m^2 (100 psig).

Turning to injector design, the overriding practical considerations were compatibility with the existing tuyere design (the injectors were to be inserted into the furnace through the existing tuyeres), simplicity of design and the availability of construction materials. These requirements were met by using a length of standard straight pipe as an injector, see Fig. 4.1. The upper limit to the inside diameter of the injector was 20.92 mm (0.824 in) based on the maximum diameter pipe which is accepted by the ball valve on the end of the tuyere (3/4 inch nominal, schedule 40S, steel pipe, I.D. = 0.824 in, O.D. = 1.050 in). The lower limit to the injector I.D. was 6.83 mm (0.269 in) which was determined by the smallest pipe available (1/8 inch nominal, schedule 40S, steel pipe, I.D. = 0.269 in, O.D. = 0.405 in). From arguments presented earlier on injector cross-sectional area, however, the smallest diameter injector was needed.

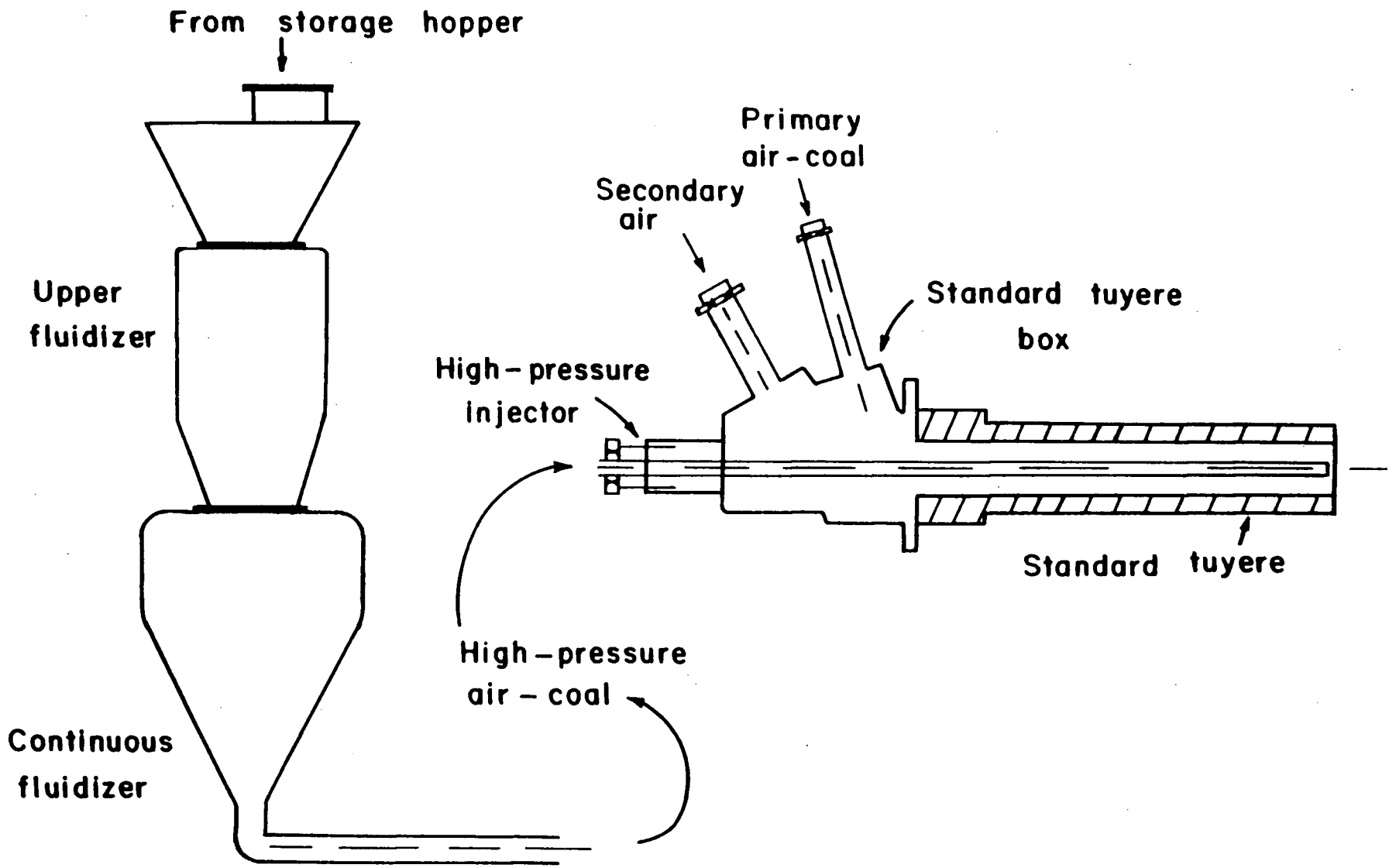

Figure 4.1 Schematic diagram showing the pneumatic conveyor, the high-pressure injector and the standard low-pressure tuyere.

Finally, because the efficacy of increased coal entrainment was to be established, it was essential that the operating parameters, particularly coal rates and air rates, of the high-pressure system be both measured and independently varied. It follows that the operating pressure and/or pressure differentials necessary to achieve these rates also had to be measured.

4.1.1.2 Summary of Design Criteria

In summary, the design and acquisition of the high-pressure coal delivery/injector system was based on the following qualitative design criterion.

[i] Maximization of stream coal to air loading - significantly greater than 0.15 (wt coal/wt air).

[ii] Maximization of injector exit velocities - significantly greater than 40-50 m/sec.

These criteria could be met, within the framework of local constraints by the following specifications for the coal delivery/injection system:

[i] coal feed rate - 45.5 kg/min.

[ii] multiple injector capability

[iii] high-pressure air flow - upper limit approximately 690 kN/m^2

[iv] small injector cross-sectional areas - initial trials with 6.83 mm I.D. pipe

[v] variable operating parameters - coal rates, air rates, and pressures

[vi] measurement of operating parameters - coal rates, air rates, and pressures

4.1.1.3 System Selection

By comparing the design criteria with the literature on solids injection systems (see Chapter II pgs. , particularly Table 2.1), the choice of coal delivery system for the high-pressure trials becomes obvious. It is clear that the blow-tank or air-into-material systems are best suited to meet the requirements of this project because of the highest operating pressures and coal-to-air loadings. Unfortunately, before this project was initiated, the system selection was based more on the overriding economics and a peristaltic-type hose pump was purchased by Cominco Ltd. As an anticipated, the system performance was shown to compromise design objectives to such an extent that it proved unacceptable for the high-pressure trials. Nevertheless, in spite of the overall failure of the hose pump tests, some valuable experience on the transporting of pulverized coal was gained.

Having established that the general classification of pneumatic delivery system would have to be a blow-tank system, it now became a question of specifications verses economics. Again compromises had to be made. Initially there was considerable incentive to build a blow-tank system using surplus equipment and on site personnel. However, because of the lack of suitable pressure vessels and the regulations governing modifications to pressure vessels, it was decided that this route would be too costly and time consuming.

It was determined that the best solution under the circumstances was rental of a blow-tank system, and installation with on site personnel and equipment. Again this was primarily a financial decision. Not surprisingly, the rental system compromised some of the previously established specifications. Of particular concern, for example, was the absence of control over coal-to-air loading, and the lack of ability to measure coal and air delivery rates. In general however, the system, according to specifications was capable of meeting the more critical criteria of delivery capacity and operating pressures.

The performance of the high-pressure pneumatic conveyor essentially dictated the duration and scope of the high-pressure trials. Thus it is felt that some detailed discussion of the operation of this system would be valuable.

4.1.1.4 The High-Pressure Delivery System: Operation

The pneumatic conveyor essentially consisted of two pressure vessels mounted vertically, one on top of the other, see Fig. 4.2. The lower pressure vessel or continuous fluidizer, continuously delivered material at a relatively constant pressure. Continuous operation is achieved by periodically cycling the upper fluidizer between atmospheric pressure (where it is charged with the material to be conveyed) and a pressure slightly above that of the continuous fluidizer (where it charges the continuous fluidizer). By adjusting the rate at which the upper fluidizer cycles according to the rate of which material is being conveyed, it is possible to maintain continuous delivery.

Starting at time t=0 with the delivery system empty and at atmospheric pressure, it is possible to break down a complete cycle into the following steps (see Fig. 4.2 for reference):

[i] t=0; The air to the upper fluidizer is switched on (Valve No. 6) and at the same time the dome valve (No. 5) moves up and is closed. The pressure in the lower fluidizer begins to increase until it reaches P_1, the delivery pressure - air is being conveyed.

[ii] $t=t_1$; The butterfly valve (No. 1) opens and pulverized coal falls under gravity from a storage hopper through the conveyor feed funnel into the upper fluidizer.

[iii] $t=t_2$; The butterfly valve closes - the upper fluidizer is full.

[iv] $t=t_3$; The air to the upper fluidizer is switched on (Valve No. 3) and simultaneously the dome valve (No. 2) closes - the pressure in the upper fluidizer begins to increase. When the pressure has reached approximately P_1, the dome value (No. 5) opens. The pressure in the upper fluidizer continues to rise until it reaches P_2 (several psi greater than P_1) - material is being conveyed to the lower fluidizer. At approximately the same time material begins to be conveyed from the lower fluidizer.

[v] $t=t_4$; The air to the upper fluidizer is switched off (Valve No. 3) and simultaneously the vent valve (No. 4) opens. Almost immediately dome valve (No. 5) closes. The pressure in the upper fluidizer drops to atmospheric and the dome valve (No. 2)

opens. The continuous fluidizer is now approximately half full and continues to convey material at P_1.

[vi] $t=t_5$; The butterfly valve (No.1) opens and the cycle is repeated as from time $t=t_1$.

From a localized control panel the operator has control over upper and continuous fluidizer pressures, P_2 and P_1 respectively, the timers which dictate $t_2 - t_1$ (butterfly valve open or charge time), $t_4 - t_3$ (upper fluidizer air on time) and, $t_5 - t_4$ (time to cycle repeat).

With respect to injection dynamics, it is interesting to note that there is a slight variation in conveying pressure and coal-to-air loading over the course of a complete cycle. This behaviour is a consequence of the mechanics of the cycle. In particular, the variation in conveying pressure and coal-to-air loading that are associated with switching the conveying air from P_1 to P_2 during those periods when the upper fluidizer air is on and is effectively the source of conveying air.

In order to measure high-pressure air and coal rates, which is fundamental to the objectives of this project, it was necessary to instrument the rental delivery system without modifying it. With respect to coal rate measurement, this was achieved by placing a small intermediate feed hopper on a 0 -

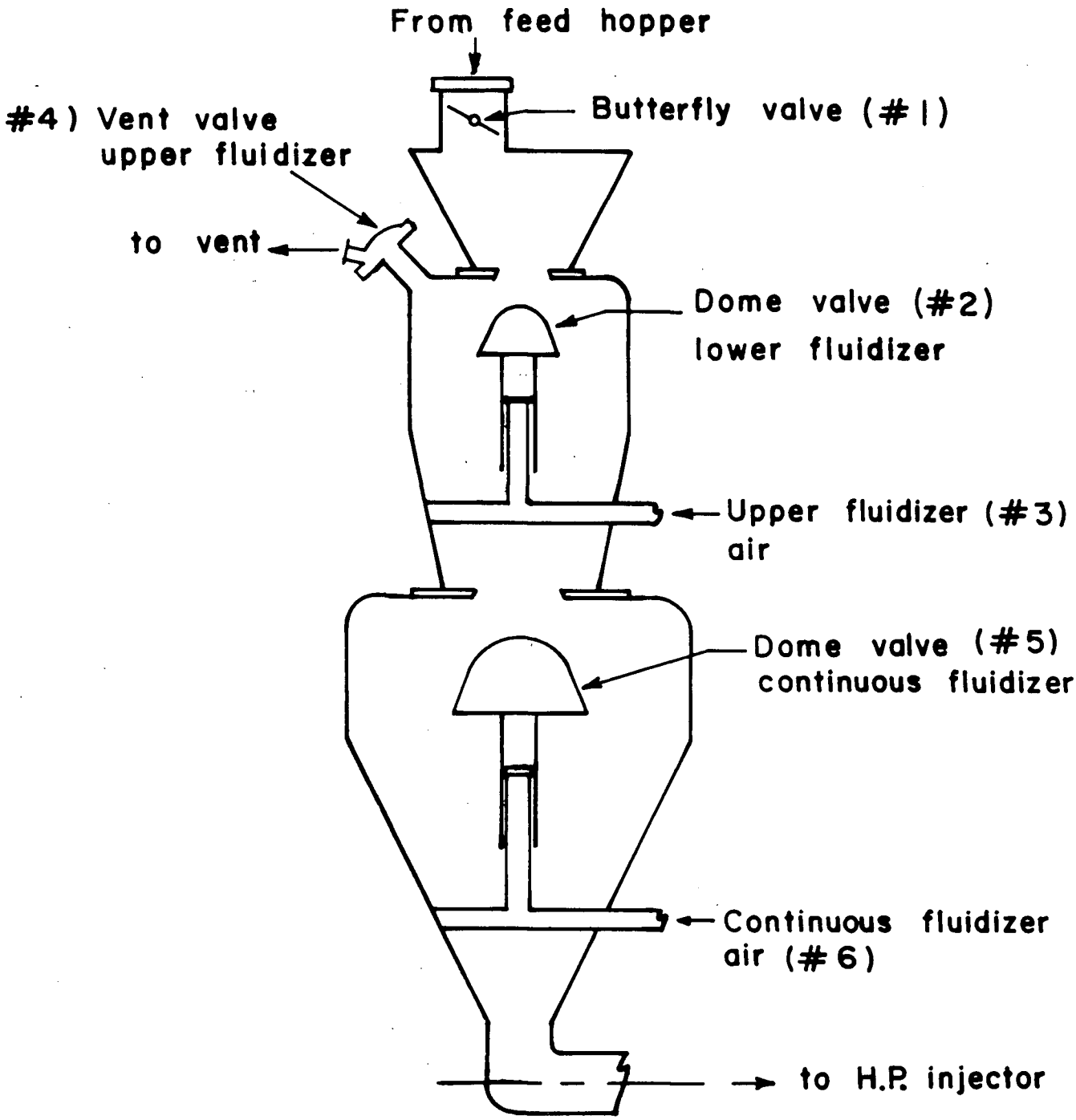

Figure 4.2 Schematic diagram showing the pneumatic conveyor in detail

227.3 kg (0-500 lb) tension load cell to measure the coal charged each cycle (t_2-t_1). Coal vented from the upper fluidizer (at t_5) was captured in a modified forty-five gallon drum. This was necessary because the rental system had a tendency to vent pulverized coal through valve No. 4, see Fig. 4.2, when the upper fluidizer was depressurized. By measuring the amount of coal charged to the delivery system and the amount of coal vented, the net amount reporting to the furnace could be determined. The total high-pressure air flow rate to the delivery system was measured with a 0 - 2.83 Nm^3 /min (0 - 100 Scfm) orifice flow meter (Ori-Flow Meter, Tokyo Keiso Ltd.).

High-pressure air to the delivery system was supplied by a 11.3 Nm^3/min (400 Scfm) portable diesel compressor. This proved to be the only means of attaining a reliable source of 690 kN/m^2 (100 psig) air. Unfortunately, moisture levels in the air supply were high and eventually necessitated the use of a 11.3 Nm^3/min (400 Scfm) in line water trap.

The pulverized coal from the Cominco storage hopper was passed through a 2 mm (0.08 inch) screen prior to entering the intermediate feed hopper and charging to the delivery system. This was necessary due to the presence of large lumps in the pulverized coal which could not be tolerated by the small diameter high-pressure injector.

The transport pipe consisted of two sections of 31.75 mm (1.25 inch) I.D. drawn-over-mandrel steel tubing, approximately 8 m (26 feet) in total length, and a small section of flexible 25.4 mm (1 inch) I.D. rubber hose, approximately 1.2 m (4 feet) in length. In addition, three 90^{o}, high-wear, material-on-material elbows were employed. The flexible rubber hose was used prior to coupling with the high pressure injector to facilitate rapid installation and removal of the injector assembly.

4.2 Experimental Techniques

As discussed, the underlying objective of this project was to establish the efficacy of increased coal entrainment quantitatively. In order to achieve this, specific information on furnace behaviour as function of operating conditions during the high-pressure trials must be obtained. The following sections discuss the experimental techniques used to obtain this industrial data.

4.2.1 Industrial Tests

It was decided that in the initial trials, the high-pressure coal would be introduced part of the way through a "normal fuming cycle", and that simultaneously with the onset of high-pressure injection, the normal low-pressure coal rate would be reduced by

an amount approximately equivalent to the high-pressure coal injection rate. It was reasoned that this procedure would best reveal the effect of increased coal entrainment. Furthermore, it was also decided that only one high-pressure injector would be used in these trials because this would allow valuable experience to be gained, both in terms of furnace behaviour and high-pressure system operation.

Since the zinc slag fuming process operates on a batch basis, the effect of increased coal entrainment on furnace behaviour can be determined from the manner in which the slag composition changes as a function of the high and low-pressure coal and air rates.

4.2.1.1 Slag Sampling

Of particular interest in the trials were the rates of change of zinc, lead, ferrous and ferric iron composition and bath temperature. To obtain information on slag composition, a technique employed previously by Richards [1a] was adopted. A 1.5 m (4.95 ft) bar was inserted into the slag through a tuyere then was withdrawn 3 - 4 seconds later and quenched with water.

To ascertain the degree of longitudinal bath mixing, the effect of injecting the high-pressure coal in a localized area was measured by taking two slag samples simultaneously; one in

the vicinity of the high-pressure injector and the other as far removed from it as possible. This procedure was followed only during the initial run. In subsequent tests, all slag samples were taken from tuyeres located directly opposite from the high-pressure injector.

Under normal operating conditions the temperature in Cominco Ltd.'s No. 2 slag furnace is monitored continuously with a thermocouple placed in the slag through a non-operational tuyere. For the high-pressure coal runs this temperature data was retrieved from the charts on which it was routinely recorded.

Furnace charge details, in particular total weight and constitution with respect to hot and cold additions, were obtained from plant personnel.

4.2.1.2 Operating Procedures

Two sets of operating parameters had to be recorded over the course of a high-pressure run. The first group encompassed the measurement of the standard furnace operating parameters which include the normal low-pressure coal rate and the low-pressure air-blast volume flow rates. In order to measure the normal coal rate, the No. 2 furnace Omega coal feeder had to be calibrated. This was achieved by recording feeder belt current (measured in percent) over measured time intervals starting with a full

storage hopper. The amount of coal needed to refill the hopper then was measured. Once calibrated, a record was kept of No. 2 Omega feeder settings for the high-pressure runs and these were converted to coal rates. Blast volume flow rates are recorded under normal operating conditions.

The second set of operating conditions pertained to the high-pressure coal delivery system which included coal and air injection rates and pressures. High-pressure coal rates, as mentioned, were determined by measuring the amount of material charged to the delivery system and the amount of coal vented from it as described earlier. The instrumented intermediate hopper was filled from the larger Cominco storage hopper during those periods when the delivery system was not charging. After filling, the intermediate hopper then was used to charge the delivery system. This procedure was repeated for every cycle. The output from the load cell on the intermediate hopper was recorded on a strip chart recorder. The amount of coal vented from the delivery system per cycle was collected and also recorded. From the load cell output the total amount charged to the delivery system over the course of high-pressure run could be determined. The difference between this amount and the amount vented then could be divided by the length of the run to determine the average high-pressure coal injection rate. The average amount of high-pressure conveying air injected into the furnace with the coal was assumed to be equal to the high-

pressure air flow rate measured during a period when only the continuous fluidizer air supply was on (t_5-t_4), see Section 4.1.1.4.

4.2.1.3 Summary: Industrial Testing Procedure

The procedure during a high-pressure coal run can be summarized as follows:

[i] After the furnace had been fully charged and allowed to reach a temperature of 1280-1300^{o} C, normal fuming operation was started. Slag sampling was carried out every 5-10 minutes.

[ii] After 15-20 minutes of normal fuming, high-pressure coal was injected. Simultaneously, the low-pressure coal rate was reduced and the slag subsequently sampled every 5 minutes.

[iii] Following the termination of high-pressure coal injection, the slag was sampled for a period of 10-15 minutes.

[iv] All pertinent operating data was collected.

Unfortunately, failure of the high-pressure coal delivery system generally dictated the length of the high-pressure runs.

4.2.2 Chemical Analysis of Slag Samples

Chemical analysis of the slag samples was performed by the assay labs of Cominco. Assays for all metals (Zn, Pb, Fe), oxides (CaO, SiO_2, Al_2O_3) and non-metal (S) were done by X-ray emission spectrography. Analysis for ferrous iron was carried out by a wet chemical oxidative technique using potassium dicromate. The procedure is summarized elsewhere. [1a]

Ferric iron reported in this thesis is the difference between total iron determined by X-ray analysis and ferrous iron determined by wet chemistry. The effect of slag sulphide iron on the ferrous iron assay has been investigated elsewhere. [1a] Ferrous iron assays reported in this thesis are assumed not to require correction for sulphur.

4.2.3 Uncertainty

The uncertainty in slag assays has been estimated by Richards[1a] through a process of submitting sixteen duplicate samples for analysis at the Cominco assay laboratory. It is assumed that laboratory procedures and equipment have not changed appreciably and therefore that the uncertainties for the assays presented in this thesis are the same as those found by Richards, see Table 4.1.

TABLE 4.1

Estimated Uncertainty of Analysis

	Average Absolute Difference	Average Relative Difference	Estimated Uncertainty
Zn	0.25 pct	7.8 pct	± 4 pct
SiO_2	3.00 pct	10.0 pct	± 5 pct
CaO	0.74 pct	4.1 pct	± 2 pct
Fe	0.74 pct	2.6 pct	± 1.3 pct
Fe^{2+}	0.39 pct	1.9 pct	± 1 pct
Fe^{3+}	0.71 pct	34.0 pct	± 17 pct

CHAPTER V

EXPERIMENTAL RESULTS AND PRELIMINARY ANALYSIS

Problems with the high-pressure delivery system limited the number of trials to three runs with a single injector. The results from these runs will be discussed in the following chapter.

5.1 Results

Assays of the slag samples and operating conditions for the three high-pressure runs are presented in Figs. 5.1 - 5.12 and are tabulated in Appendix I.

It should be noted that problems with the high-pressure coal supply were encountered in two of the three trials. The length of the period of high-pressure injection in Runs 2 and 3 was cut short by delivery system failure. Fortunately, operating parameters remained within acceptable limits until failure occurred.

5.2 Preliminary Analysis and Discussion

Before the effect of high-pressure coal injection on furnace performance can be discussed it is necessary to evaluate the

high-pressure injection dynamics to establish if improvements in key parameters have in fact been achieved. Of primary importance are the magnitudes of high-pressure injector exit velocity and stream coal-to-air loading.

5.2.1 High-Pressure Injection Dynamics

High-pressure coal-to-air loadings and stream exit velocities have been estimated for three high-pressure runs and are presented in Table 5.1. Loadings and velocities typical of the standard low-pressure tuyeres used in the Cominco No. 2 fuming furnace also are presented in Table 5.1 for comparison. High-pressure injector loadings are expressed in terms of weight of coal conveyed per weight of conveying air. Stream exit velocities were calculated assuming the coal to be travelling at the air velocity.

The resulting increases in stream exit momentum per unit area for the high-pressure tuyere relative to the standard low-pressure tuyeres have been calculated for the three high-pressure runs and are included in Table 5.1. Based on the magnitude of the momentum increases (factor of 171 for Run 1, 249 for Runs 2 and 222 for Run 3), it is evident that a considerable gain in the driving force for slag entrainment (momentum) has been achieved with the high-pressure injector.

TABLE 5.1

High-Pressure Injection Dynamics

Run No.	Coal rate (kg/min)	Air rate (Nm^3/min)	Coal to (wt./wt.)	Estimated coal exit velocity (m/s)	*Estimated momentum increase
Run 1	12	0.37	25	~114	~171x
Run 2	18	0.37	36	~116	~249x
Run 3	16	0.37	32	~115	~222x
Normal Operation (low pressure tuyere)	/	/	0.16	~42	/

*These numbers represent an estimate for the increase in momentum per unit area for the high-pressure injector relative to the standard low-pressure tuyeres.

Having established that the injection dynamics are consistent with the original objectives, the question of assessing the effect of high-pressure injection on furnace performance can now be addressed. At the onset of the project it was realized that this would not be an easy task. In particular, there is a problem associated with defining "normal" furnace performance against which the high-pressure runs can be compared.

Originally, this problem was to be avoided by introducing the high-pressure coal part of the way through the proper fuming stage of the fuming cycle (see Chapter IV for outline of this procedure). By adopting this procedure it was reasoned that a direct comparison between furnace performance during normal operation and high-pressure injection could be made on a run by run basis. The comparison simply would be an exercise of calculating the corresponding fuming rates (% Zn per min) and efficiencies (kg zinc fumed per kg coal injected) which are normally used to measure furnace performance.

Unfortunately, practical constrains prevented this procedure from being fully implemented. As a result, normal fuming operation and performance must be carefully defined to permit a valid comparison to be made.

5.2.2 Normal Fuming Practice at Cominco

At the Trail Smelter of Cominco under "normal" conditions (see Appendix I, Table I for approximate slag composition with respect to Pb, Fe^{2+}, Fe^{3+}, CaO and SiO_2), the fuming cycle can be broken down into two stages, as previously described in Chapter I. During Stage 1, the heating period, the secondary blast rate and coal rate are generally in the range of 340-400 Nm^3/min (12,000-14,000 Scfm), and 46-55 kg/min (100-120 lbs/min), respectively. Typically, this stage ends when the bath temperature reaches 1300-1325^{o}C.

Not surprisingly, the length of the heating period is very dependent on the charge constitution with respect to hot and cold additions. For example, under conditions when there is a 100% hot charge, this period may last 15-20 minutes, whereas for a 50:50 hot-cold charge, the period may last upward of 75 minutes- half a normal fuming cycle. In this situation, cold granulated slag may be continually charged to the furnace over the course of the heating period. Bath zinc concentrations at the end of the heating period are typically 16-14 wt%. However, when the heating period is long, concentrations may fall to 8-10 wt%.

At the onset of the second stage, proper fuming, the secondary blast rate is fixed at 340 Nm^3/min (12,000 Scfm) and the coal rate is raised to between 64 and 68 kg/min (140-150

lbs/min). During this stage, for a 100% hot charge, fuming rates are typically about 0.082 % Zn/min. and efficiencies are approximately 0.7 kg Zn/kg coal (values are an average based on one month of operation for 100% hot charges only, and were calculated from the zinc assays; zinc fuming efficiencies were calculated assuming a constant initial bath weight).

It should be noted that fuming rates and efficiencies calculated in this manner appear to be sensitive to the temperature of the charge. For example, for charges consisting of 30% and 50% cold material, the fuming rate falls to 0.067 and 0.055 % Zn/min. and efficiencies fall to 0.55 and 0.48 kg zinc/kg coal respectively. As the proportion of cold material charged to the furnace increases, the calculated fuming rate and efficiency decrease. This effect is believed to be due to the manner in which these quantities are calculated. Clearly, if any solid (cold) zinc-rich material melts during the fuming period, it will tend to influence the slag assay because its zinc content is greater than that of the bulk of the bath. The net result will be an increase in the zinc concentration of the bath and a decrease in the fuming rate and efficiency based on zinc assays. The same should also hold for lead if the melting material is rich in lead.

Taken one step further, this implies that the actual fuming rate (kg zinc reporting to fume) and fuming efficiency (kg zinc

reporting to fume/kg coal injected) during the period of proper fuming should be insensitive to charge temperature for a given set of operating conditions. This behaviour is more in accordance with what would be expected.

As a final note, based on the preceding discussion it appears necessary to include information on charge temperature prior to quantifying normal furnace performance.

Having established normal operation and performance for the Cominco No. 2 fuming furnace, it is possible to proceed with the preliminary analysis of the high-pressure runs.

5.2.3 High-Pressure Coal Injection Preliminary Analysis

In Run 1, the charge to the furnace was 50,909 kg (56 tons), and consisted of 50% hot slag and 50% cold crushed material. As anticipated, this resulted in a prolonged heating period and a low bath zinc concentration (approximately 9 wt %) at the onset of the proper or normal fuming period. Of particular concern, however, is the effect that the charge temperature had on fuming rate and efficiency. This must be considered when interpreting the results.

Analysis of Run 1 is complicated further by difficulties which were experienced with charging the high-pressure delivery

system in the initial stages of high-pressure injection. As a result, from 15 to 25 minutes elapsed time, the total coal rate to the furnace (low-pressure plus high-pressure) ranged between 4.5 and 9 kg/min. (10-20 lbs/min) less than normal for the fuming stage, see Fig. 5.4. In addition, because the bath temperature leveled off during this period, the low-pressure coal rate was raised to 61.4 kg/min (135 lbs/min) for approximately five minutes.

The simultaneous effect of all of these factors complicates interpretation of the results in Run 1. Qualitatively, there does not appear to be any consistent increase in either the zinc or lead elimination rates with the onset of high-pressure injection, see Fig. 5.1. It is worth noting, however, that the maximum rate of decrease of zinc concentration coincides exactly with the point at which steady state high-pressure injection was achieved.

If the ferric and ferrous iron assays are considered, see Fig. 5.2, the effect of high-pressure coal injection is more clearly seen. There is a general increase in the ferrous iron level and a corresponding decrease in ferric level coincident with steady high-pressure injection. This behaviour is consistent with increased coal entrainment and more reducing conditions in the slag.

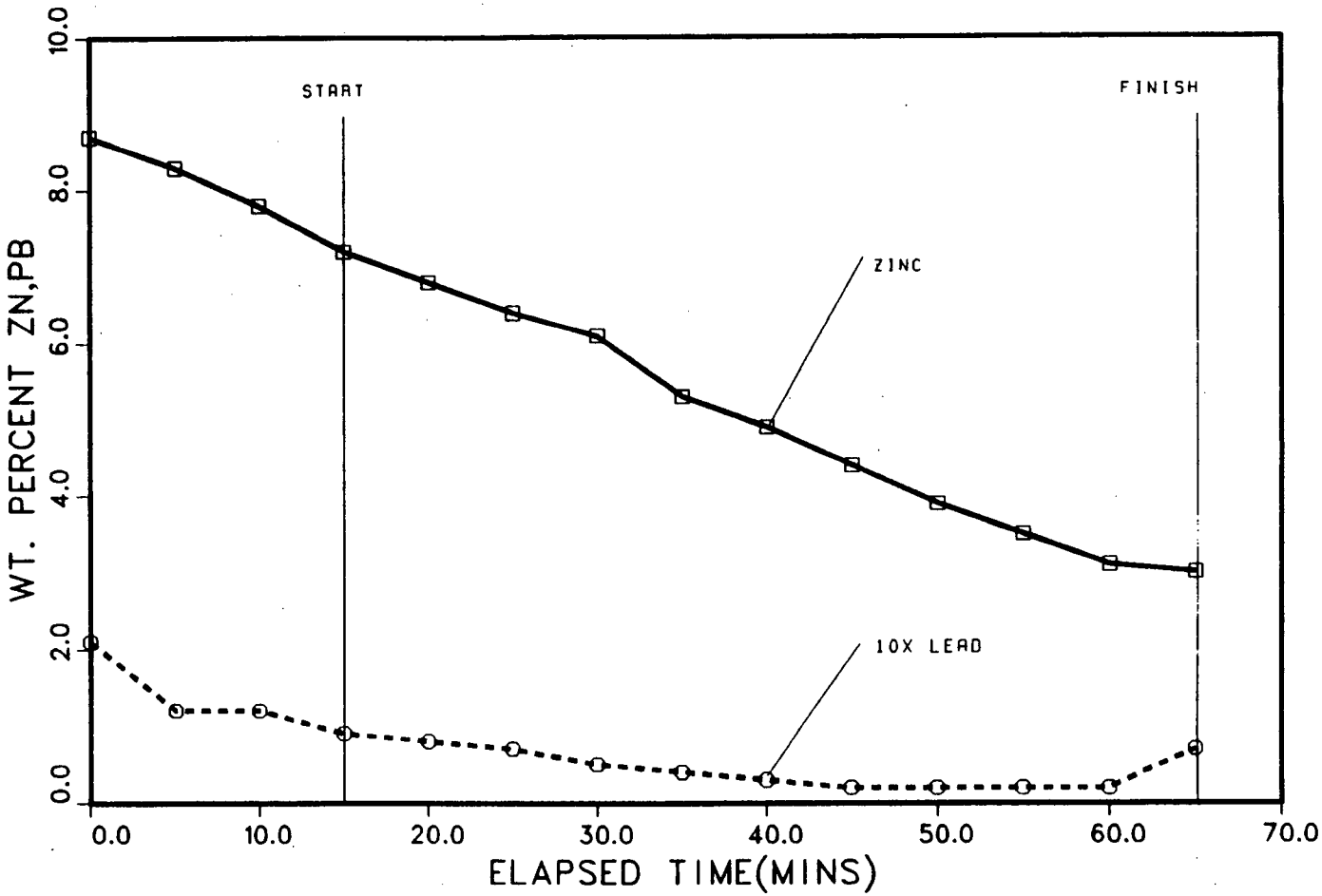

Figure 5.1 Zn and Pb profiles for Run 1

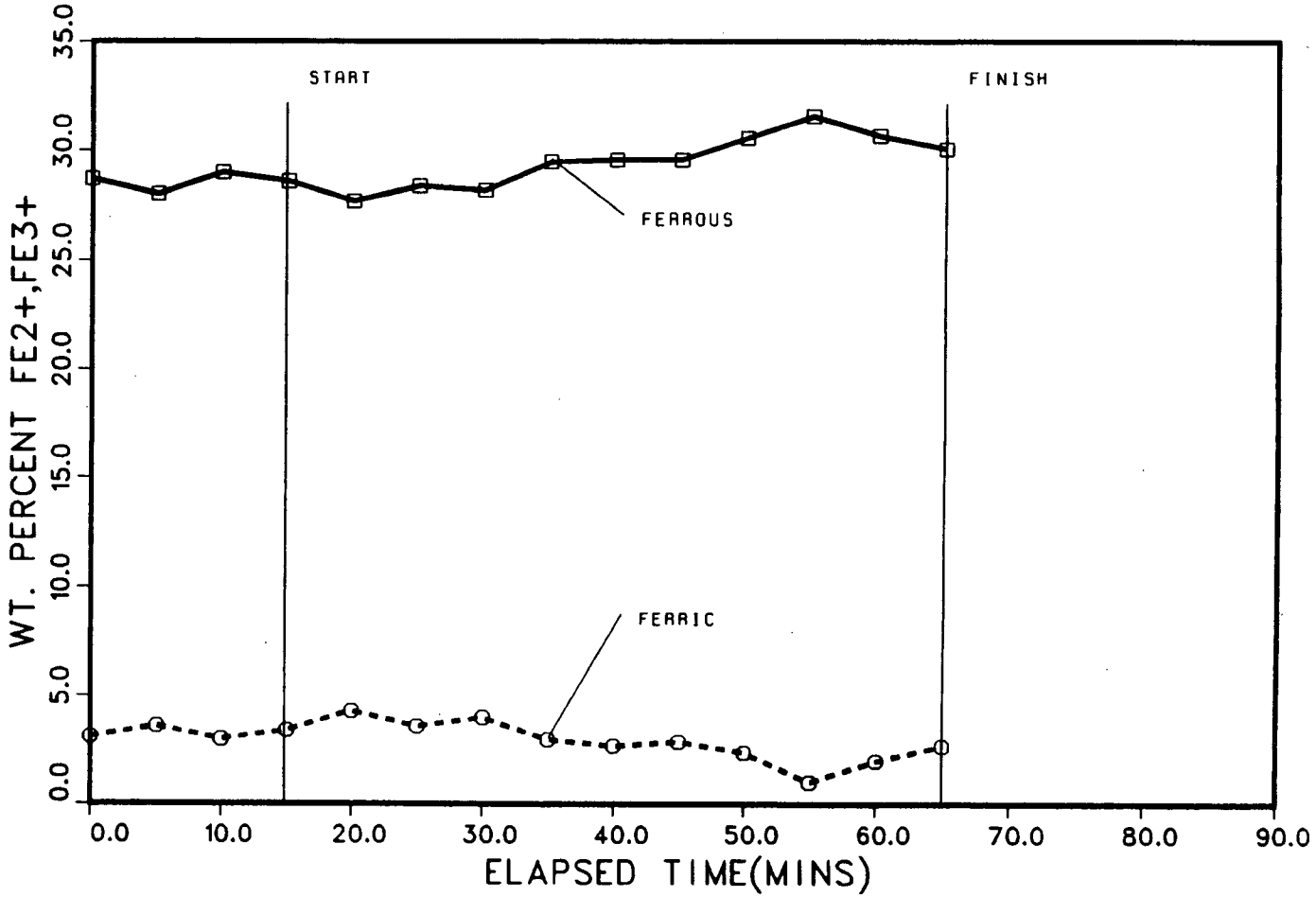

Figure 5.2 Fe^{2+} and Fe^{3+} profiles for Run 1

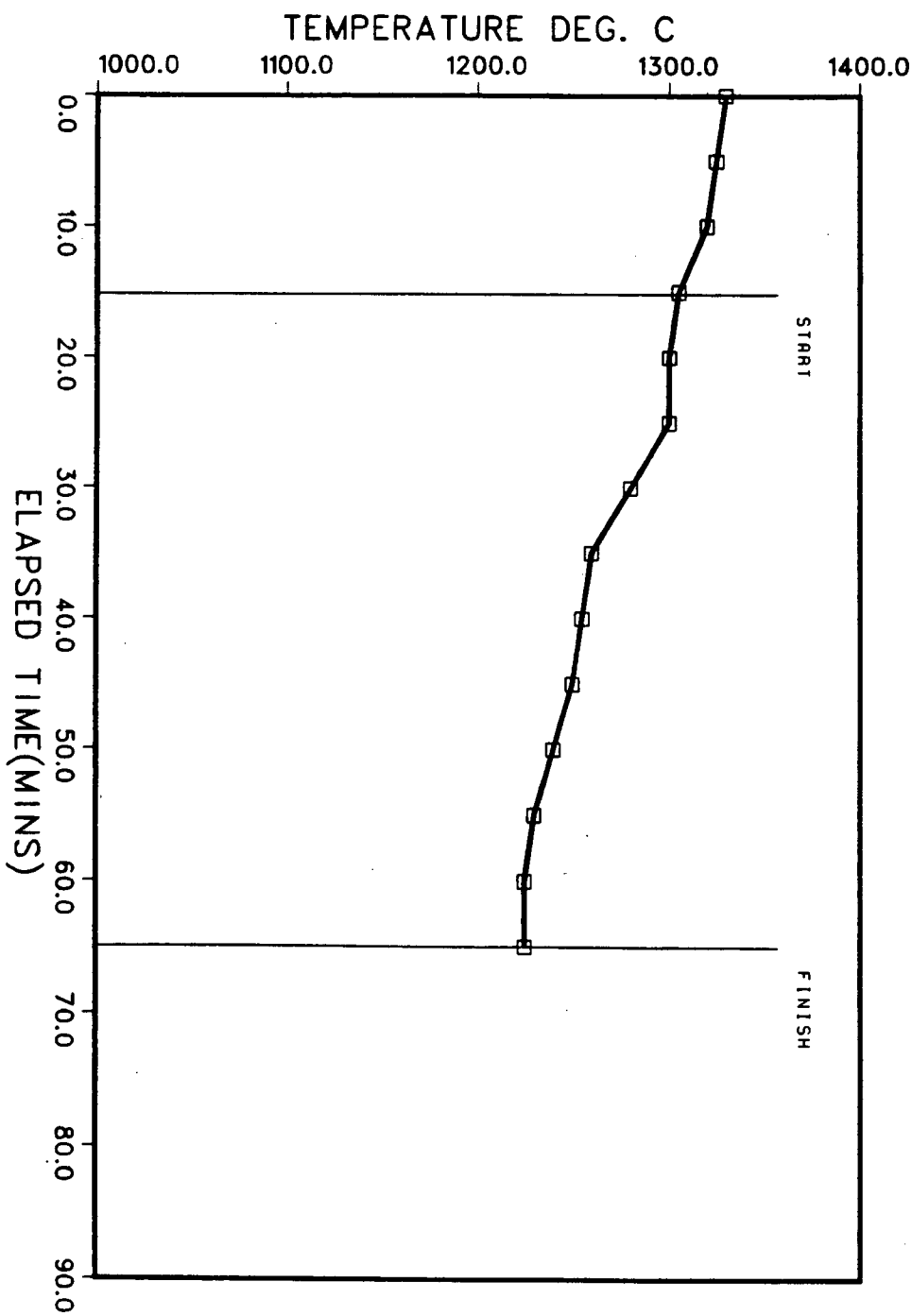

Figure 5.3 Temperature profile for Run 1

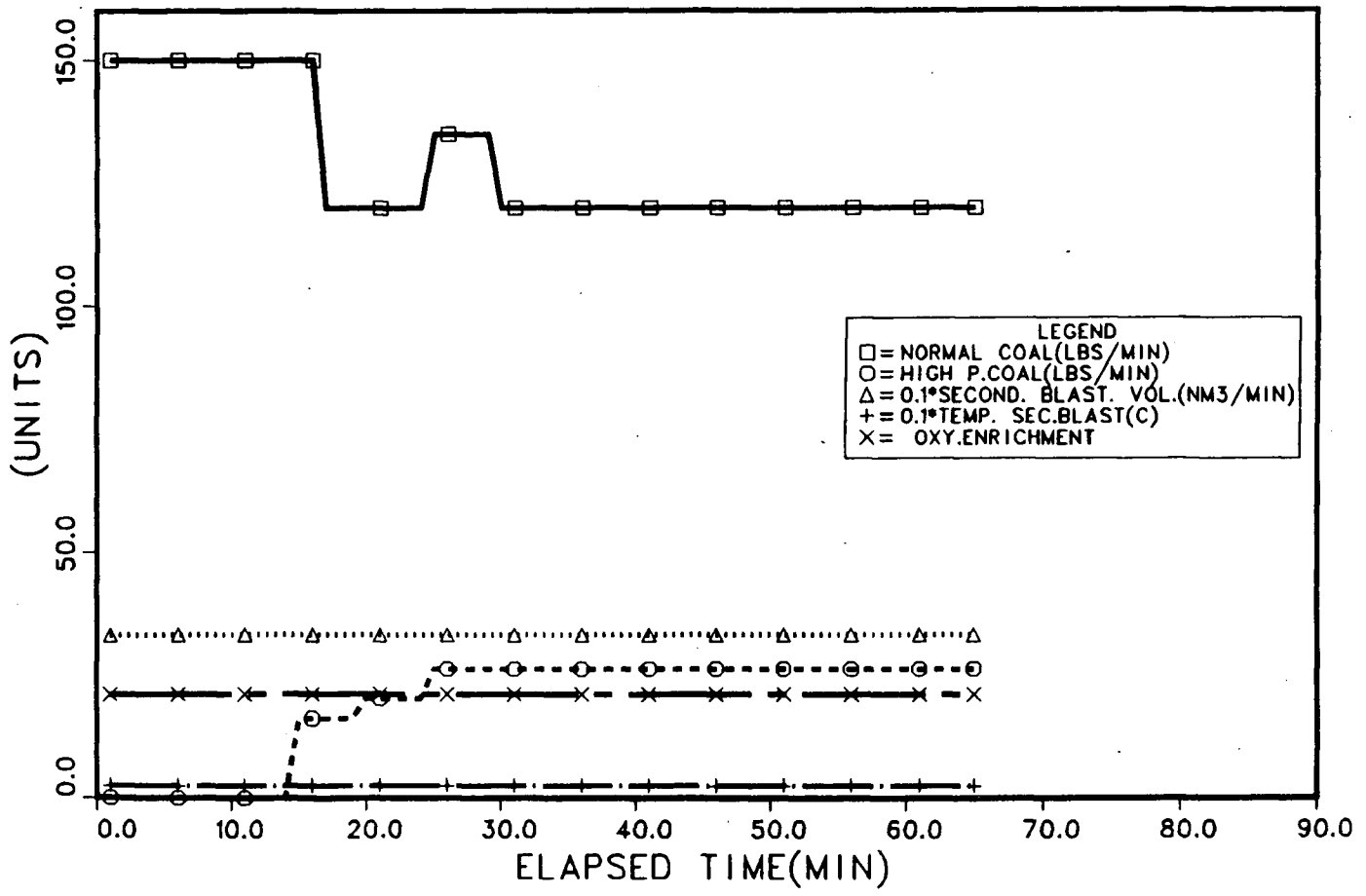

Figure 5.4 Furnace operating conditions for Run 1

The temperature profile, see Fig. 5.3, exhibits a roughly continuous decline during high-pressure injection. It should be noted that the maximum rate of temperature drop coincided with the short term increase in the low-pressure coal rate and not with the period of maximum zinc decrease.

In quantitative terms, a fuming rate and efficiency have been calculated for the period of steady-state, high-pressure injection (30-65 minutes elapsed time) in Run 1, see Table 5.2. These values can be compared with the average fuming rate and efficiency for a 50:50 hot-cold charge - also shown in Table 5.2. From this comparison it is clear that substantial improvements have been achieved with high-pressure injection (factor of 1.69 increase in fuming rate and 1.68 increase in fuming efficiency).

It should be noted that the results of the double sample tests (procedure described earlier in Chapter IV) indicate that there is a high degree of longitudinal bath mixing. The differences in the zinc concentrations of the double samples (see Appendix I, Table 1) are within $\pm$0.04 weight percent. Therefore, it can be concluded that the slag samples taken in the vicinity of the high-pressure tuyere are representative of the entire bath composition.

It is worth mentioning that in Fig. 5.1 there is some evidence to suggest that the melting of zinc a lead-rich

TABLE 5.2

Fuming Rates and Efficiencies

Run No.	Fuming rate	Fuming efficiency	*Estimated increase in fuming rate	*Estimated increase in fuming efficiency	Predicted fuming efficiency
	%Zn / min	kg.Zn / kg.coal			kg.Zn+kg.Pb / kg.coal
Run 1	0.10	0.635	~1.69x	~1.68x	0.77 **0.92
Run 2	0.124	1.02	~1.85x	~1.86x	1.2
Run 3	0.150	1.27	~1.85x	~1.89x	1.4

* These numbers represent increases in fuming rate relative to normal furnace performance.

** This value was obtained from the model using a term to account for the melting of zinc-rich material.

material was occurring throughout the run. In particular, there is a noticeable decrease in the zinc and lead elimination rates toward the end of the run which was unaccompanied by a change in the furnace operating parameters. With regard to the behaviour of lead, there is some justification for questioning the validity of this result in light of the relative uncertainties in assay results at the low concentrations involved. Nevertheless, both of these observations are consistent with the addition of zinc and lead to the bulk of the bath, and therefore, the melting of zinc and lead-rich material.

As a final note, steam generation in No. 2 boiler increased substantially during high-pressure injection in Run 1. In fact, levels increased to the point where they exceeded the rated maximum of the boiler. It was postulated that this was due to the high-fuming rates and/or excessive amounts of high-pressure coal stripping through the bath and combusting in the boiler. Therefore, it was decided that low-pressure coal rates would have to be lower during high-pressure injection in subsequent runs.

In Run 2, the charge to the furnace was 52,727 kg. (58 tons) and consisted of 70% hot slag and 30% hot pot shell. Not surprisingly, this charge required a relatively short heating period and as a result, bath zinc concentrations were relatively high - approximately 16 wt% at the onset of the fuming period. This made Run 2 particularly well suited for testing the high-

pressure injection.

Unfortunately, problems with interpretation of the results still prevailed. In this run, the problem was associated with the magnitude of the coal rate during the period of normal fuming preceding the start of high-pressure injection, see Fig. 5.8. Although not considered to be oxidizing, the low-pressure coal rate was definitely low in comparison with those more representative of normal fuming practice. As a result, furnace performance during high-pressure injection could not be compared quantitatively to the initial period of low-pressure fuming. It is interesting to note that this problem was a direct result of the more conservative approach taken by plant operators in response to the problems with excessive steam generation in Run 1.

Qualitatively, in Run 2 there was a considerable increase in the elimination rates of both zinc and lead with the onset of high-pressure coal injection, see Fig. 5.5. This is particularly evident with respect to the behaviour of lead. In contrast, if the behaviour of the ferric - ferrous couple is considered, see Fig. 5.6, there appears to be a slight decrease in the generation rate of ferrous iron with high-pressure injection. This is in direct contradiction with the behaviour observed in Run 1, and appears to be inconsistent with conditions becoming more reducing in the slag. Interestingly, the difference in low-pressure coal

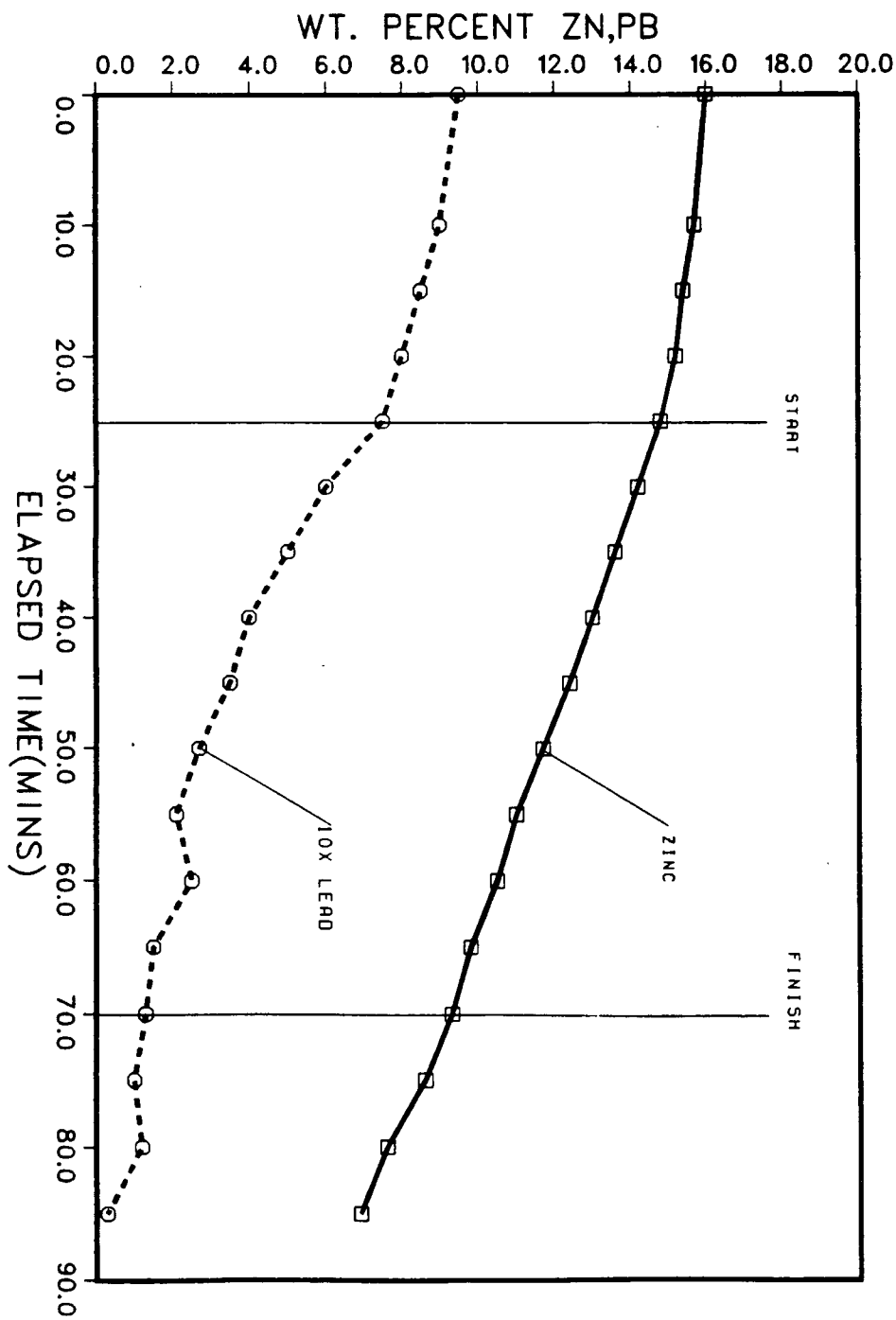

Figure 5.5 Zn and Pb profiles for Run 2

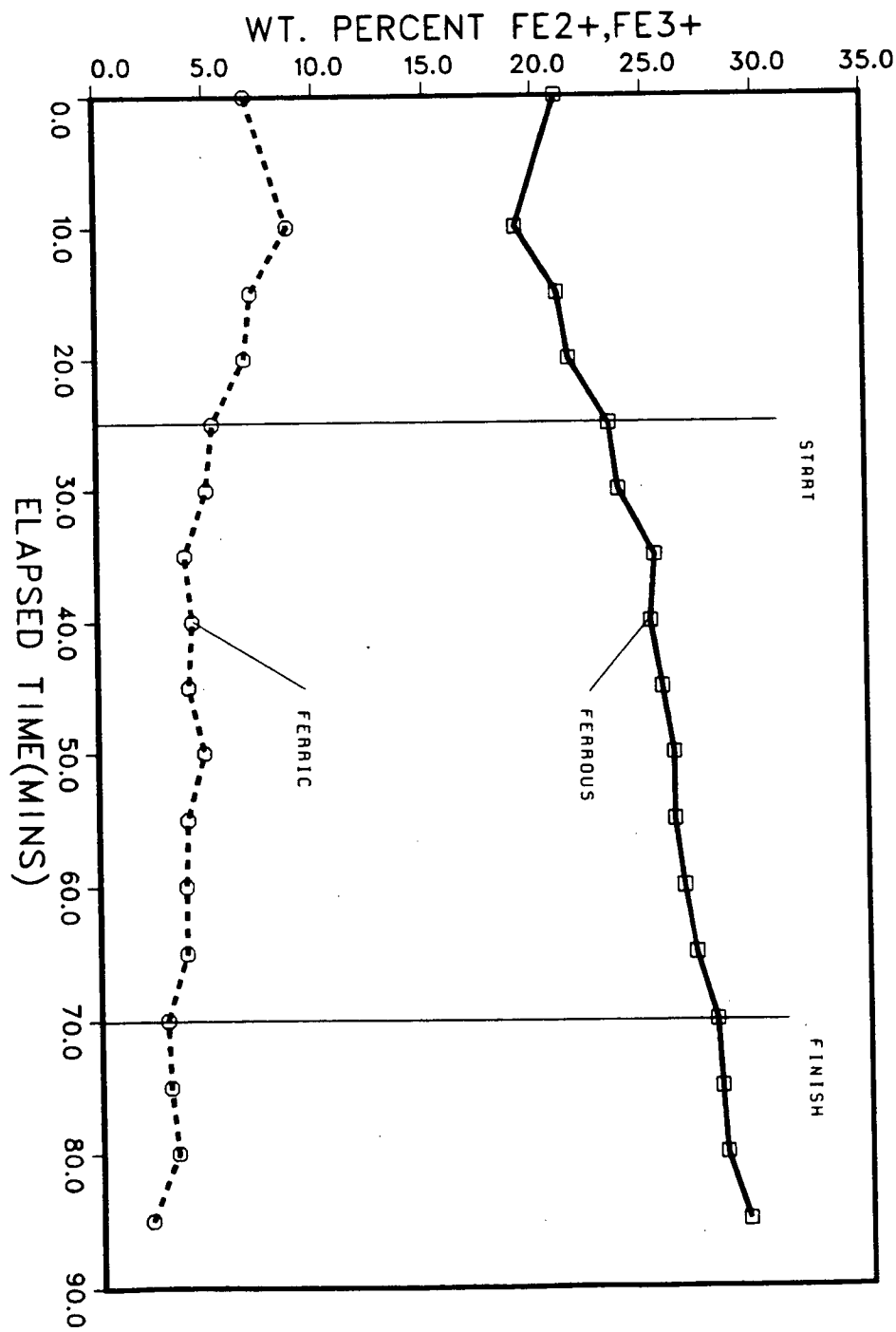

Figure 5.6 Fe^{2+} and Fe^{3+} profiles for Run 2

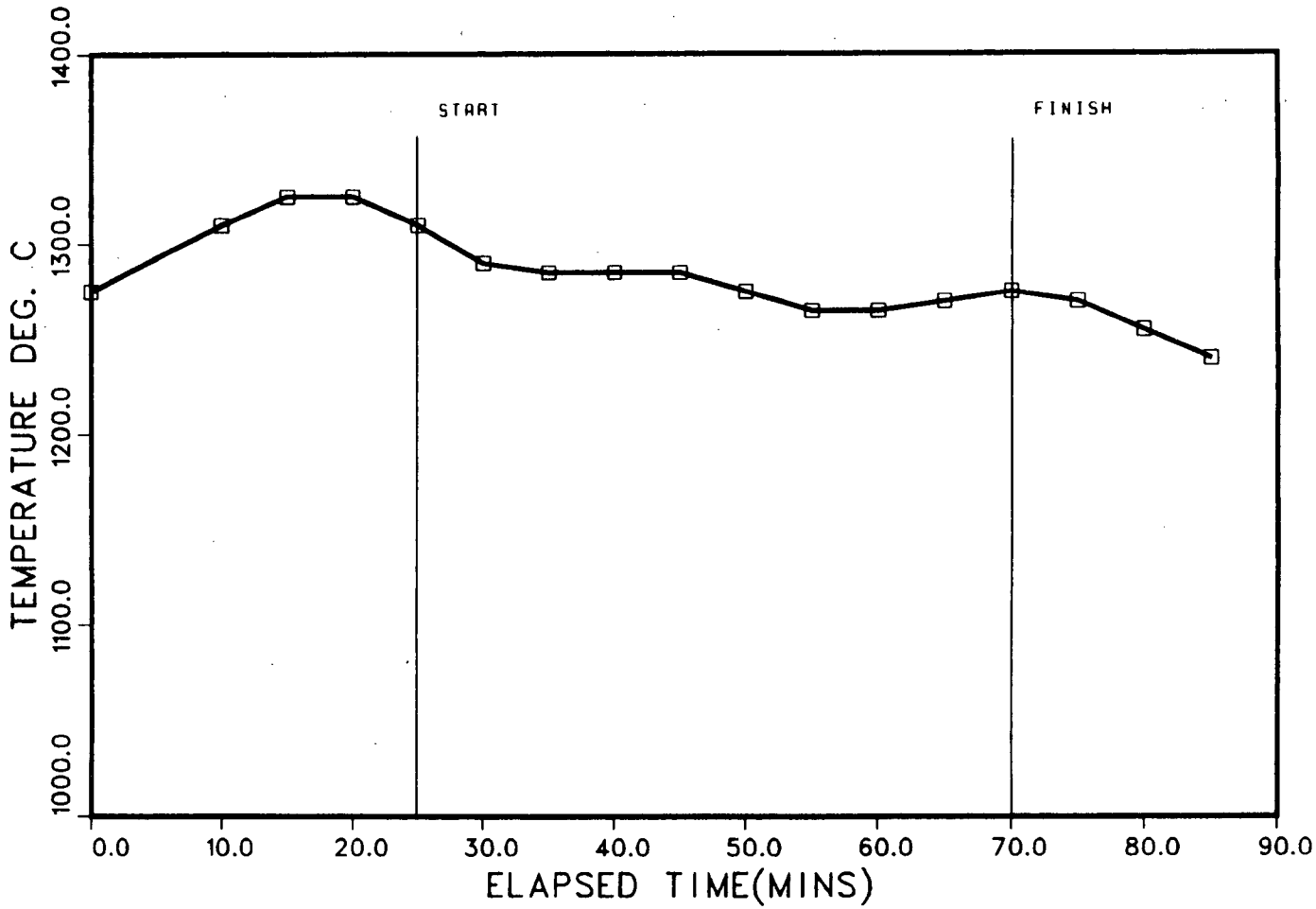

Figure 5.7 **Temperature profile for Run 2**

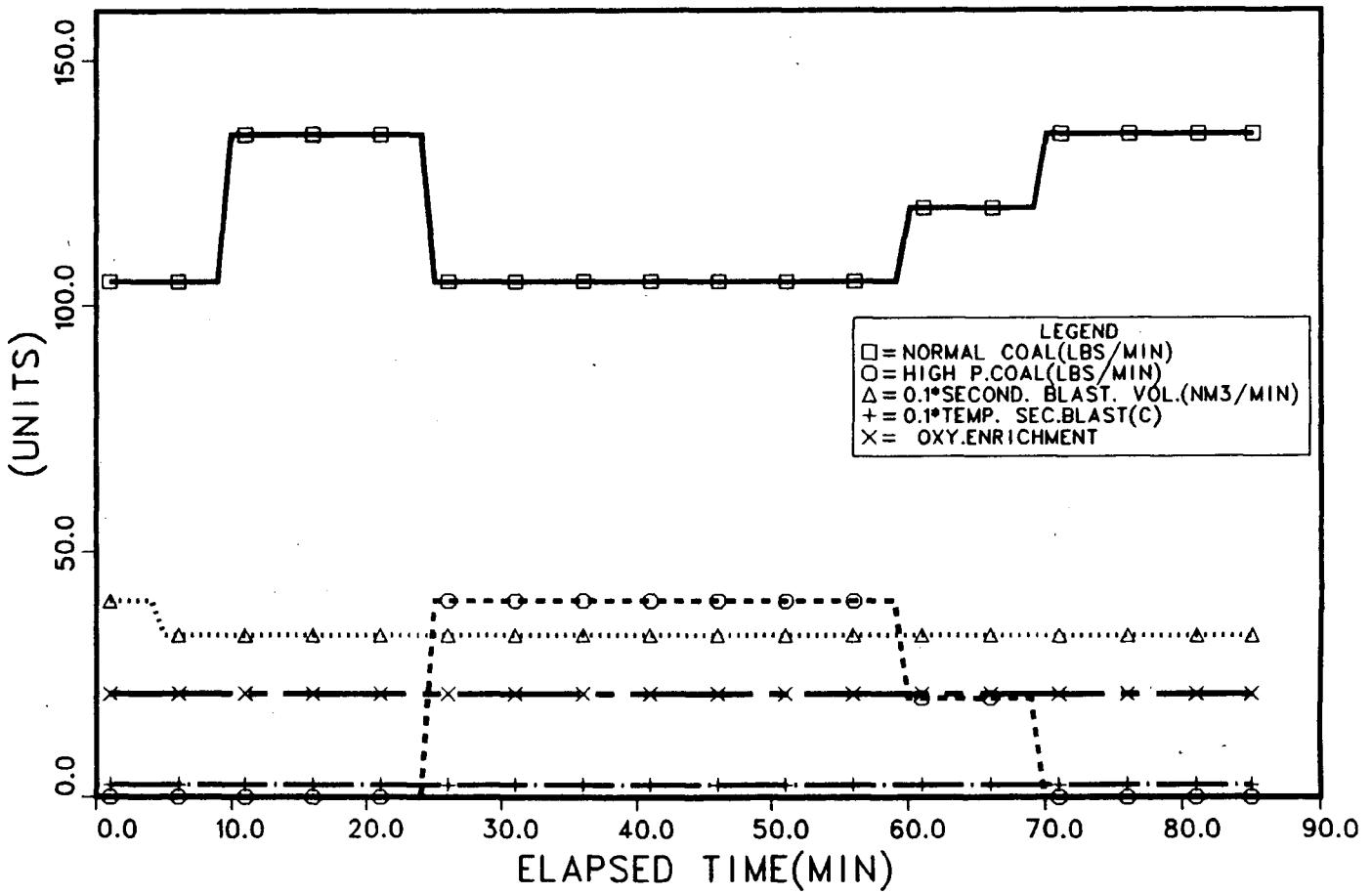

Figure 5.8 **Furnace operating conditions for Run 2**

rates between Runs 1 and 2 provides some insight into this seemingly contradictory behaviour. This is worthy of further discussion before proceeding with analysis of the results.

Following from the mathematical model of Richards et al [1a,b] the mechanism for generation of ferrous iron is reduction of ferric iron by entrained coal, and the mechanism for consumption is oxidation by the tuyere gas column. Under normal operating practice, the rates at which reduction and oxidation of ferrous iron proceed are inversely related. It is impossible to envisage a situation where one is not increased at the expense of the other. However, if the model is correct, with a second high-pressure coal source, this should no longer be the case. There is evidence to support this inference in Run 2. In this case, reduction was increased during high-pressure injection (increased zinc and lead elimination rates) and simultaneously, oxidation was increased in the tuyere gas column (increase in the rate of generation of ferric iron). The fact that this behaviour was not observed in Run 1 is probably due to the difference in the low-pressure coal rate during fuming. Moreover, by reducing the low-pressure coal rate from 54.5 kg/min (120 lbs/min) in Run 1 to 47.7 kg/,om (105 lbs/min) in Run 2, the rate of oxidation of ferrous iron was increased by an amount which was not completely off-set by the higher-reduction rate. This will be borne out by the modelling analysis presented in a later Chapter.

Additional evidence for these mechanisms comes from the temperature profile, see Fig. 5.7. Qualitatively, in Fig. 5.7 it is clear that there is a net decrease in the bath temperature during high-pressure injection. This trend is in itself consistent with normal fuming practice. However, the consistency and magnitude of the temperature drop are less than that expected with an equivalent fuming rate obtained under normal operation.[44] This behaviour, in particular the magnitude of the drop, is consistent mechanistically with increased ferrous iron oxidation which is a source of heat.

The results of a quantitative analysis of furnace performance in Run 2 are presented in Table 5.2. The high-pressure fuming rate and efficiency obtained in Run 2 can be compared with average values representative of low-pressure operation for a 70:30 hot-cold charge, shown also in Table 5.2. Based on this comparison, substantial gains have again been realized with high-pressure injection (factor of 1.85 increase in fuming rate and 1.86 increase in efficiency).

In Run 3, the charge to the furnace was 58180 kg. (64 tons) and consisted of 100% hot slag. In this particular run an attempt was made to avoid excessive generation of ferric iron during the heating period (as in the case of Run 2) by maintaining a secondary blast rate of 340 Nm^3/min (12,000 Scfm), see Fig. 5.12. As a result, the heating period was a little longer in

comparison with Run 2. The zinc concentration at the onset of normal fuming was approximately 13 wt.%, see Fig. 5.9.. Problems with interpretation of the results are again encountered because of the relatively low low-pressure coal rate during the period of fuming prior to high-pressure injection, see Fig. 5.12.

Qualitatively, from Fig 5.9, a considerable increase in the elimination rates of both zinc and lead was observed at the initiation of high-pressure injection at 30 mins. elapsed time. The behaviour of the ferrous - ferric couple, see Fig. 5.10, was consistent with observations in Run 2. The rate of increase in ferrous iron concentration was slowed during high-pressure injection in comparison with the preceding period of low-pressure fuming.

If the temperature profile is considered, see Fig. 5.11, the results are again consistent with expectations of a net temperature drop over the period of high-pressure injection. Moreover, the magnitude of the drop, 50^{o}C is similar to that observed in Run 2 - small for the observed fuming rate. Both of these observations, the behaviour of the ferrous-ferric couple and bath temperature, give further support to the mechanism proposed by Richards et al.[1a,b]

The results of a quantitative analysis are summarized in Table 5.2. These can be compared with average values

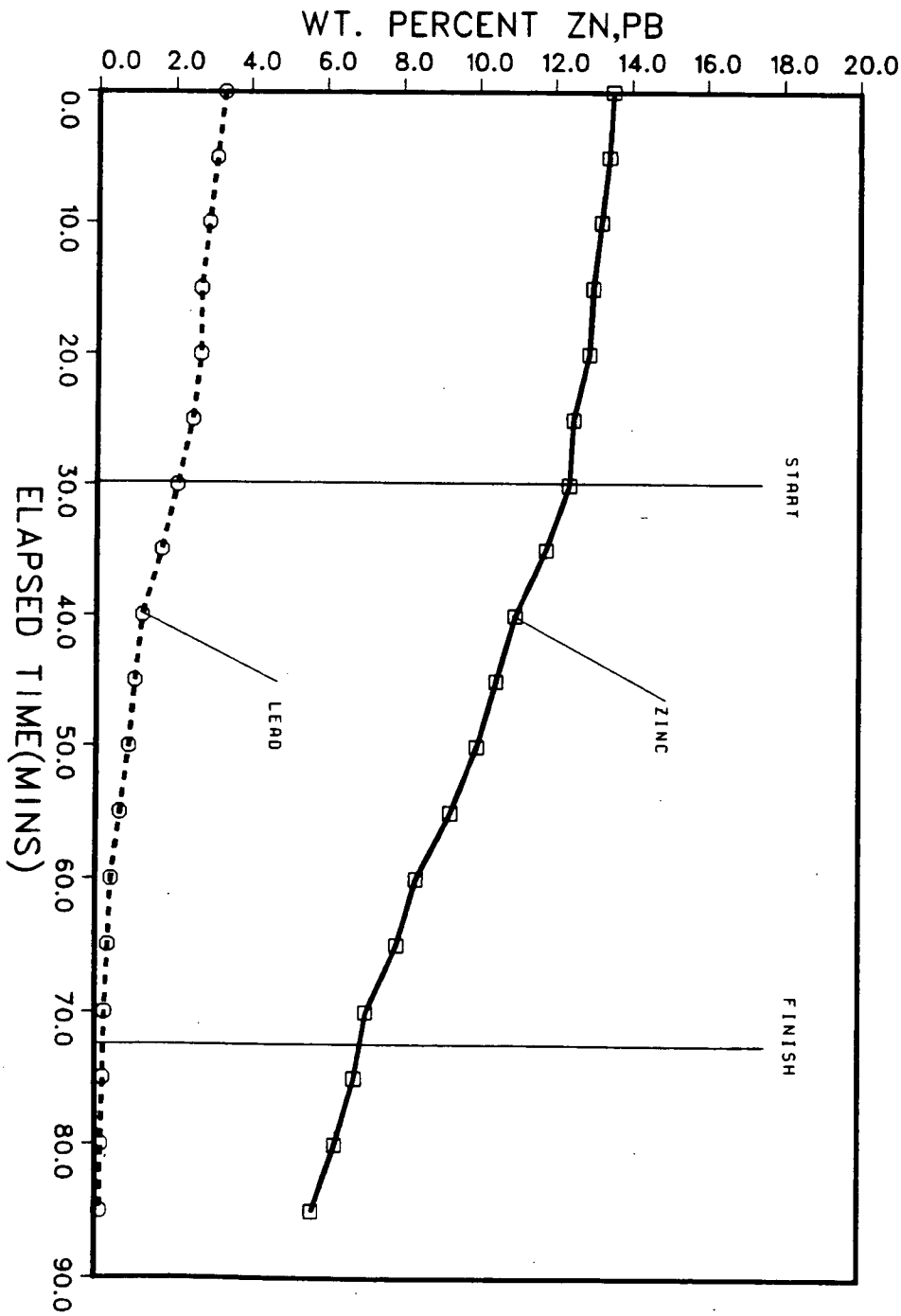

Figure 5.9 Zn and Pb profiles for Run 3

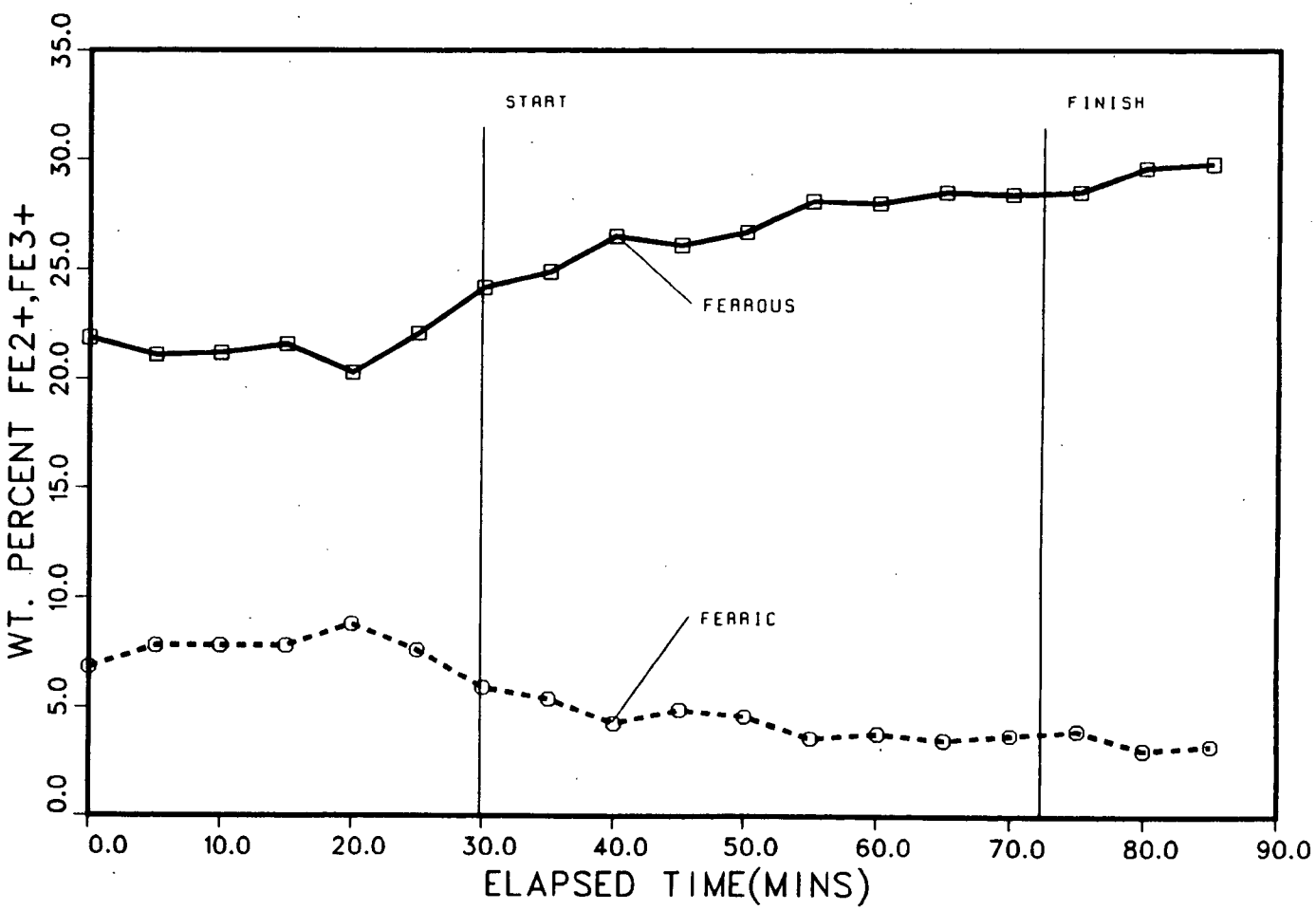

Figure 5.10 Fe^{2+} **and** Fe^{3+} **profiles for Run 3**

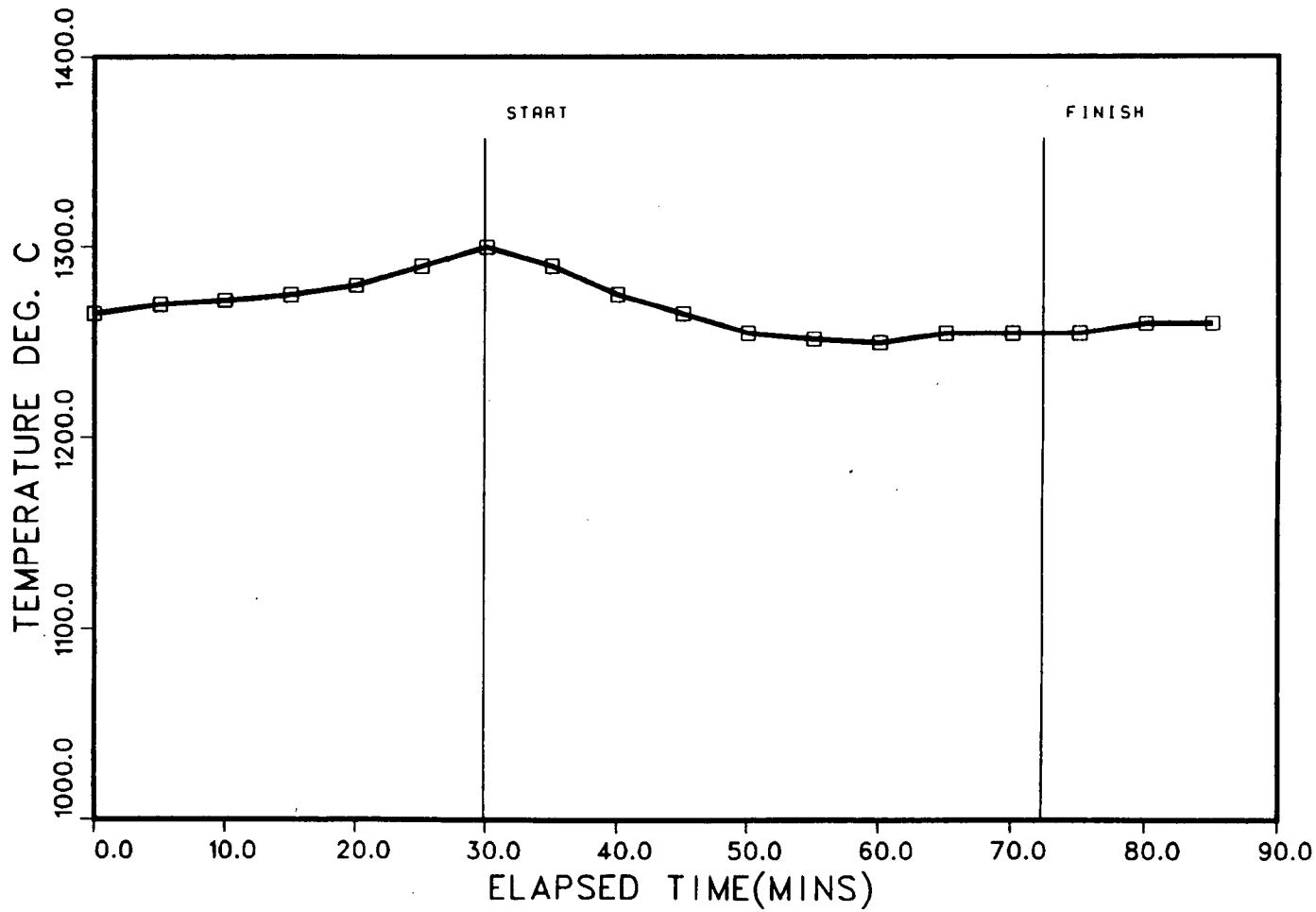

Figure 5.11 **Temperature profile for Run 3**

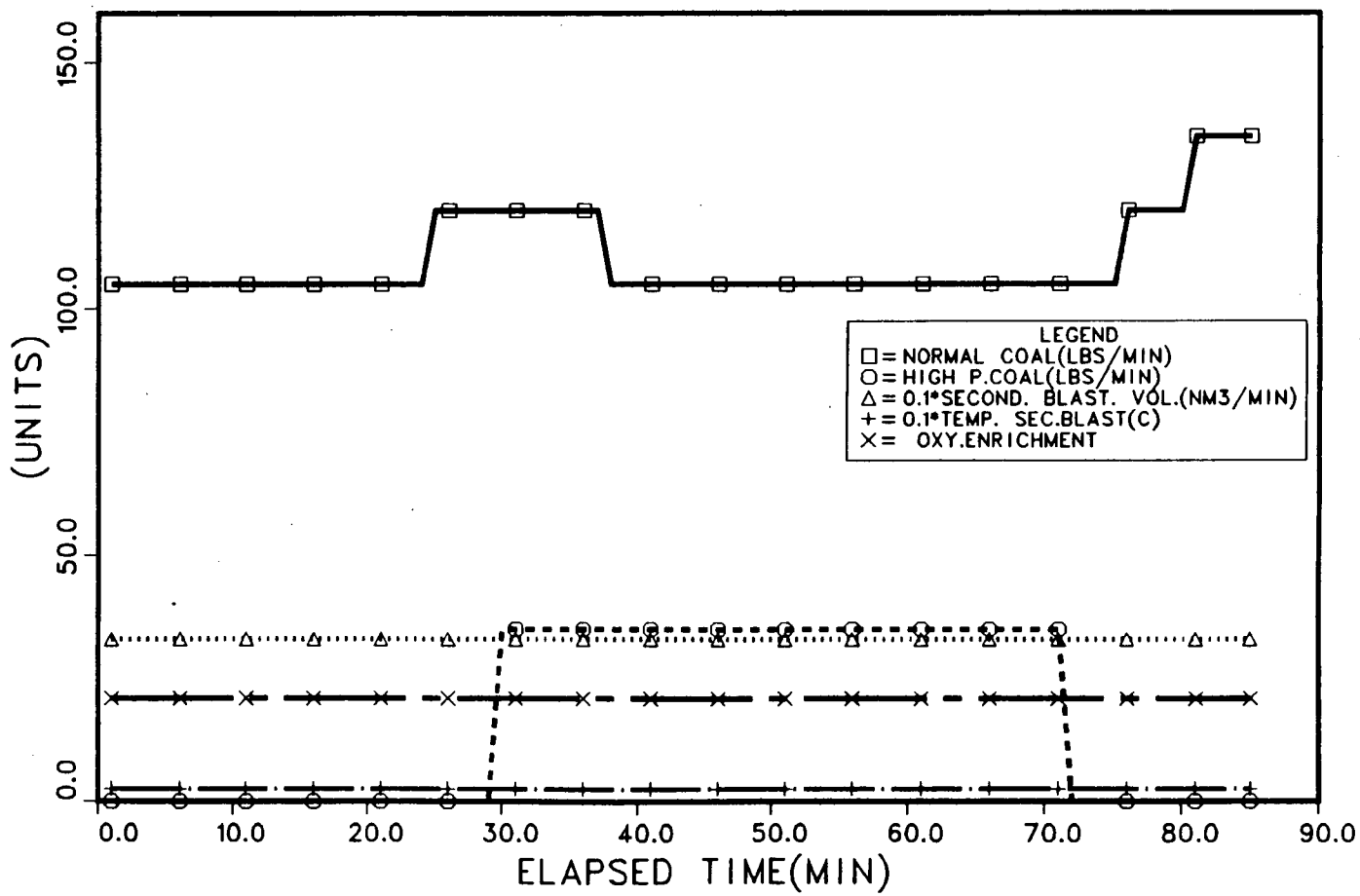

Figure 5.12 Furnace operating conditions for Run 3

representative of low-pressure fuming for a 100% hot charge, also presented in Table 5.2. Again, as with the two previous trials, substantial improvements in furnace performance have been achieved with high-pressure injection (a factor of 1.83 increase in fuming rate and a 1.89 increase in fuming efficiency).

Before proceeding with a summary of the preliminary analysis, it must be emphasized that the quantitative comparisons made with normal low-pressure operation are based on average plant data which is assumed to best represent normal operation. Emphasis has been placed on maintaining as much similarity between operating conditions prevailing during high-pressure injection and those runs used to establish normal operations. In particular, the importance of charge temperature has been considered. It is felt that in terms of a preliminary analysis, this is the only valid approach possible.

5.3 Summary

In summary, the preliminary analysis of the results in Runs 1 to 3 reveals that considerable improvement in both fuming rates and efficiencies have been realized with high-pressure injection. In Run 1, the zinc fuming rate and efficiency were increased by factors of 1.69 and 1.68 over normal operation, respectively. In Run 2, the increase was a factor of 1.85 and 1.86, while, in Run 3, the factors were 1.83 and 1.89, respectively. These results

are in direct contradiction to any predictions based on an equilibrium model. It remains to be established if a model based on kinetics can account for these results.

CHAPTER VI

MATHEMATICAL MODEL OF ZINC FUMING PROCESS AND DISCUSSION OF MODEL FITTING

As mentioned previously, the concept of high-pressure coal injection in the zinc slag fuming process followed from the work of Richards et al[1a,b] and in particular, their mathematical model of the process. It is logical therefore, that the Richards kinetic model be used to further analyze the results of the three high-pressure runs in an attempt to predict entrainment factors for the high-pressure coal. In its present form the kinetic model is fully capable of doing this. The procedure would involve calculation of entrainment factors for the total combined (low-pressure and high-pressure) coal supply to the furnace for each of the three high-pressure runs. This information then would be used in conjunction with the individual coal rates and an assumed low-pressure entrainment factor to estimate the factor of high-pressure coal entrained. The low-pressure entrainment factor could be obtained by fitting the model to data taken from the Cominco No. 2 furnace under normal low-pressure operating conditions.

At the outset, however, it was decided to modify the existing program by including a separate high-pressure coal supply distinct from the normal low-pressure coal. It was felt that this separation would simplify the fitting procedure.

Moreover, it would serve to emphasize the different roles of the two coal supplies within the furnace: one acting as a source of reductant, and the other as a source of heat. This modification was largely a book keeping exercise and does not warrant further discussion.

The opportunity did arise however, to modify the Richards model in a more fundamental manner. The area for potential improvement was associated with the behaviour of lead in the bath. The desire to include lead reduction in a kinetic model of the process was largely precipitated by two factors: firstly, the unusually high lead concentration at the start of Run 3, and secondly, the desire to elucidate the mechanisms of lead reduction in general.

With regard to the former, it was felt that at a concentration of 3 wt%, the influence of lead on zinc fuming rates and efficiencies could no longer be neglected. Therefore, in order to complete a valid analysis of one third of the high-pressure data (Run 3) the existing model would have to be modified to include lead reduction.

The latter reason follows from the emergence of the newer technologies for the smelting of lead concentrates. These technologies, as indicated previously, rely heavily on slag cleaning stages and in particular the removal of lead from high

lead content slags. It is essential, therefore, that the mechanisms surrounding the reduction and removal of lead be well understood in these processes. With this in mind, it was felt that the incorporation of lead reduction in the zinc fuming model would aid in elucidating the mechanisms of lead reduction and removal in general.

6.1 Modifications to the Richards Model

The following sections discuss the modifications made to the Richards[1a] kinetic model of the process.

6.1.1. The Kinetic Conceptualization of the Process

As discussed previously, the key to Richards[1a] mechanistic breakdown of the zinc fuming process is the separation of the furnace into two reaction zones: the slag bath or reduction zone, and the tuyere gas column or oxidation zone. Thus it is obvious that the modification surrounding lead reduction will be limited to the reduction zone and in particular the coal particle-slag reaction system developed by Richards et al. [1a,b]

6.1.1.1 The Coal Particle - Slag Reaction Model

At the instant a coal particle becomes entrained in the slag it is subjected to very rapid heating due to direct contact with

the slag. Under these conditions, according to Richards, pyrolysis occurs virtually instantaneously. The following assumptions were made in the original model in an attempt to characterize the exceedingly complex pyrolysis process.

(a) all proximate volatile hydrogen is released as H_2,
(b) all proximate volatile nitrogen is released as N_2,
(c) all proximate volatile oxygen reacts with volatile carbon to form CO, and
(d) the remaining proximate volatile carbon precipitates on the char particle.

Following pyrolysis it is assumed that the remaining char particle resides in the slag surrounded by an atmosphere of H_2, N_2 and CO. This char particle - secondary bubble then begins reaction with the slag.

The reducing conditions prevailing in the secondary bubble initiate the diffusion of ZnO, PbO and Fe_2O_3 to the bubble-slag interface (formerly only ZnO and Fe_2O_3 were considered). At the bubble-slag interface these species then are reduced by CO or H_2 via the following reactions:

$$ZnO_{(sl)} + CO_{(g)} = Zn_{(g)} + CO_{2(g)} \quad \ldots (6.1)$$

$$PbO_{(sl)} + CO_{(g)} = Pb_{(v)} + CO_{2(g)} \quad \ldots (6.2)$$

$$Fe_2O_{3(sl)} + CO_{(g)} = 2FeO_{(sl)} + CO_{2(g)} \quad \ldots (6.3)$$

and

$$ZnO_{(sl)} + H_{2(g)} = Zn_{(g)} + H_2O_{(g)} \quad \ldots (6.4)$$

$$PbO_{(sl)} + H_{2(g)} = Pb + H_2O_{(v)} \quad \ldots (6.5)$$

$$Fe_2O_{3(sl)} + H_{2(g)} = 2FeO_{(sl)} + H_2O_{(g)} \quad \ldots (6.6)$$

The CO_2 and H_2O produced via Reactions (6.1) - (6.6) then diffuses through the gas phase to react with the char particle via the following reactions:

Boudouard

$$C_{(char)} + CO_{2(g)} = 2CO_{(g)} \quad \ldots (6.7)$$

Char - Steam

$$C_{(char)} + H_2O_{(g)} = H_{2(g)} + CO_{(g)} \quad \ldots (6.8)$$

This marks the second divergence from the original Richards[1a] reaction model which only considers the Boudouard reaction.

In the initial stages as this reaction system rises through the slag, the vapour pressures of Zn and Pb increase, and the char particle gradually shrinks as carbon is consumed by the Boudouard and Char - Steam reactions. The rate of increase in the partial pressure of CO_2 and H_2O are a function of the rates

at which they are generated via Reactions (6.1)-(6.6), and the rates at which they are consumed by Reactions (6.7)-(6.8).

An interesting problem with respect to model formulation arises as the char particle - secondary bubble continues to react with the slag. The problem is associated with the form of metallic lead. At slag fuming temperatures, 1200-1325^{o} C, lead is stable as a liquid (m.pt. 327.50, b.pt. 1740^{o} C) unlike metallic zinc which is a vapour (m.pt. 419.58, b.pt. 907^{o} C). Mechanistically, it can be argued that the vapour pressure of lead will continue to rise in the secondary bubble until the partial pressure reaches that in equilibrium with liquid metallic lead at the temperature of the slag bath, ie.

$$Pb_{(v)} = Pb_{(l)} \qquad \ldots (6.9)$$

From this point on, as lead vapour continues to be produced at the bubble - slag interface, liquid lead is simultaneously precipitated at such a rate so as to maintain Reaction (6.9) at equilibrium. For the purpose of modelling it is assumed that the liquid lead produced collects in the bottom of the secondary bubble. The reaction system which develops is schematically illustrated in Fig. 6.1.

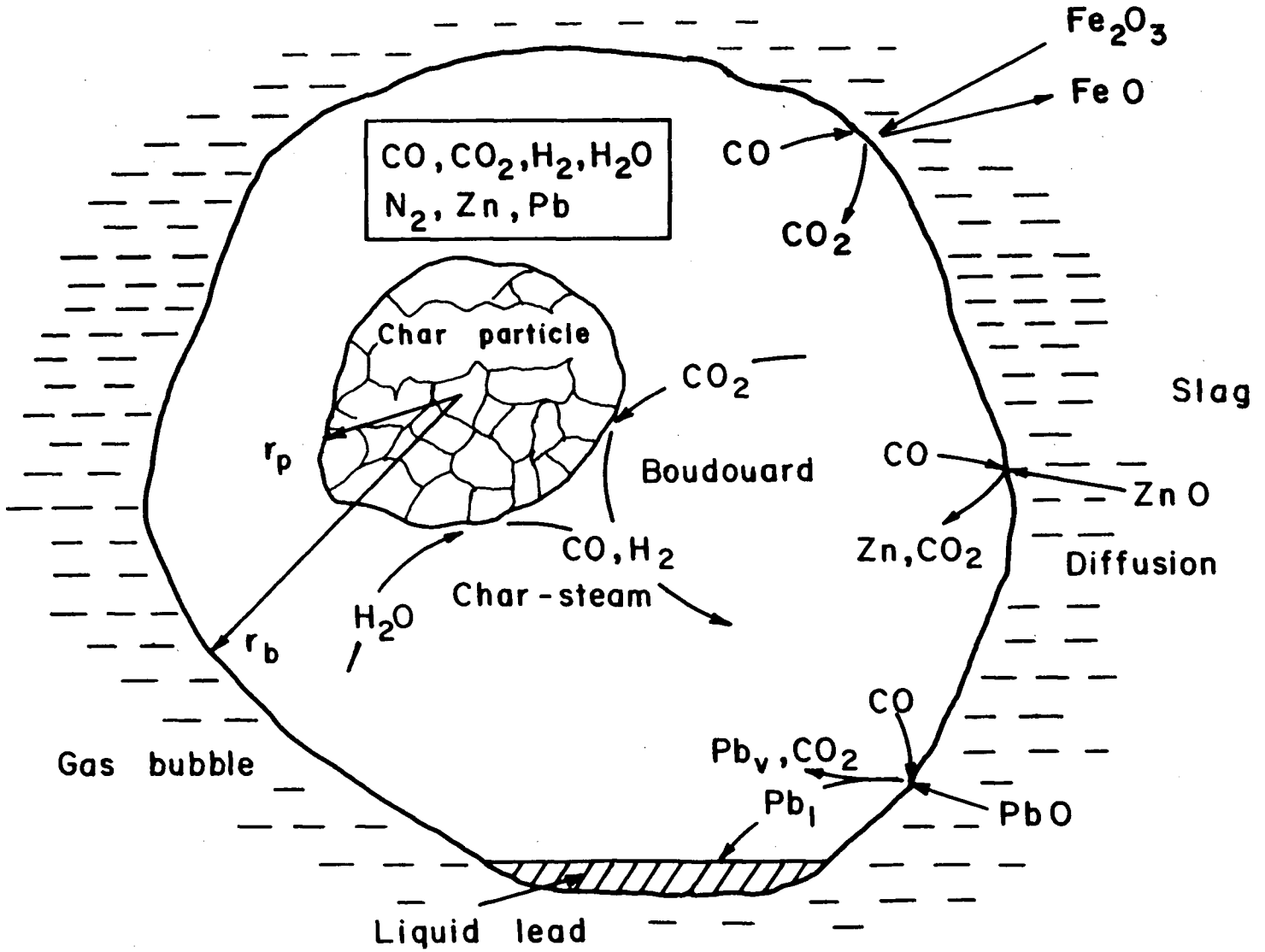

Figure 6.1 The char particle-slag reaction system

As discussed previously in Chapter II, substantial evidence in support of this reaction was provided by Richards[1a] Similar evidence for the lead reduction modification is available from aphotomicrograph of a quenched and polished slag sample of Cominco lead blast furnace slag. Fig 6.2 shows a white metallic inclusion, or lead prill, in contact with black gas pores (secondary bubbles) as postulated.

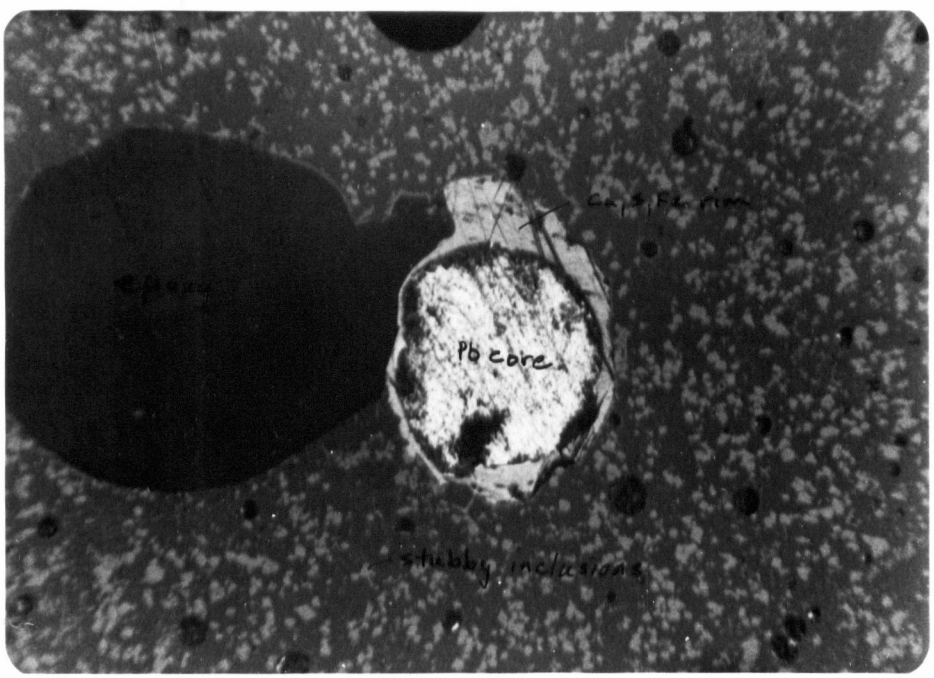

Note: Course stubby inclusions are more Fe rich than slag. Metallic inclusion contains a fairly pure Pb core with a rimming of Cu, S and minor Fe. The slag and stubby inclusions are Zn and S rich. Reflected light, x 160 magnifications.

Fig 6.2 Photomicrograph of quenched and polished slag sample

In this system, as with Richards, it is assumed that electron transfer via the ferric-ferrous couple does not play a significant role in the reduction of ferric iron (Fe^{3+}). Evidence to this effect has been discussed previously in Chapter II. The treatment of diffusion processes in and around the reaction system is identical to that of Richards except for the inclusion of better rheological data. Equilibrium is assumed within the gas phase of the secondary bubble and locally at the bubble-slag interface. This assumption was justified[1a] from an assessment of the relative rates of mass-transfer within the secondary bubble and surrounding slag. Mass-transfer coefficients were estimated as follows.

The terminal rise velocity of the secondary bubble according to Stoke's Law is:

$$V_{terminal} = 4gr_b^2 \Delta p/18\,\mu \qquad \ldots (6.10)$$

where according to Altman et al[35], for lead blast furnace slag

$$\log \mu = 0.0160 \log (CR) + \frac{680.12}{T^\circ K} 0.39881 \qquad \ldots (6.11)$$

where,

$$CR = \frac{\% SiO_2 + \% Al_2O_3 + \% MgO}{\% CaO + \% FeO + \% ZnO + \% S} \qquad \ldots (6.12)$$

(percentages are in weight percent).

From Clift et al[36], for rigid spheres in creeping flow, for species i:

$$Sh_i = 1 + (1+Pe_i)^{1/3} \quad \ldots (6.13)$$

where Pe is the Peclet Number;

$$Pe_i = 2r_b V_b / D_i \quad \ldots (6.14)$$

and, Sh is the Sherwood Number;

$$Sh_i = 2k_i r_b / D_i \quad \ldots (6.15)$$

For the purpose of modelling, additional assumptions also must be made. Following from Richards[1a], these are:

(a) the char particle is spherical,

(b) the char particle reacts only with CO_2 and H_2O, and

(c) the system is isothermal at bath temperature.

A sample model of the original reaction system has been developed by Richards. Eight unknown time-dependent variables, C^b_{Zn}, C^b_{CO}, $C^b_{CO_2}$, $C^b_{H_2}$, $C^b_{H_2O}$, $C^b_{N_2}$, r_p and r_b, in addition to three time-dependent modelling parameters, W_p, V_g and M^C_c, have been considered where C^b_i, is the concentration of species i in the secondary bubble, r_p is the radius of the secondary bubble, and M^C_c is the molar amount of carbon in the char particle. The incorporation of lead reduction adds two more variables: C_{Pb_v}

and M_{Pb_v}, the concentration of lead vapour in the secondary bubble and the molar amount of liquid lead respectively. This makes a total of thirteen time dependent quantities. Thirteen equations must be developed.

The development of these equations is sufficiently changed by the consideration of lead reduction to warrant a repeat of their derivation here.

6.1.1.1.1 Zinc Balance

The mass-transfer of zinc oxide to the secondary bubble can be characterized by the empirical equation:

$$\dot{n}_{ZnO} = A_b \, k_{ZnO} \, (C^{Sl}_{ZnO} - C^{i}_{ZnO}) \qquad \ldots (6.16)$$

A zinc mass balance on the secondary bubble yields:

$$\dot{n}_{ZnO} = \frac{d}{dt} (C^{b}_{Zn} \, V_g) = V_g \frac{d}{dt} (C^{b}_{Zn}) + C^{b}_{Zn} \frac{d}{dt}(V_g) \qquad \ldots (6.17)$$

Thus

$$\frac{d}{dt} (C^{b}_{Zn}) = \frac{1}{V_g} \left[\dot{n}_{ZnO} - C^{b}_{Pb_v} \frac{d}{dt}(V_g) \right] \qquad \ldots (6.18)$$

6.1.1.1.2 Lead Balance

The mass-transfer of lead oxide to the secondary bubble can be characterized by the empirical equation:

$$\dot{n}_{PbO} = A_b k_{PbO} (C^{sl}_{PbO} - C^{i}_{PbO}) \quad \ldots (6.19)$$

For conditions when the partial pressure of Pb_v in the secondary bubble is less than that in equilibrium with liquid lead, a mass balance on the gas phase yields:

$$\dot{n}_{PbO} = \frac{d}{dt}(C^{b}_{Pb_v} V_g) = V_g \frac{d}{dt}(C^{b}_{Pb_v}) + C^{b}_{Pb_v} \frac{d}{dt}(V_g) \quad \ldots (6.20)$$

$$\frac{d}{dt}(C^{b}_{Pb_v}) = \frac{1}{V_g}\left[\dot{n}_{PbO} - C^{b}_{Pb_v} \frac{d}{dt}(V_g)\right] \quad \ldots (6.21)$$

For conditions when the partial pressure of lead vapour equals that in equilibrium with liquid lead, a portion of lead reduced at the bubble-slag interface ends up in the gas phase. This portion serves to maintain the partial pressure of lead at equilibrium with liquid lead. Separating the total flux of PbO into two components:

n_{PbO_v} = portion of total PbO flux reporting to gas phase,

n_{PbO_l} = portion of total PbO flux reporting to liquid.

From Equation (6.9), assuming one atmosphere total pressure, it follows that

$$K_{6.9} = P_{Pb_v} = \frac{C^b_{Pbv}}{p^m_g} \quad \ldots (6.22)$$

Rearranging Equation (6.22)

$$C^b_{Pb_v} = K_{6.9}\, p^m_g \quad \ldots (6.23)$$

and differentiating gives

$$\frac{d}{dt}\left(C^b_{Pb_v}\right) = \frac{d}{dt}\left(K_{6.9}\, p^m_g\right) = 0 \quad \ldots (6.24)$$

A mass balance for lead in the gas phase yields:

$$\dot{n}_{PbO_v} = \frac{d}{dt}\left(C^b_{Pb_v} V_g\right) \quad \ldots (6.25)$$

Expanding and rearranging,

$$\frac{d}{dt}\left(C^b_{Pb_v}\right) = \frac{1}{Vg}\left[\dot{n}_{PbO_v} - C^b_{Pb_v}\frac{d}{dt}(V_g)\right] \quad \ldots (6.26)$$

Substituting Equations (6.23) and (6.24) into Equation (6.26), and rearranging,

$$\dot{n}_{PbO_v} = K_{6.9}\, p^m_g \frac{d}{dt}(V_g) \quad \ldots (6.27)$$

This then is the portion of the total flux of PbO which enters the gas phase. The portion of the total flux of PbO reporting to liquid lead is simply

$$\dot{n}_{PbO_l} = \frac{d}{dt} (M_{Pb_l}) \quad \ldots (6.28)$$

Finally, a mass balance on the total lead (vapour and liquid) in the system yields:

$$\dot{n}_{PbO} = \dot{n}_{PbO_v} + n_{PbO_l} \quad \ldots (6.30)$$

Substituting Equations (6.27) and (6.28) into (6.29) gives:

$$\dot{n}_{PbO} = K_{6.9} p_g^m \frac{d}{dt}(V_g) + \frac{d}{dt} (M_{Pb,l}) \quad \ldots (6.30)$$

6.1.1.1.3 Carbon Balance

Carbon does not leave the secondary bubble. Carbon enters the gas phase by the Boudouard and char-steam reactions, Equations (6.7) and (6.8) respectively. Thus

$$\dot{r}_{C_{input}} = \hat{B}_r + \hat{S}_r \quad \ldots (6.31)$$

where $\hat{B}_r$ and $\hat{S}_r$ are the rates of the Boudouard and char-steam reactions respectively. A mass balance for carbon in the gas

phase yields

$$\dot{B}_r + \dot{S}_r = V_g \frac{d}{dt}(C^b_{CO}) + \frac{d}{dt}(C^b_{CO}) + \frac{1}{2}\frac{d}{dt}(V_g)\quad C^b_{CO} + C^b_{CO_2} \qquad \ldots (6.32)$$

rearranging,

$$\dot{B}_r + \dot{S}_r = V_g \left[\frac{d}{dt}(C^b_{CO}) + \frac{d}{dt}(C^b_{CO_2})\right] + \frac{d}{dt}(V_g)\left[C^b_{CO} + C^b_{CO_2}\right] \qquad \ldots (6.33)$$

6.1.1.1.4 Oxygen Balance

Oxygen enters the gas phase via Reactions (6.1), (6.2) and (6.3). There is no generation or consumption. Thus:

$$\dot{t}_{O_2,\,input} = \frac{1}{2}\dot{n}_{ZnO} + \frac{1}{2}\dot{n}_{PbO} + \frac{1}{2}\dot{n}_{Fe_2O_3} \qquad \ldots (6.34)$$

where $\dot{n}_{Fe_2O_3}$ is the rate of mass transfer of Fe_2O_3 to the secondary bubble.

A mass balance for oxygen in the gas phase yields

$$\dot{t}_{O_2,\,input} = \frac{1}{2}\frac{d}{dt}(C^b_{CO}\,V_g) + \frac{d}{dt}(C^b_{CO_2}\,V_g) + \frac{1}{2}\frac{d}{dt}(C^b_{H_2O}\,V_g) \qquad \ldots (6.35)$$

rearranging,

$$\dot{n}_{ZnO} + \dot{n}_{PbO} + \dot{n}_{Fe_2O_3} = \frac{d}{dt}(V_g)\left[C^b_{CO} + 2C^b_{CO_2} + C^b_{H_2O}\right] + V_g\left[\frac{d}{dt}C^b_{CO} + 2\frac{d}{dt}C^b_{CO_2} + \frac{d}{dt}C^b_{H_2O}\right] \quad \ldots (6.36)$$

6.1.1.1.5 Hydrogen Balance

There is no net input, output, generation or consumption of hydrogen in the secondary bubble. Thus a mass balance for hydrogen in the secondary bubble yields

$$\frac{d}{dt}(M^b_{H_2}) = 0 = \frac{d}{dt}(V_g C^b_{H_2}) + \frac{d}{dt}(V_g C^b_{H_2O}) \quad \ldots (6.37)$$

Rearranging,

$$0 = \frac{d}{dt}(V_g)\left[C^b_{H_2O} + C^b_{H_2}\right] + V_g\left[\frac{d}{dt}C^b_{H_2} + \frac{d}{dt}C^b_{H_2O}\right] \quad (6.38)$$

6.1.1.1.5.1 Equilibrium of the Water-Gas Reaction

Following from the assumption of equilibrium within the secondary bubble a fourth equation in $\frac{d}{dt}(C^b_{CO})$, $\frac{d}{dt}(C^b_{CO_2})$, $\frac{d}{dt}(C^b_{H_2})$ and $\frac{d}{dt}(C^b_{H_2O})$, can be developed.

From the equilibrium of the water-gas reaction:

$$CO + H_2O = H_2 + CO_2 \quad \ldots (6.39)$$

it follows that;

$$K_{6.39} = \frac{P_{H_2}\ P_{CO_2}}{P_{CO}\ P_{H_2O}} = \frac{C^b_{H_2}\ C^b_{CO_2}}{C^b_{CO}\ C^b_{H_2O}} \quad \ldots (6.40)$$

Differentiating and rearranging

$$K_{6.32}\left[C^b_{CO}\frac{d}{dt}C^b_{H_2O}+\frac{d}{dt}C^b_{CO}\right]=C^b_{CO_2}\frac{d}{dt}C^b_{H_2}+C^b_{H_2}\frac{d}{dt}C^b_{CO_2} \quad \ldots (6.41)$$

Combining Equations (6.33), (6.36) and (6.38) with the Water-Gas equilibrium, Equation (6.41) gives four equations in four unknowns;

$$\frac{d}{dt}(C^b_{CO_2})=\frac{K_{6.32}\,C^b_{CO}(D_1-D_3)+K_{6.32}\,C^b_{H_2O}\,D_3-C^b_{CO_2}(D_1-D_2+D_3)}{\left[C^b_{H_2}+C^b_{CO_2}+K_{6.32}\,C^b_{H_2O}+K_{6.32}\,C^b_{CO}\right]} \quad \ldots (6.42)$$

$$\frac{d}{dt}(C^b_{CO})=D_3-\frac{d}{dt}(C^b_{CO_2}) \quad \ldots (6.43)$$

$$\frac{d}{dt}(C^b_{H_2})=D_1-D_2+D_3+\frac{d}{dt}(C^b_{CO_2}) \quad \ldots (6.44)$$

and,

$$\frac{d}{dt}C^b_{H_2O}=D_2-D_3-\frac{d}{dt}C^b_{CO_2} \quad \ldots (6.45)$$

where

$$D_1=\frac{1}{V_g}\frac{d}{dt}(V_g)\left[C^b_{H_2O}+C^b_{H_2}\right] \quad \ldots (6.46)$$

$$D_2=\frac{1}{V_g}\frac{d}{dt}\left[\dot{n}_{ZnO^+}\,\dot{n}_{Pbo^+}\,\dot{n}_{Fe_2O_3^-}\frac{d}{dt}(V_g)\left[C^b_{CO}+2C^b_{CO^+}+C^b_{H_2O}\right]\right] \quad \ldots (6.47)$$

and

$$D_3=\frac{1}{V_g}\left[\dot{B}_r+\dot{S}_r-\frac{d}{dt}(V_g)\left[C^b_{CO}+C^b_{CO_2}\right]\right] \quad \ldots (6.48)$$

6.1.1.1.6 <u>N_2 Balance</u>

There is no input, output, generation or consumption of nitrogen. Thus:

$$\frac{d}{dt}\left[C^b_{N_2} V_g \right] = 0 \qquad \ldots (6.49)$$

$$\frac{d}{dt}\left(C^b_{N_2}\right) = \frac{-C^b_{N_2}}{V_g} \frac{d}{dt}\left(V_g\right) \qquad \ldots (6.50)$$

6.1.1.1.7 Bubble Radius

Following from the assumption of spherical geometry, the gas volume can be written as

$$V_g = \frac{4}{3} r_b^3 - \frac{4}{3} r_p^3 \qquad \ldots (6.51)$$

Differentiating and rearranging

$$\frac{d}{dt} r_b = \frac{1}{r_b^2}\left[\frac{1}{4}\frac{d}{dt}(V_g) + r_p^2 \frac{d}{dt} r_p\right] \qquad \ldots (6.52)$$

6.1.1.1.8 Char Particle Radius

Relating the radius of the char particle to its weight, it follows that:

$$\frac{4}{3} r_p^3 = \frac{Wp}{pc} \qquad \ldots (6.53)$$

It is assumed the density of the char particle is equal to that of the original coal. Differentiating

$$\frac{d}{dt}\left(r_p\right) = \frac{1}{4} r_p^2 \frac{1}{Pc} \frac{d}{dt}(W_p) \qquad \ldots (6.54)$$

6.1.1.1.9 Char Particle Weight

Assuming that the char particle loses weight in proportion to the rate of the Boudouard and char-steam reactions in follows that:

$$\frac{d}{dt}(W_p) = -(\dot{B}_r + \dot{S}_r) \frac{W_{CAP}}{I_{PWT}} * 12.01 \quad \ldots (6.55)$$

where

W_{CAP} = the weight of carbon remaining in the char after pyrolysis,

I_{PWT} = the initial particle weight after pyrolysis (carbon plus ash).

The factor 12.01 is the molecular weight of carbon in kg/kg.mole.

6.1.1.1.10 Gas Volume

The secondary bubble gas volume changes as a function of the reduction reactions and, the Boudouard and char-steam reactions. For conditions when the partial pressure of lead in the secondary bubble is below that in equilibrium with liquid lead:

$$\dot{r}_{g,gen} = 2\dot{n}_{ZnO} + 2\dot{n}_{PbO} + 2\dot{B}_r + 2\dot{S}_r \quad \ldots (6.56)$$

$$\dot{r}_{g,cons} = \dot{n}_{ZnO} + \dot{n}_{PbO} + \dot{B}_r + \dot{S}_r \quad \ldots (6.57)$$

A mass balance for the secondary bubble yields:

$$\dot{n}_{ZnO} + \dot{n}_{PbO} + \dot{B}_r + \dot{S}_r = \frac{d}{dt}(P_g^m V_g) \quad \ldots (6.58)$$

Rearranging,

$$\frac{d}{dt}(V_g) = \frac{1}{P_g^m}\left[\dot{n}_{ZnO} + \dot{n}_{PbO} + \dot{B}_r + \dot{S}_r\right] \quad \ldots (6.59)$$

where P_g^m is the molar gas density at temperature.

For conditions when the partial pressure of lead equals that in equilibrium with liquid lead, a mass balance for the secondary bubble yields

$$\dot{n}_{ZnO} + \dot{n}_{PbO_v} + \dot{B}_r + \dot{S}_r = \frac{d}{dt}(P_g^m V_g) \quad \ldots (6.60)$$

Substituting Equation (6.27) into Equation (6.60) and rearranging gives

$$\frac{d}{dt}(V_g) = \frac{1}{[P_g^m (1-K_{6.9})]}\left[\dot{n}_{ZnO} + \dot{B}_r + \dot{S}_r\right] \quad \ldots (6.61)$$

6.1.1.1.11 Initial Conditions

The initial gas volume and composition are calculated using the original procedure of Richards.[1a] Equations (6.7) and (6.8)

are assumed to be at equilibrium and a mass balance is conducted on the volatile constituents, oxygen, nitrogen and hydrogen. This yields five equations and five unknowns, C^b_{CO} , $C^b_{CO_2}$, $C^b_{H_2}$ $C^b_{H_2O}$, $C^b_{N_2}$. The zinc and lead vapour concentrations are assumed to be zero. Having established the gas concentration, the initial gas volume can be found. The initial charge particle weight and carbon content follow from a mass balance. The initial values of r_p and r_b also may be calculated. Finally, the initial amount of liquid lead is assumed to be zero.

6.1.1.1.12 Thermodynamic Data

The necessary thermodynamic data together with references are shown in Table 6.1.

6.1.1.1.13 Mass Transfer

The calculation of the mass-transfer rates of ZnO and PbO is a relatively straight forward exercise. Calculation of the mass-transfer rates of FeO and Fe_2O_3 is more complex.

A review of the literature by Richards [1a] has indicated that a significant portion of the ferric iron present in zinc fuming slags may be associated with non-stoichiometric wustite (Fe_x O). This behaviour was accounted for in the original Richards[1a] model

TABLE 6.1

Thermodynamic Data for Reactions, $\Delta G^{o} = \Delta H^{o} - T\Delta S^{o}$

Reaction	H^{o} (J)	S^{o} (JK^{-1})	Reference
$Zn_{(g)} + \frac{1}{2} O_2 = ZnO_{(s)}$	-460240	-198.3	36
$Pb_{(g)} + \frac{1}{2} O_2 = PbO_{(l)}$	-181167	-68.03	36
$C + O_2 = CO_{2(g)}$	-395350	0.544	36
$C + \frac{1}{2} O_2 = CO_{(g)}$	-114390	85.75	36
$H_2 + \frac{1}{2} O_2 = H_2O_{(g)}$	-247484	-55.86	36
$Fe_{(s)} + \frac{1}{2} O_2 = FeO_{(s)}$	-264889	-65.35	42
$2Fe_{(s)} + \frac{3}{2} O_2 = Fe_2O_{3(s)}$	-814123	-250.66	36

*Standard states for gases are the pure gas at 1 atm at temperature, for the liquids, the pure liquid at temperature and for the solids, the pure solid at temperature.

TABLE 6.1 CONT'D

Activity Coefficient of Slag Species

Species	Activity Coefficient	Reference
ZnO	$\ln \gamma_{ZnO_{(s)}} = \frac{16400\,(S^*) - 12000}{T} - 10.75\,(S^*) + 8.8$	1a,37,43
PbO	$\ln \gamma_{PbO_{(l)}} = \frac{1573}{T} \ln 1.20\,(\%CaO/\%SiO_2) - .37(\%Fe/\%SiO_2) + 0.27$	39
FeO Fe_2O_3	γ_{FeO} and $\gamma_{Fe_2O_3}$ have been calculated using the three-suffix Margules model developed by Goel et al.[44]	

where S^* = the molar ratio of CaO/SiO_2

*Standard states for liquids are the pure liquid at temperature and for solids, the pure solid at temperature.

by rewriting Equation (6.3) in the form:

$$Fe_2O_3 + (3 - 2/X)CO = (2/X)Fe_xO + (3 - 2/X)CO_2 \quad . . . (6.62)$$

In addition to making mass-transfer calculations more cumbersome, there are some fundamental problems with this approach. One problem, as indicated by Richards, is the implication that diffusion of Fe^{2+} is occurring against a concentration gradient- clearly not possible. A second problem, not considered is the influence that the non-stoichiometric factor has on chemical potentials. For example, as x approaches 0.667 the driving force for Reaction (6.64) clearly tends to zero.

A different approach is necessary to resolve these problems. The following section discusses the method followed in the modified model.

6.1.1.1.13.1 Mass Transfer of Fe^{2+} and Fe^{3+}

To access the influence of the non-stoichiometric factor x on the mass-transfer of Fe_2O_3 and FeO, Reaction (6.3) must be broken down into the following more fundamental reactions:

$$2Fe^{3+}_{(sl)} + 2\bar{e} = 2Fe^{2+}_{(sl)} \quad . . . (6.63)$$

$$O^{2-}_{(sl)} = 1/2\ O_{2(g)} + 2\bar{e} \quad . . . (6.64)$$

and,

$$CO_{(g)} + 1/2\ O_{2(g)} = CO_{2(g)} \quad \ldots (6.65)$$

On the basis of this breakdown it is clear that the overall reaction essentially is an oxygen exchange reaction. Moreover, the driving force is simply the difference in oxygen potential between the slag and the secondary bubble. The former is established by the Fe^{3+}/Fe^{2+} ratio in the slag and the latter by the Co_2/CO ratio in the secondary bubble.

From this simplistic analysis several comments can be made. Firstly, if the slag composition is expressed in terms of Fe^{3+} and Fe^{2+}, then clearly the stoichiometry of Reaction (6.3) would apply and would be independent of x. Since this is in fact the case, Reaction (6.3) is applicable for mass-transfer calculations. Secondly, it is evident that the oxygen potential of the slag must be calculated in order to determine mass-transfer rates. For this purpose, the following information is need for typical zinc fuming slags:

[i] the slag composition,

[ii] the activity coefficient of Fe_xO,

[iii] the activity coefficent of Fe_2O_3,

[iv] the equilibrium constant for the reaction:

$$Fe_xO = 1/2\ O_2 + xFe \qquad \ldots (6.66)$$

and,

[v] the equilibrium constant for the reaction:

$$Fe_2O_3 = 2Fe + 3/2\ O_2 \qquad \ldots (6.67)$$

Clearly two of these quantities are dependent on x: the activity coefficient of Fe_xO, and the equilibrium constant for Reaction (6.65). Unfortunately, these values are not available in the literature. The best reported data for the activity coefficient of wustite in slags approximating zinc fuming slags (see Table 6.1), are given relative to $FeO_{(s)}$ as the standard state. This being the case, the equilibrium constant for Reaction (6.66) also must be evaluated relative to $FeO_{(s)}$ (x=1) in order to be consistent thermodynamically. Therefore, there is little alternative other than to set x=1 for mass-transfer calculations.

The mass transfer of FeO and Fe_2O_3 through the slag to the bubble slag interface may be characterized empirically as

$$\dot{n}_{Fe_2O_3} = A_b\ k_{Fe_2O_3} \left[C^{sl}_{Fe_2O_3} - C^{i}_{Fe_2O_3} \right] \qquad \ldots (6.68)$$

$$\dot{n}_{FeO} = A_b\ k_{Fe_2O_3} \left[C^{i}_{FeO} - C^{sl}_{FeO} \right] \qquad \ldots (6.69)$$

From the stoichiometry of Reaction (6.3) and assuming the positive direction to be away from the bubble slag interface, it

follows that

$$\dot{n}_{FeO} = 2\dot{n}_{Fe_2O_3} \quad \ldots (6.70)$$

Substituting Equations (6.68) and (6.69) with Equation (6.70) yields

$$C^i_{FeO} = \frac{2k_{Fe_2O_3}}{k_{FeO}} \left(C^{sl}_{Fe_2O_3} - C^i_{Fe_2O_3}\right) + C^{sl}_{FeO} \quad \ldots (6.71)$$

Since Equation (6.3) is at equilibrium at the bubble-slag interface

$$K_{6.6} = \frac{a^2_{FeO} \; P_{CO_2}}{a_{Fe_2O_3} \; P_{CO}} \quad \ldots (6.72)$$

Combining Equations (6.71) and (6.72), and solving for $C^i_{Fe_2O_3}$ yields

$$0 = D_4(C^i_{Fe_2O_3}) - \left[D_6 - D_5 \left(C^i_{Fe_2O_3}\right)\right]^2 \quad \ldots (6.73)$$

where

$$D_4 = K_{6.6} \; P^m_{sl} \; \frac{\gamma_{Fe_2O_3} \; PCO}{\gamma^2_{FeO} \; PCO_2} \quad \ldots (6.74)$$

$$D_5 = \frac{2k_{Fe_2O_3}}{k_{FeO}} \quad \ldots (6.75)$$

$$D_6 = D_5 \; C^{sl}_{Fe_2O_3} + C^{sl}_{FeO} \quad \ldots (6.76)$$

Equation (6.69) can be solved analytically or numerically for $C^{i}_{Fe_2O_3}$ and then substituted back into Equation (6.68) to calculate $\dot{n}_{Fe_2O_3}$.

6.1.1.1.13.2 Mass Transfer Coefficients

In order to calculate $\dot{n}_{ZnO}$, $\dot{n}_{PbO}$, and $\dot{n}_{Fe_2O_3}$, it is necessary to calculate the mass-transfer coefficients: k_{ZnO}, k_{PbO}, $k_{Fe_2O_3}$. The method of calculation is identical to that of Richards.[1a] Since, as discussed previously, the secondary bubble behaves as a rigid sphere, the mass-transfer coefficients are characterized by Equations (6.13)-(6.15). The necessary physico-chemical data can be calculated from Equations (6.10)-(6.12). The diffusivities are those used by Richards. Due to a lack of data, the following assumptions have been made:

$$D_{ZnO} = D_{FeO} \quad \ldots (6.77)$$

$$D_{PbO} = D_{FeO} \quad \ldots (6.78)$$

$$D_{Fe_2O_3} = 0.1 D_{FeO} \quad \ldots (6.79)$$

D_{FeO} is assumed to be empirically characterized by the following equation for the self-diffusivity of iron in a $CaFeSiO_4$ melt over a temperature range of 1250 to 1540°C.[36]

$$\log D_{Fe^{2+}} = \log D_{FeO} = \frac{5450 \pm 620}{T} 5.93 \pm 0.37 \qquad (6.80)$$

where $D_{Fe^{2+}}$ is expressed in units of m^2/s.

6.1.1.1.14 Boudouard and Char-Steam Reactions

The last terms to evaluated in the char particle - slag reaction model are the rates of the Boudouard and char-steam reactions occurring on the char particle. From Skinner and Smoot[37], for a pulverized bituminous coal char (70% through -200 mesh), the rate of the Boudouard reaction is first order in the quantity of carbon left unreacted and the partial pressure of CO_2 as follows

$$\dot{B}_r = A_o^B \exp (E_a^B / RT) P_{CO_2} \qquad . . . (6.81)$$

where $A_o^B = 3.13 \times 10^6$ (kg mole kg mole^{-1} kPa^{-1} s^{-1})

$E_a^B = 196200$ (kJ kg mole^{-1})

As an addition to Richards[1a] model, the char-steam reaction has been included. Again from Skinner and Smoot[37], for a pulverized bituminous coal char, the rate of the char-steam reaction is first order in the quantity of carbon left unreacted and the

partial pressure of H_2O:

$$S = A_o^s \exp (E_a^s / RT) P_{H_2O} \quad \ldots (6.82)$$

where $A_o^s = 1.0 \times 10^6$ (kg mole kg mole^{-1} kPa^{-1} S^{-1})

$$E_a^s = 183739 \text{ (kJ kg. mole}^{-1}\text{)}$$

6.1.1.1.15 Model Solution

The resulting model is an initial-value problem in a system of thirteen ordinary differential equations. These were solved using a fourth order Runga-Kutta technique in double percision available through the UBC Computing Centre.

6.1.1.2 The Kinetics of Lead Removal

Having completed the addition of lead reduction to the char particle-slag reaction model, an interesting problem arises since mass balances on operating furnaces indicate that all of the lead reports to fume.[38] The question is how is the liquid lead removed from the furnace?

Within the context of the present model the liquid lead will be left behind after the gaseous contents of the secondary bubble are released to the furnace atmosphere. The resulting "lead prill" then will be carried back down into the bulk of the bath by slag motion. Thermodynamically the metallic lead will be unstable in the slag. It is proposed, therefore, that the lead prill will react with the slag via the following reaction:

$$Fe_2O_{3(sl)} + Pb_{(l)} = 2FeO_{(sl)} + PbO_{(sl)} \quad \ldots (6.83)$$

By this mechanism, the metallic lead prill is oxidized into the bulk of the slag where it can be re-reduced and removed, in part, as vapour. Obviously, as with the secondary bubble slag reactions, kinetics will play an important role in determining the rate at which oxidation will proceed. A lead prill-slag reaction model has been developed to account for these kinetics.

6.1.1.2.1 The Lead Prill-Slag Reaction Model

In order to simplify the mathematics involved, it is assumed that the metallic lead present in the furnace at any given time is in the form of spherical lead prills with an average radius, r_p^{Pb}.

Diffusion in the slag is assumed to be the rate-limiting step. This is not unreasonable since no mass-transfer need take place within the prill itself and, Reaction (6.83) should proceed rapidly at slag fuming temperatures. The resulting reaction system is shown schematically in Fig. 6.3.

6.1.1.2.1.1 Mass Balance on Liquid Lead

Liquid lead in the prill is consumed by oxidation at a rate equal to the mass - transfer rate of Fe_2O_3 in the slag. This establishes the rate of back oxidation of liquid lead per prill and, therefore, can be used to determine the overall rate of metallic lead oxidation within the furnace.

6.1.1.2.1.2 Mass Transfer

The mass-transfer rates of PbO, Fe_2O_3 and FeO can be characterized empirically by the following equations:

$$\dot{n}_{PbO} = k_{PbO,Pb} A_{Pb} [C^{i,Pb}_{PbO} - C^{sl}_{PbO}] \quad \ldots (6.84)$$

$$\dot{n}_{Fe_2O_3} = k_{Fe_2O_3,\,Pb} A_{Pb} [C^{sl}_{Fe_2O_3} - C^{i,Pb}_{Fe_2O_3}] \quad \ldots (6.85)$$

$$\dot{n}_{FeO} = k_{FeO,Pb} A_{Pb} [C^{i,Pb}_{FeO} - C^{sl}_{FeO}] \quad \ldots (6.86)$$

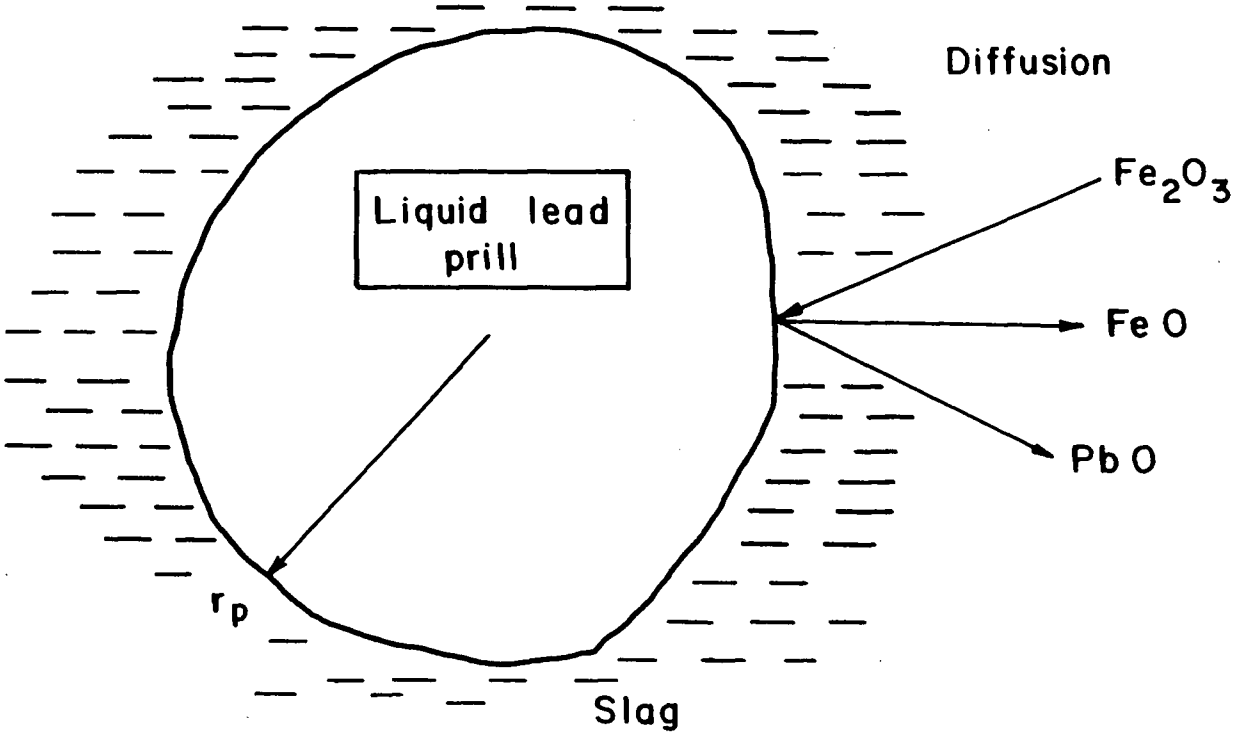

Figure 6.3 The lead prill-slag reaction system

From the stoichiometry of Equation (6.83) it follows that:

$$\dot{n}_{Fe_2O_3} = \dot{n}_{PbO} = -\frac{1}{2} n_{FeO} \quad \ldots (6.87)$$

and, from the assumption of local equilibrium at the prill-slag interface,

$$\frac{(C^{i,Pb}_{FeO})^2 \; C^{i,Pb}_{PbO}}{C^{i,Pb}_{Fe_2O_3}} = \frac{K_{6.78} \; \gamma_{Fe_2O_3}}{\gamma^2_{FeO}} \; \frac{(P^m_{sl})^2}{\gamma_{PbO}} \quad \ldots (6.88)$$

Combining Equations (6.84) - (6.88) and solving for $C^i_{Fe_2O_3}$ it can be shown that

$$0 = [\, D_9 - (D_7)\, C^{i,Pb}_{Fe_2O_3} \,]^2 \; [\, D_{10} - D_8\, (C^{i,Pb}_{Fe_2O_3})] - C^i_{Fe_2O_3} (D_{11}) \quad \ldots (6.89)$$

where

$$D_7 = \frac{2k_{Fe_2O_3}}{k_{FeO}} \quad \ldots (6.90)$$

$$D_8 = \frac{k_{Fe_2O_3}}{k_{PbO}} \quad \ldots (6.91)$$

$$D_9 = D_7\, (C^{sl}_{Fe_2O_3}) + C^{sl}_{FeO} \quad \ldots (6.92)$$

$$D_{10} = D_8\, (C^{sl}_{Fe_2O_3}) + C^{sl}_{PbO} \quad \ldots (6.93)$$

$$D_{11} = \frac{K_{6.78} \; \gamma_{Fe_2O_3} \; (P^m_{sl})^2}{\gamma^2_{FeO} \; \gamma_{PbO}} \quad \ldots (6.94)$$

Equation (6.89) can be solved analytically or numerically for $C^i_{Fe_2O_3}$. The resulting value of $C^i_{Fe_2O_3}$ then can be substituted

into Equation (6.85). Only the mass-transfer coefficients remain be determined.

6.1.1.2.1.3 Mass-Transfer Coefficients

On the basis that the lead prills behave as rigid spheres in creeping flow, the mass-transfer coefficients, k_{PbO}, k_{FeO}, and $k_{Fe_2O_3}$, are characterized empirically by Equations (6.13)-(6.15). The necessary physico-chemical data can be calculated from Equations (6.10) - (6.12). Diffusivities are the same as those used in the char-particle slag reaction model.

6.1.2 The Furnace Model

The calculation of the secondary bubble residence time, the kinetics of the tuyere gas column, and the characterization of the melting and freezing of slag on the furnace walls and bottom are unchanged by the incorporation of lead reduction. Thus the interested reader is referred to the original mathematical model of Richards[1a] for the treatment of this material.

The overall furnace heat and mass balances must be modified to account for the reduction of lead. These modifications are largely a book keeping exercise and will not be discussed. For a general review of the mathematics involved in the overall furnace

heat and mass balances the reader is referred to the original treatment of Richards.

6.2 Discussion of Model Fitting

Before the model could be applied to analyze the high-pressure coal injection trials, it was necessary to fit it to a run typical of normal fuming practice for the Cominco No. 2 furnace. There were two main reasons for this: firstly, to elucidate the effect that the addition of lead reduction has on model predictions, and secondly, to determine the fraction of low-pressure coal entrained in the slag. The latter was necessary in order to provide a basis for the calculation of entrainment factors for the high-pressure coal.

The procedure adopted was to adjust F_{LPCE}, F_{LPCC} and F_{oxy} until good agreement was obtained between measured and predicted profiles of bath composition and temperature. F_{LPCE} is defined as the fraction of low-pressure coal entrained, F_{LPCC} is the fraction of low-pressure coal combusted; and F_{oxy} is the fraction of remaining oxygen which oxidizes ferrous iron (the remaining oxygen is defined as that portion of the total input oxygen which is unconsumed by coal combustion.)

Within the computer program, values for F_{LPCE}, F_{LPCC}, and F_{oxy} can be input for each set of operating conditions (coal rate

and secondary blast rate). Therefore, for those runs where there is a variation in operating conditions, it is possible to have a corresponding variation in the primary fitting parameters. In this way, the best possible fit for a given set of operating conditions can be obtained.

Three low-pressure runs, two of which have been previously analyzed by Richards [1a], were available for analysis. The model was fitted to all three runs; however, only the results for the run not previously analyzed by Richards[1a] will be presented for discussion. It is felt that the other two runs were not indicative of normal operation and, therefore, do not warrant detailed discussion.

6.2.1 Results of Fit to Normal Operation

The results of fitting the model to a "normal" run are presented in Figs. 6.4-6.6 The predicted values for the primary fitting parameters, F_{LPCE}, F_{LPCC} and F_{oxy} are summarized together with the predicted furnace oxygen utilization in Table 6.2. For the purpose of comparison, the results of the original analysis of the process by Richards also have been presented in Table 6.2.

It should be mentioned that the inclusion of lead reduction has necessitated the use of two additional fitting parameters: the average radius of the lead prills (r_p^{Pb}), and the initial

TABLE 6.2

Model Fitting Parameters

	Normal Operation	Run 1	Run 2	Run 3
Fraction of low-pressure coal entrained (Richards)	0.2-0.32 (0.29)	0.27	0.27	0.27
Fraction of high-pressure coal entrained	-	0.75*	0.65	0.90
Fraction of low-pressure coal combusted (Richards)	0.40-0.65 (0.54)	0.50-0.54	0.70-0.50	0.70
Fraction of high-pressure coal combusted	-	0	0	0
Fraction of uncombusted oxygen to ferrous iron oxidation (Richards)	0.03-0.30 (0.04)	0.15-0.50	0.75-0.10	0.55-0.30
Radius of Pb prill (m)	1×10^{-3}	1×10^{-3}	1×10^{-3}	1×10^{-3}
Initial fraction of Pb as metal	0.10	0.10	0.90	0.50
Slag circulation velocity (m/sec) (Richards)	3 (1)	3	3	3
Predicted oxygen utilization	0.55-0.75	0.62-0.85	0.65-0.95	0.78-0.92

*This value was obtained using a term to account for the melting of zinc-rich material at a rate of 0.3×10^{-2} kg mole Zn/s

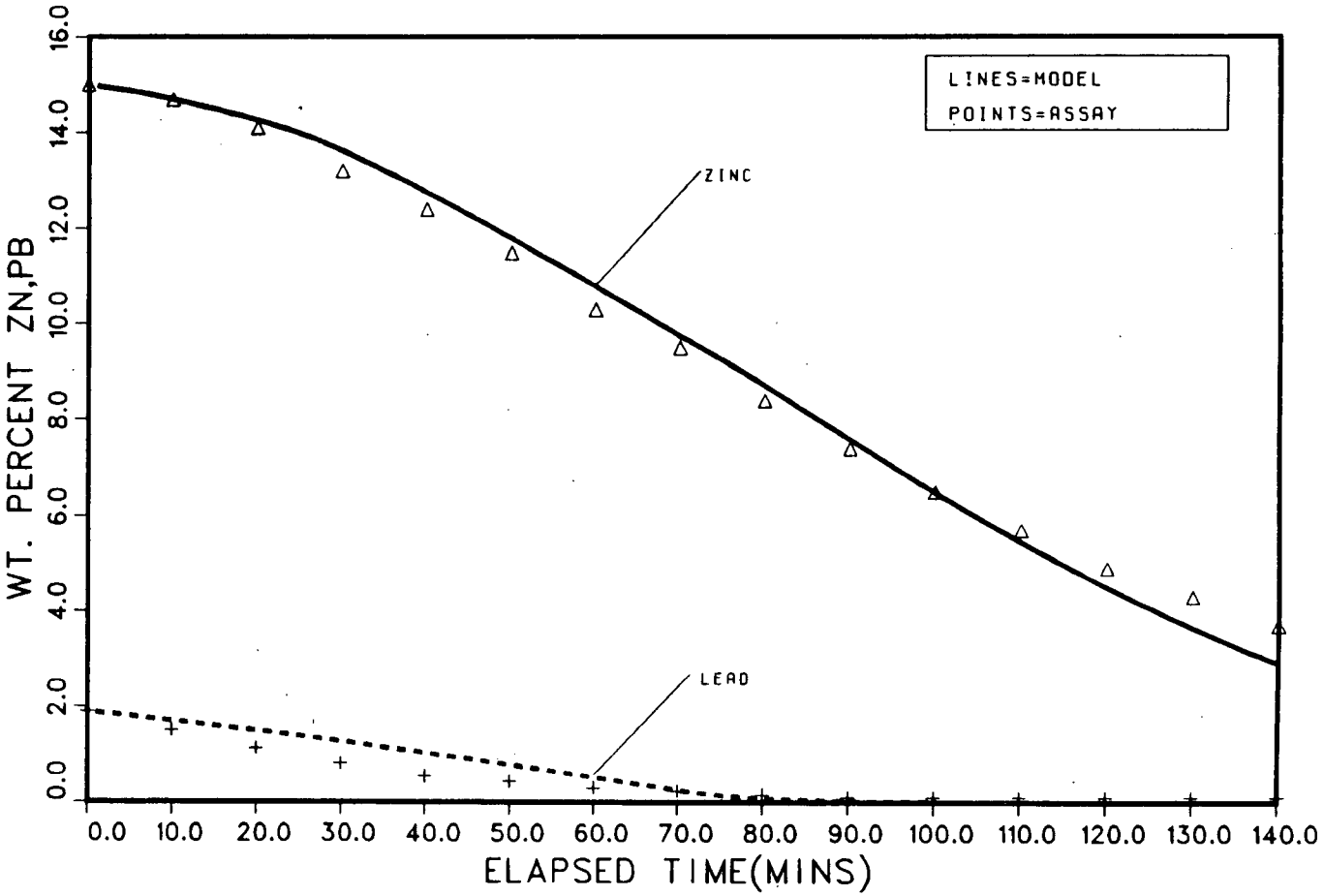

Figure 6.4 Industrial data and model fit to the Zn and Pb profiles for normal operation

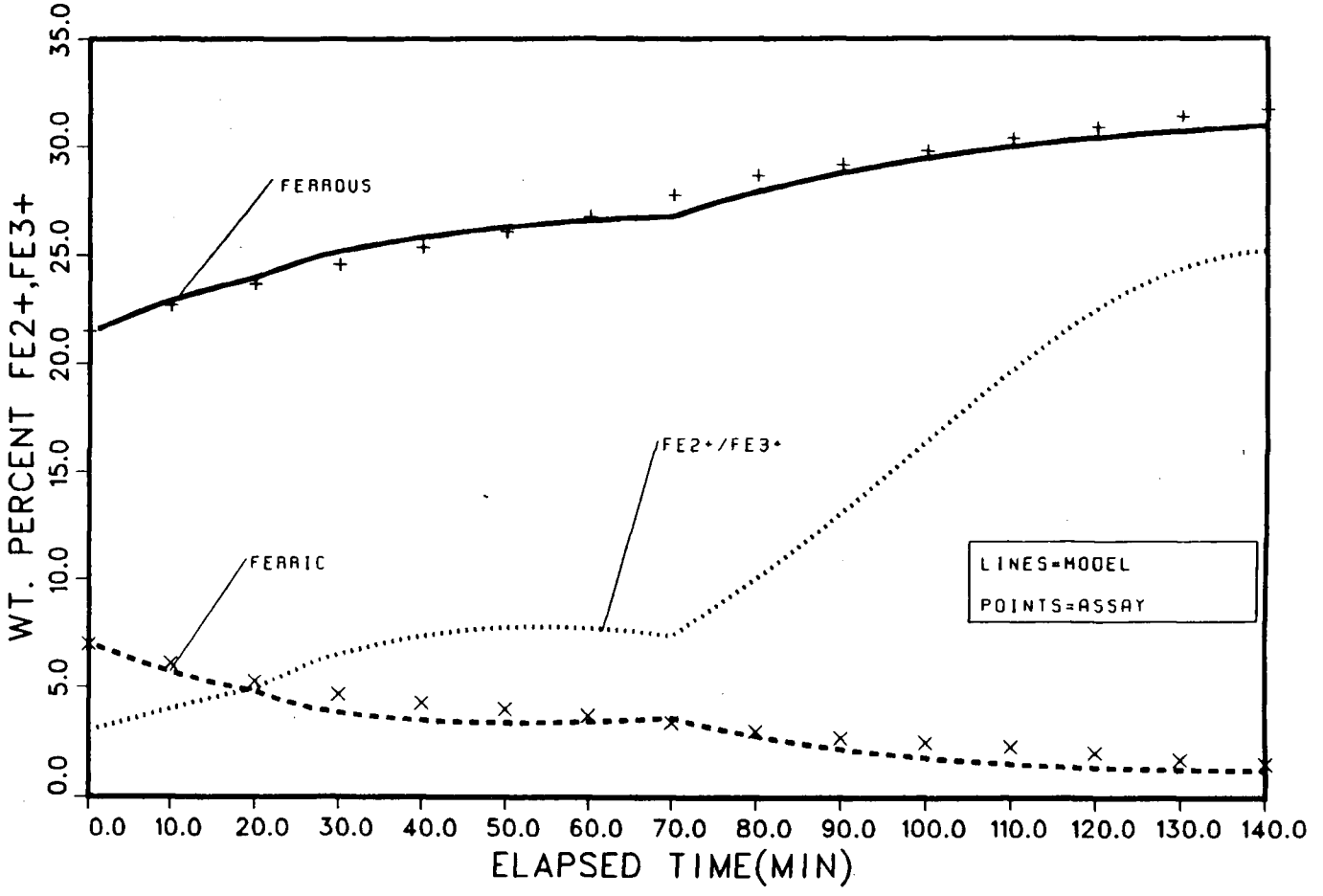

Figure 6.5 Industrial data and model fit to the Fe^{2+} and Fe^{3+} profiles for normal operation

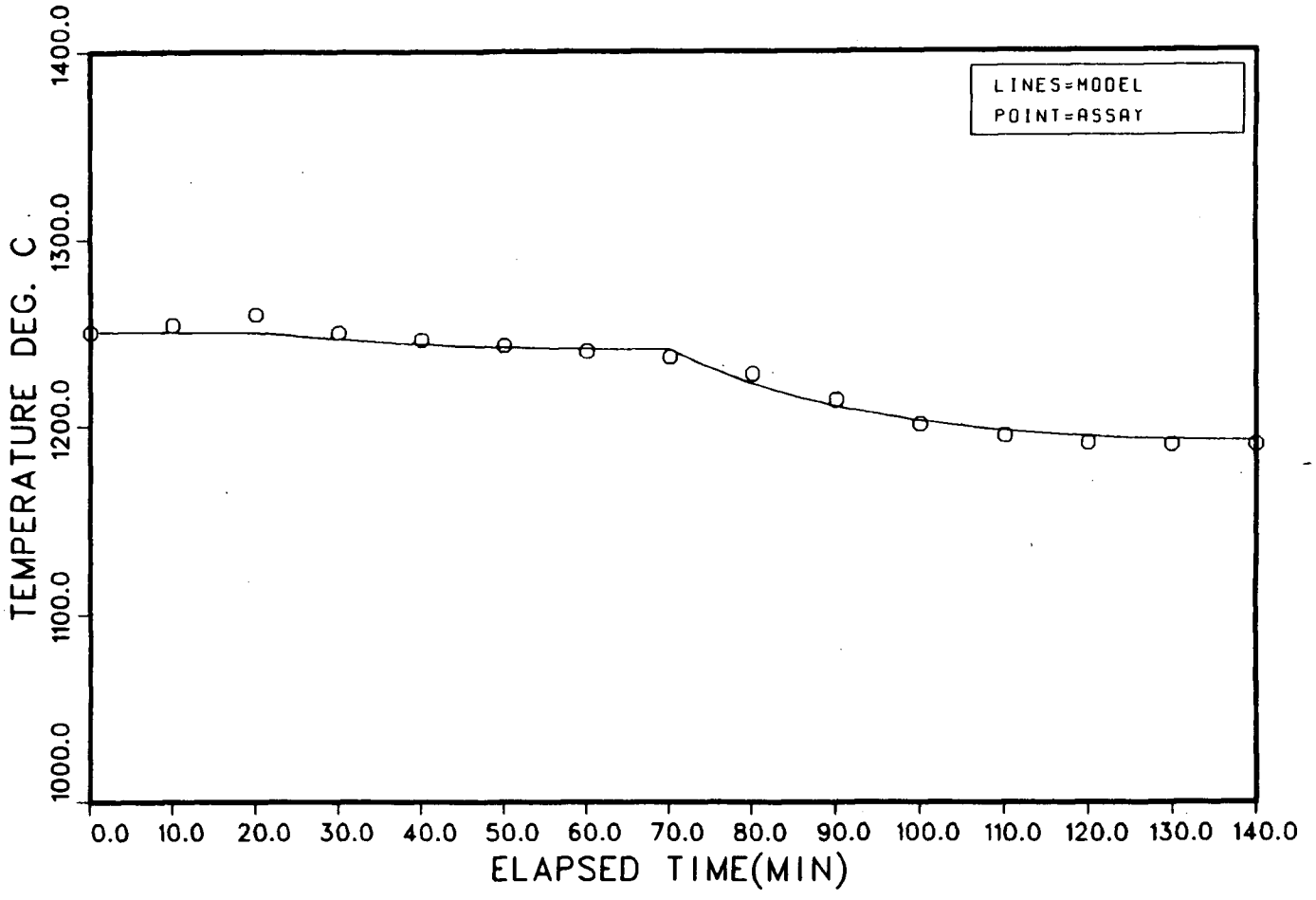

Figure 6.6 Industrial data and model fit to the temperature profile for normal operation

fraction of metallic lead F_{PBL}. The latter of these was deemed necessary since a significant portion of the lead charged to the furnace may be present in metallic form.[39] The values for r_p^{Pb} and F_{PBL} are also provided in Table 6.2.

6.2.1.1 Discussion of Fit to Normal Operation

The fit of model prediction to measurement is reasonably good, see Figs. 6.4-6.6. It should be noted, however, that all three primary fitting parameters have had to be varied over the course of the run (0.23 to 0.37 F_{LPCE}, 0.38 to 0.65 F_{LPCC} and 0.03 to 0.32 F_{oxy}), see Table 6.2. Unfortunately, on the basis of one run, it is difficult to speculate on the implications of these variations. For example, the higher entrainment factor of 0.37 (0-20 mins. elapsed time) could indicate that the model is underestimating zinc fuming rates under oxidizing conditions; and/or the lower entrainment factor of 0.23 (20-40 mins. elapsed time) could suggest the model is overestimating fuming rates under reducing conditions. Moreover, since the predicted changes in F_{LPCE} are coincident with changes in coal rate it could also be a real effect. Not surprisingly, the same holds for the variations in F_{LPCC} and F_{oxy} - there is the possibility that their behaviour could be the result of weaknesses within the model, real effects, or some combination of the two.

Having stated this, it appears that there is little alternative other than to assume an average value for F_{LPCE} which can be adopted in the analysis of the high-pressure data. Therefore, for all subsequent analysis F_{LPCE} is set equal to 0.30.

If the results of this fitting exercise are compared to the previous finding of Richards[1a] (see Table 6.2) some interesting observations can be made. Firstly, it is immediately obvious that there is a significant difference in the slag circulation velocities employed in the two models - 3m/s in the present model as compared to 1m/s in the Richards model. Clearly, this is a significant difference and as such warrants some justification. This will be postponed until a sensitivity analysis can be completed. Secondly, there is a remarkable consistency between the values predicted for coal utilization (F_{LPCE} and F_{LPCC}) with the two models, see Table 6.2. This continues to lend soundness to the kinetic foundations on which both models are based, ie. the partitioning of coal into reductant and source of heat.

Having completed fitting the model to normal operation it is now possible to fit the model to the high-pressure trials. As mentioned previously, the value of F_{LPCE} is set equal to 0.30 for this exercise.

6.2.2 Results of Fit to High-Pressure Operation

The results of fitting the model to the high-pressure operation, Runs 1-3, are presented in Figs. 6.8-6.19. The predicted values for the primary fitting parameters F_{LPCE}, F_{HPCE}, F_{LPCC} and F_{oxy} are summarized together with the predicted oxygen utilization in Table 6.2 (F_{HPCE} is defined as the fraction of high-pressure coal entrained in the slag). A summary of the values for the secondary fitting parameters r_p^{Pb} and F_{PBL} also are presented in Table 6.2.

Before proceeding with an assessment of the influence of high-pressure injection on coal entrainment, it is necessary to discuss the ability of the model to be fitted to each of the three high-pressure trials. This will help in establishing the validity of the results of the model analysis.

6.2.2.1 Discussion of Fit to High-Pressure Operation

In all three runs the model predictions are seen to fit the measurements quite well, see Figs. 6.8-6.19. The zinc concentration profiles, however, are the least satisfactory. In Run 1, the model was initially unable to account for the low fuming rate. The most likely explanation is that zinc rich material was melting in the furnace throughout the run. This is

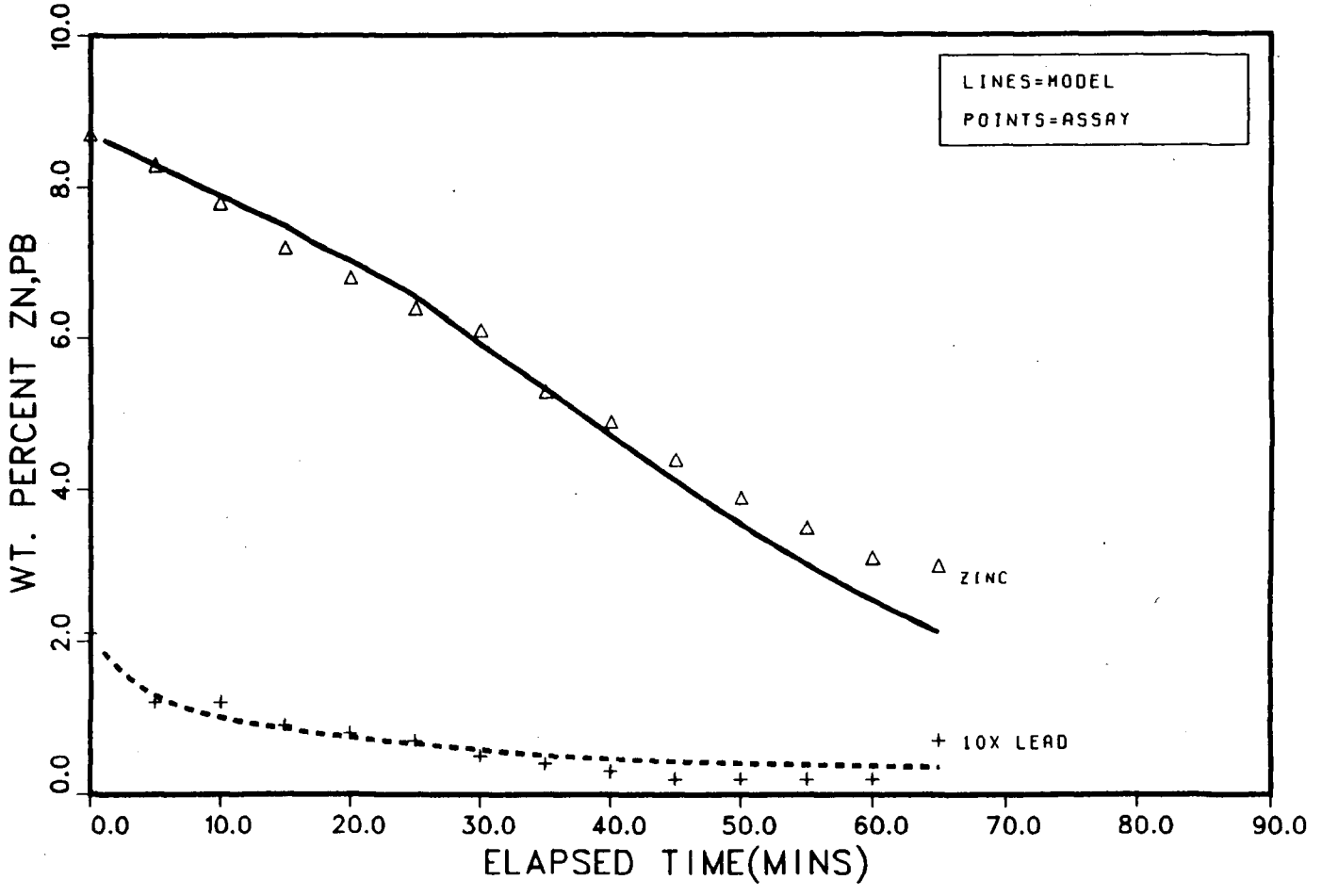

Figure 6.7 Industrial data and model fit to the Zn and Pb profiles for Run 1

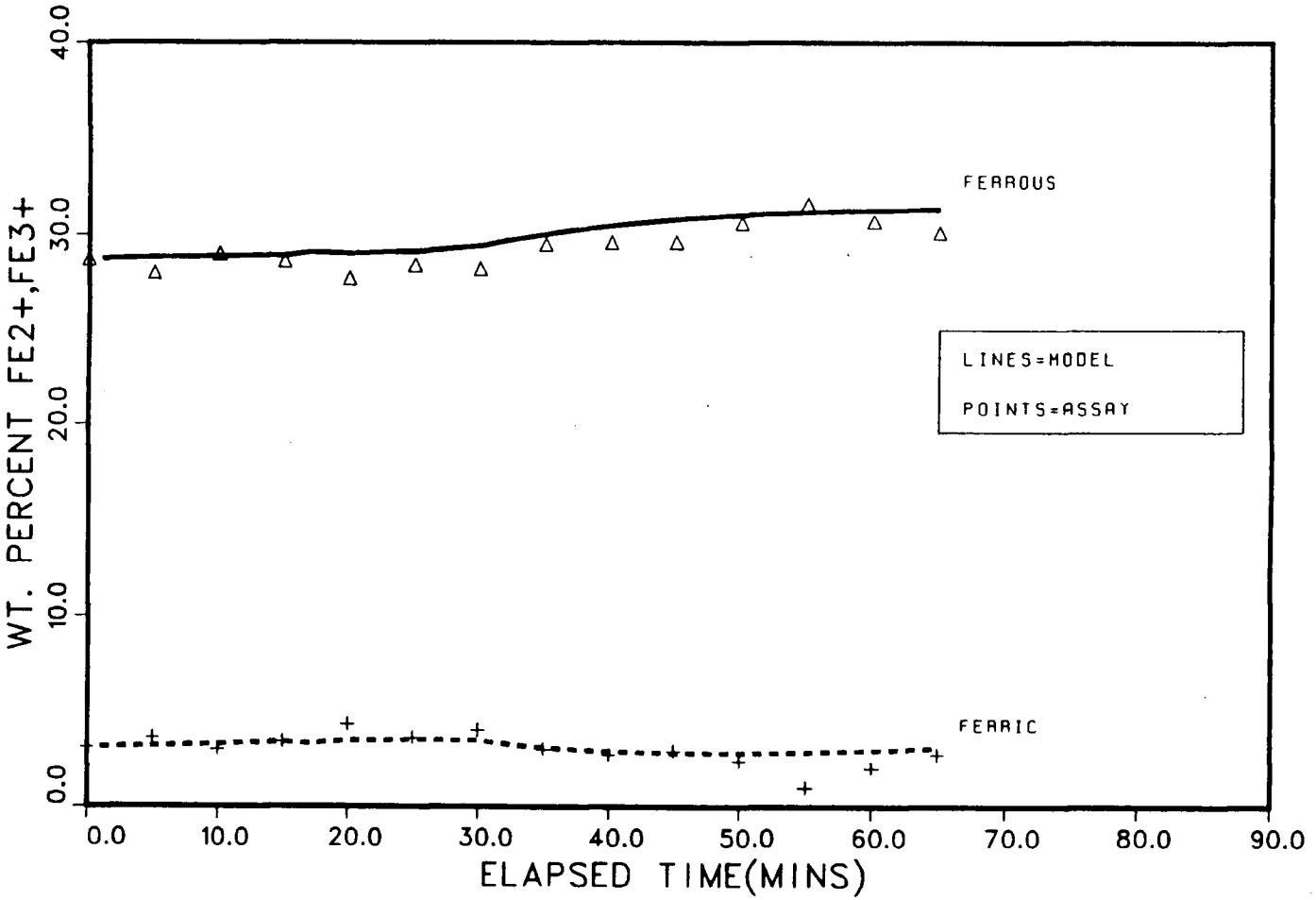

Figure 6.8 Industrial data and model fit to the Fe^{2+} and Fe^{3+} profiles for Run 1

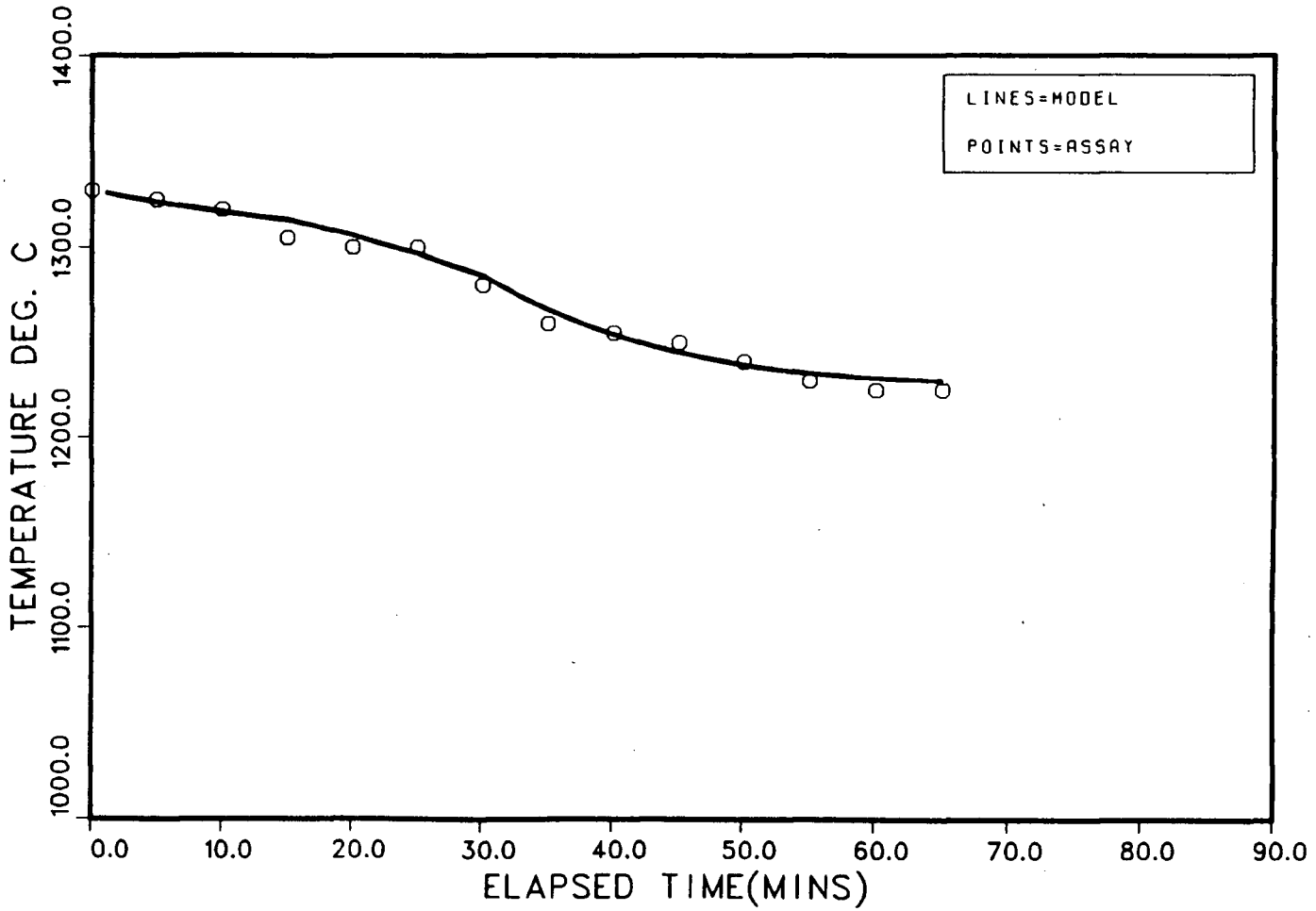

Figure 6.9 Industrial data and model fit to the temperature profile for Run 1

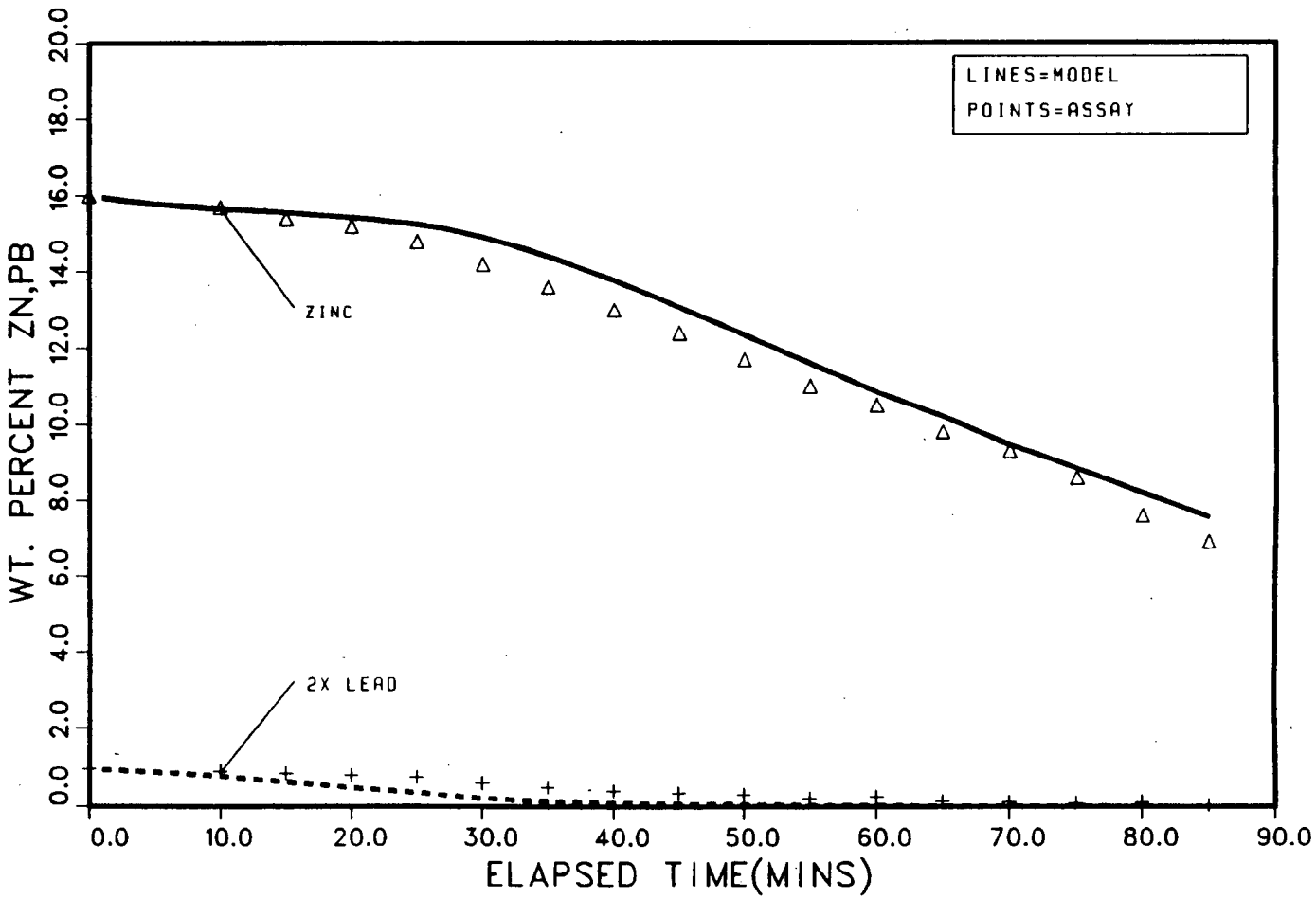

Figure 6.10 **Industrial data and model fit to the Zn and Pb profiles for Run 2**

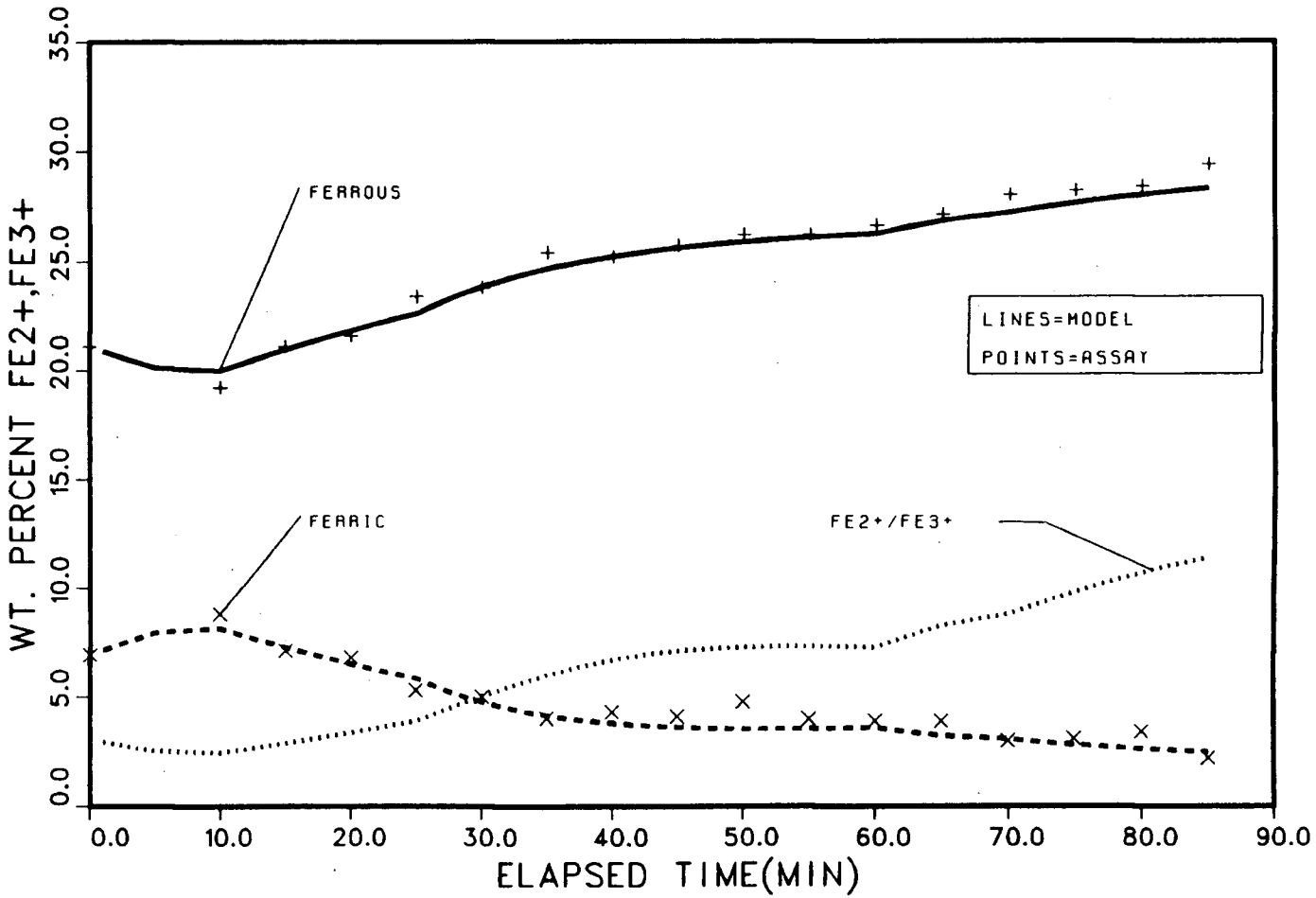

Figure 6.11 Industrial data and model fit to the Fe^{2+} and Fe^{3+} profiles for Run 2

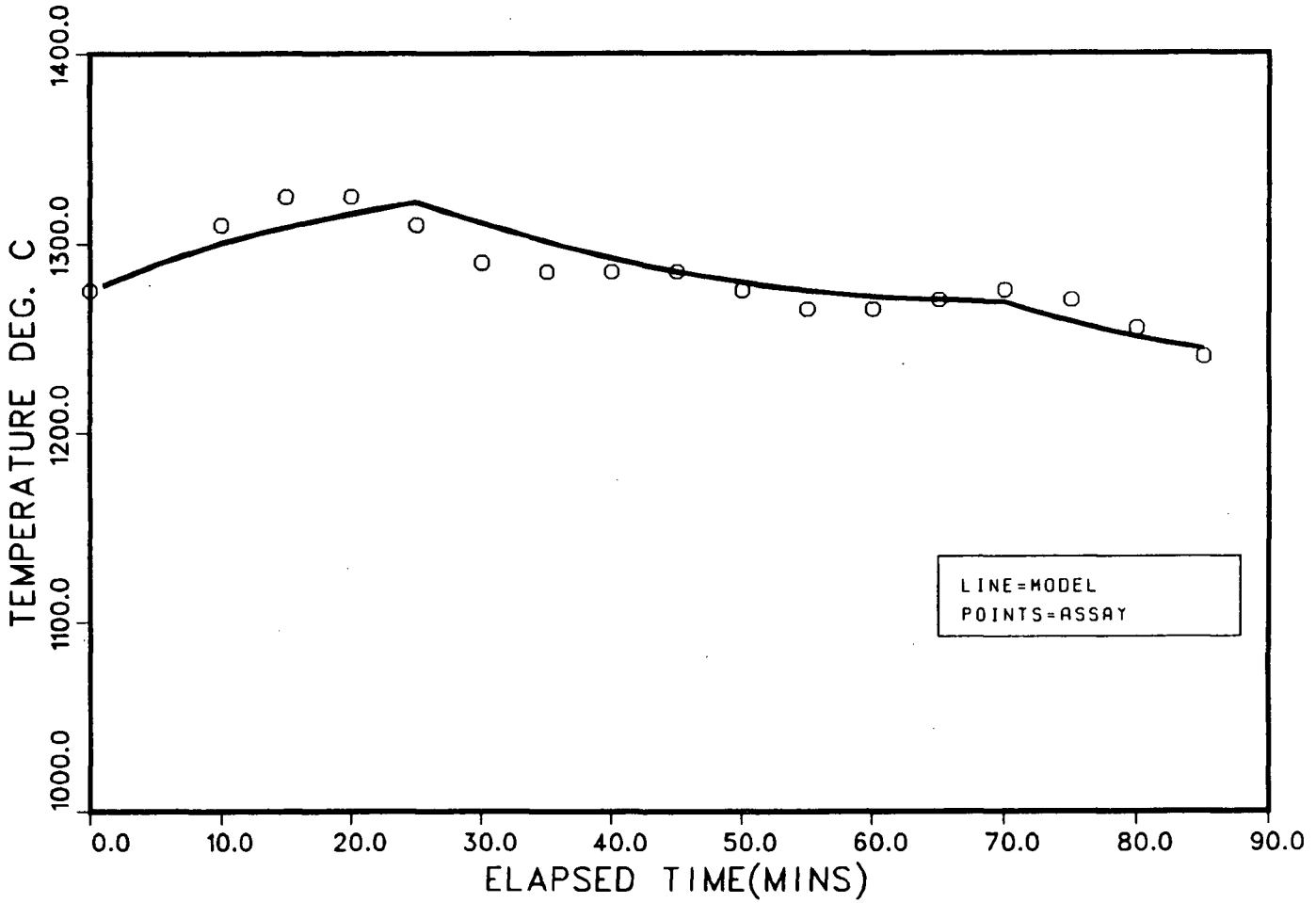

Figure 6.12 Industrial data and model fit to the temperature profile for Run 2

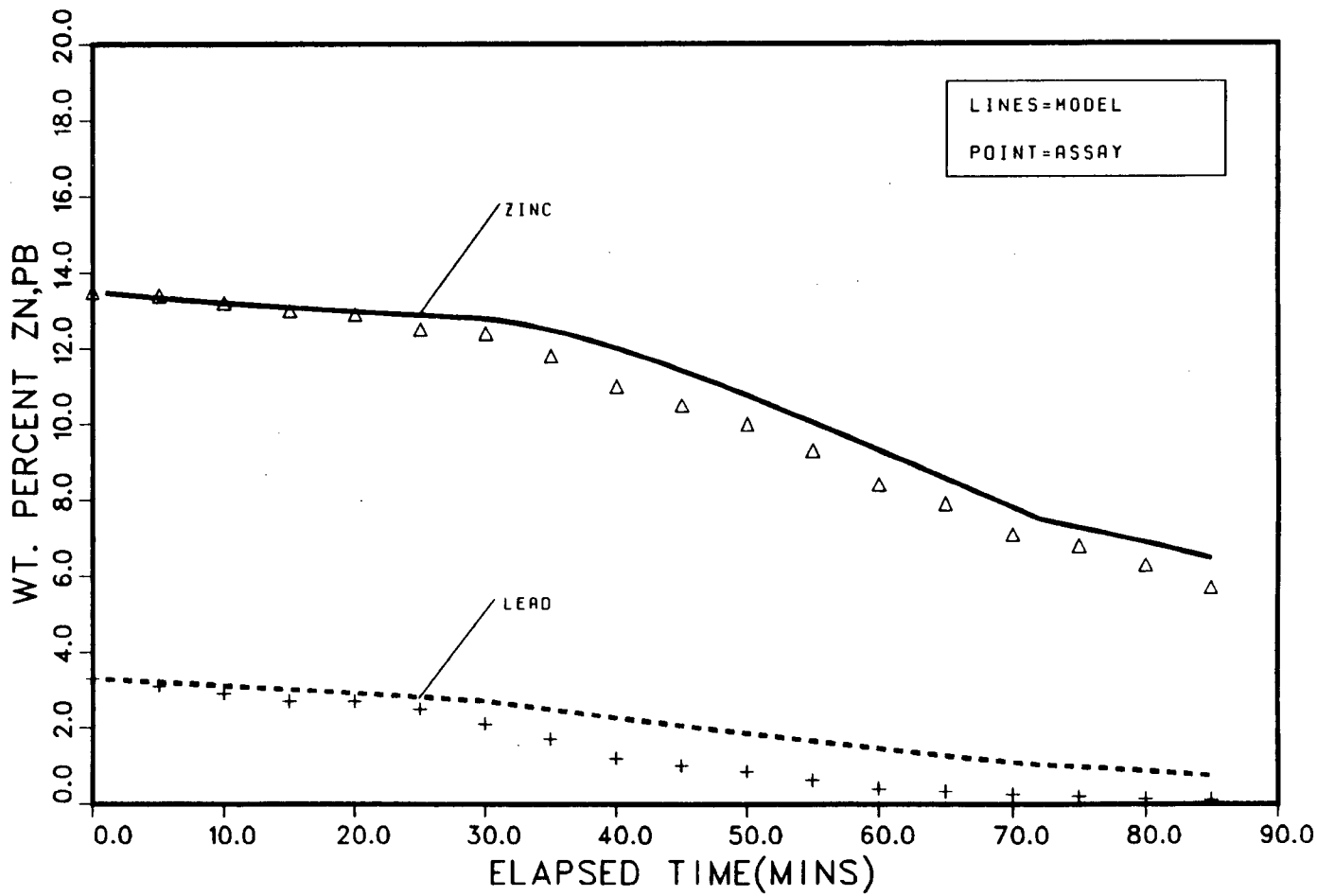

Figure 6.13 Industrial data and model fit to the Zn and Pb profiles for Run 3

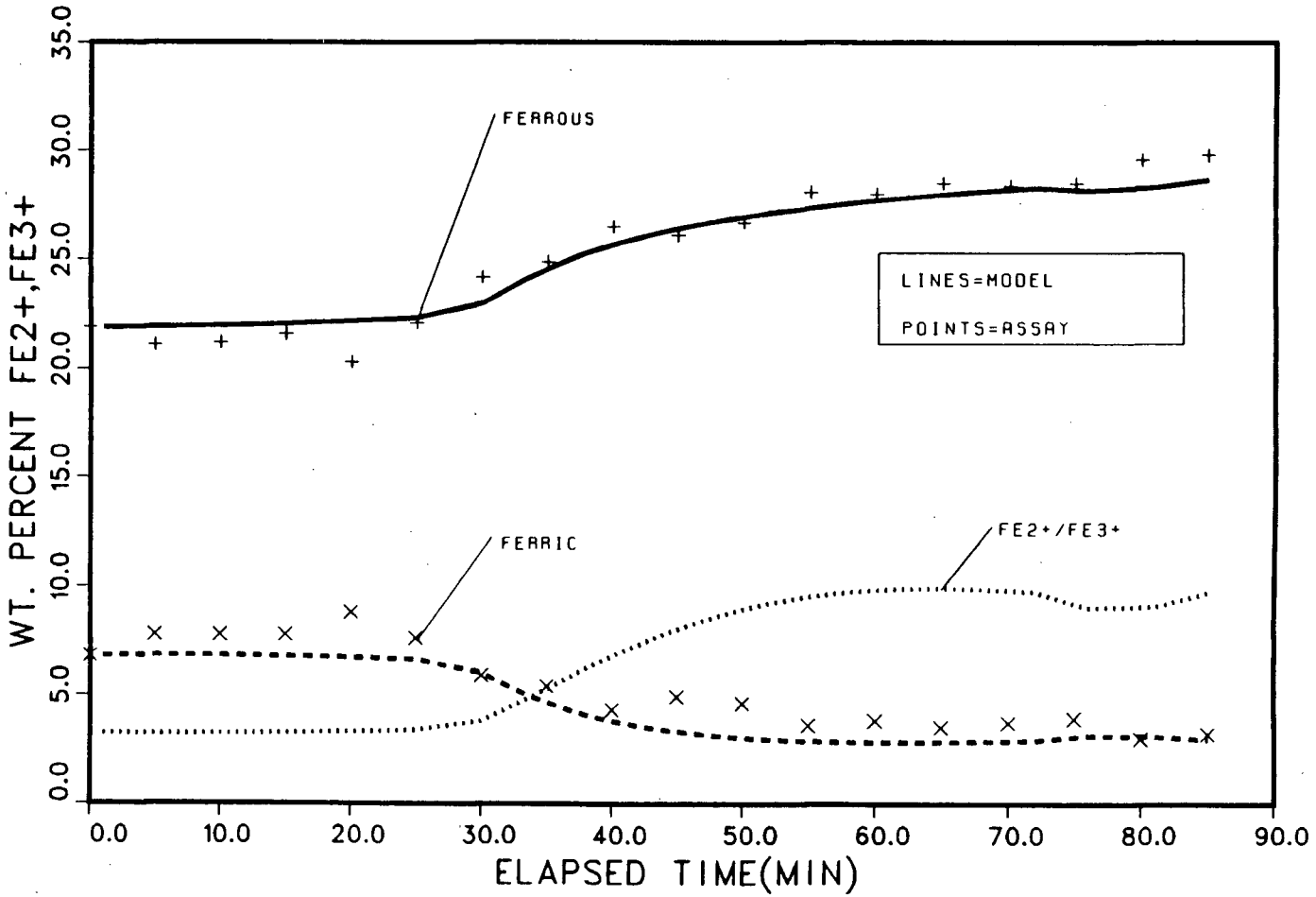

Figure 6.14 Industrial data and model fit to the Fe^{2+} and Fe^{3+} profiles for Run 3

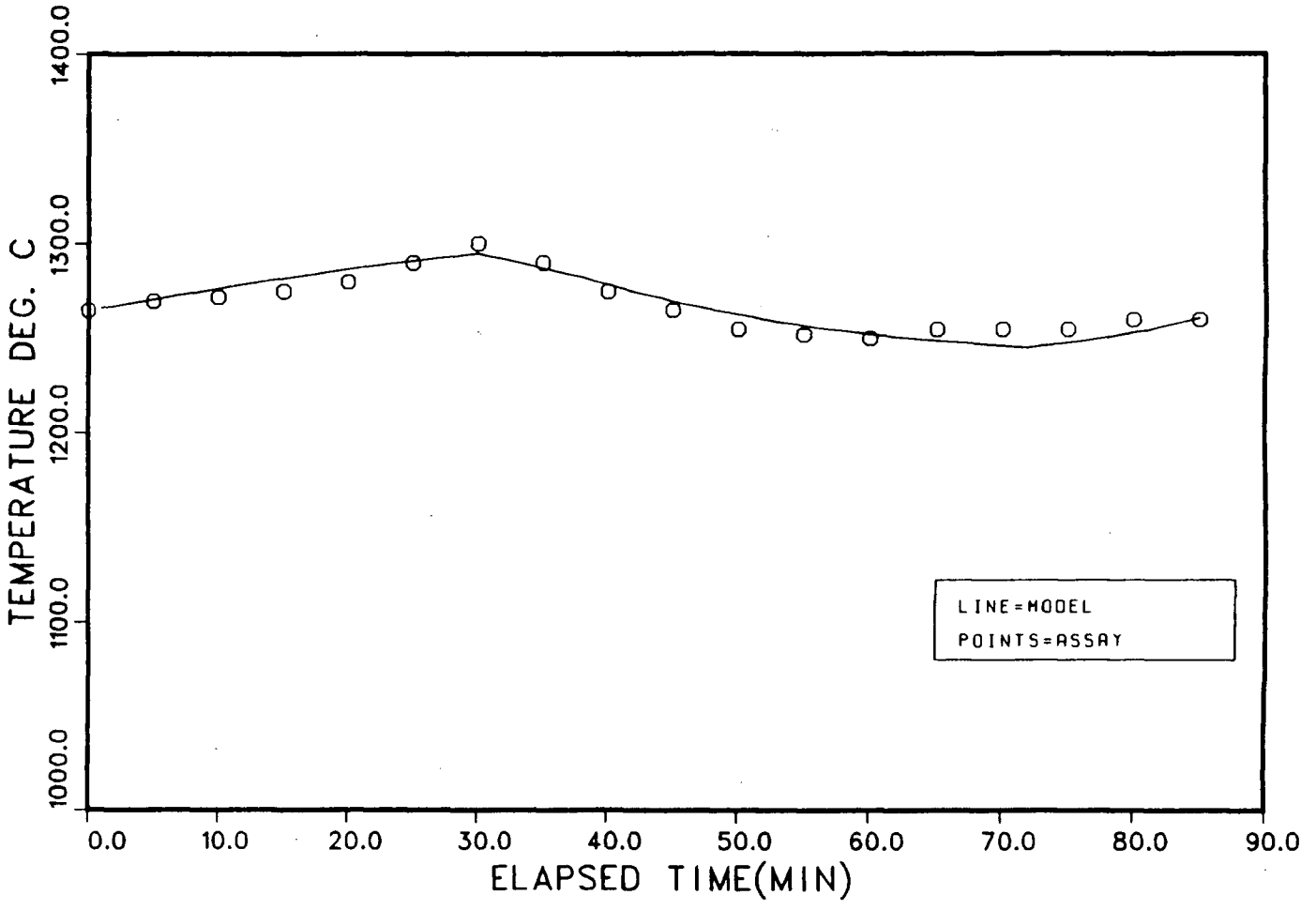

Figure 6.15 **Industrial data and model fit to the temperature profile for Run 3**

consistent with both the charge make-up, 50:50 hot-cold, and averaged plant data which indicates a decrease in the measured fuming rate for cold charges (see Chapter V).

Assuming this explanation to be correct, a term was added to the model to account for the introduction of zinc into the bath. A value of 0.75 for F_{HPCE} was assumed for Run 1 (value arrived at from the results of model analysis of Runs 2 and 3) and the model was fitted to the zinc profile, see Fig. 6.7, by adjusting the melt rate of zinc into the bath. Justification for the introduction of this term is that the average predicted fuming efficiency is increased from 0.77 to 0.92 (Kg Zn + Kg Pb)/Kg coal which is more in line with that predicted for Runs 2 and 3, 1.2 and 1.4 (Kg Zn + Kg Pb)/Kg coal respectively. This is consistent with the theory originally proposed in Chapter V that the act fuming efficiency (equivalent to predicted) and the apparent fuming efficiency (that based on assays) will be different under conditions when the melting of zinc-rich material is occurring.

If the zinc profiles of Runs 2 and 3 are considered, a different weakness in the model is evident, see Figs. 6.10 and 6.13, respectively. The model is unable to account for the observed fuming rates during periods of transition from oxidizing to reducing conditions (0-30 minutes elapsed time in both runs). This behaviour is consistent with what was observed in fitting the model to normal operation, see Fig. 6.4. Therefore, it

appears that the model, in general, has a tendency to underestimate fuming rates (by approximately 1 wt% in Runs 2 and 3) under conditions when the bath concentration of ferric iron is relatively high. There are several possible explanations for this behaviour including for example, an incorrect activity coefficient of Fe_2O_3 in the slag. It is difficult to assess the validity of this,or any other explanation, owing to the complexity of the mathematical model. Therefore, discussion will have to be left until a sensitivity analysis can be completed.

It should be noted that both F_{LPCC} and F_{oxy} have had to be varied over the course of the three runs in order to fit the Fe^{2+}/Fe^{3+} and temperature profiles (F_{LPCC}: 0.5 Run 1, 0.5 - 0.7 Run 2 and 0.68 to 0.70 Run 3; F_{oxy}: 0.15-0.5 Run 1, 0.1-0.75 Run 2 and 0.30-0.50 Run 3), see Table 6.2. This behaviour is consistent also with the results of fitting the model to normal operation. Moreover, it is interesting to note that the resulting values for oxygen utilization decrease with decreasing bath temperature. To assess the correlation on a run-to-run basis, a plot of predicted oxygen utilization versus temperature was made, see Fig. 6.16. Linear regression of the data for the three high-pressure runs and the normal operation run yields a correlation coefficient of r=0.85. To determine which of the two parameters, $F_{LPCC}$and/or F_{oxy}, are responsible for this trend, plots of both F_{LPCC} and F_{oxy} versus temperature were made, see Figs. 6.17 and 6.18, respectively. Based on this, it appears

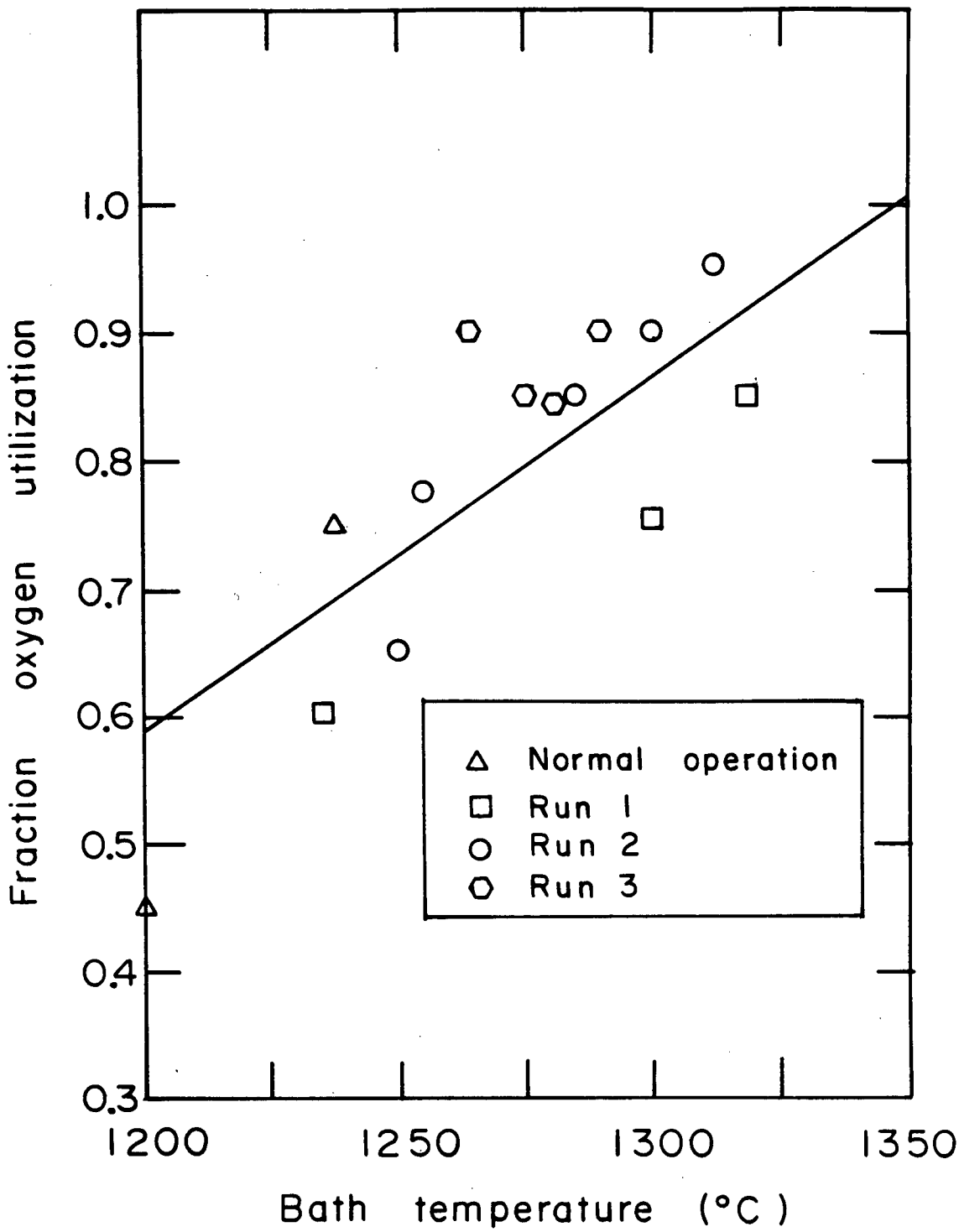

Figure 6.16 Predicted oxygen utilization as a function of bath temperature

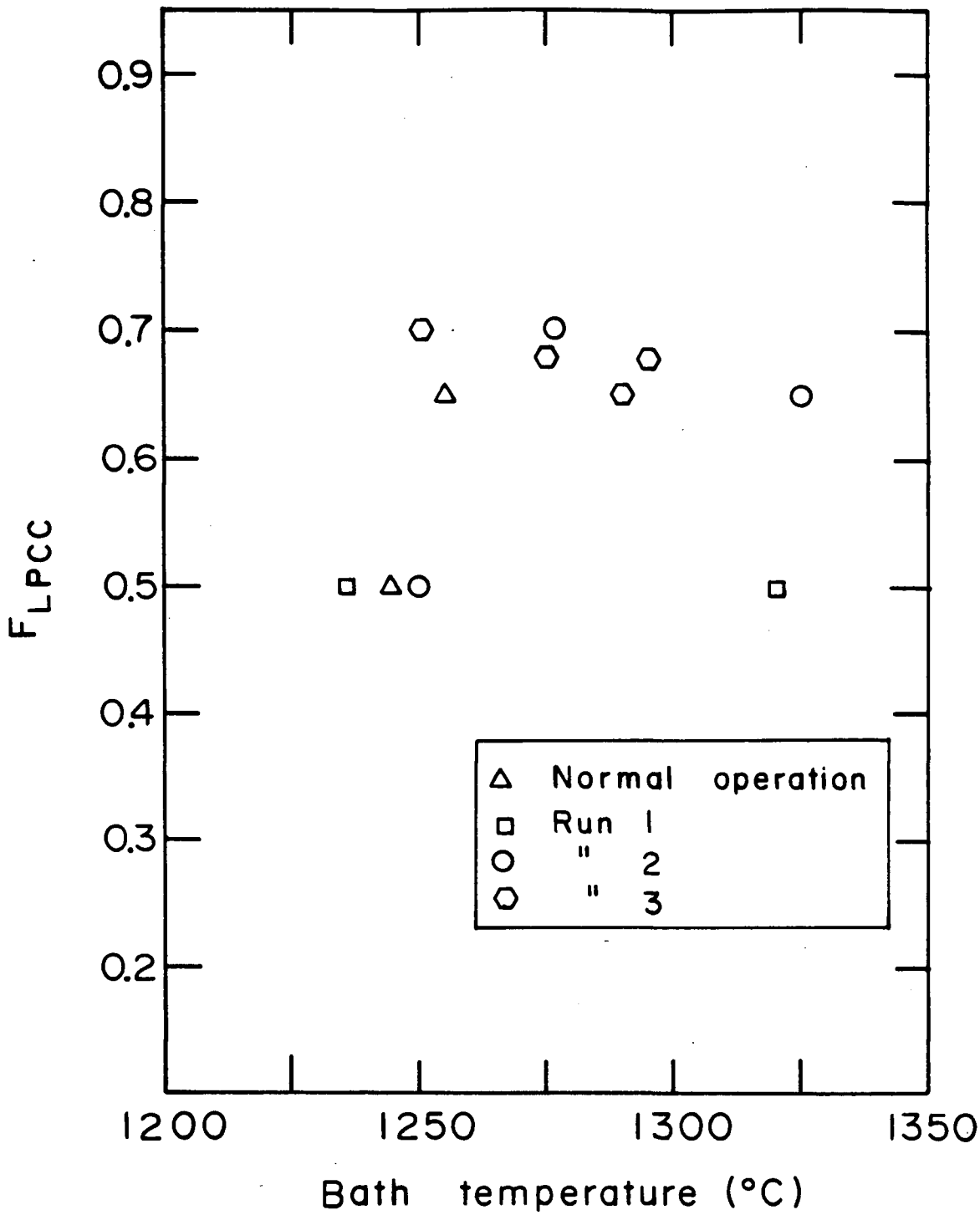

Figure 6.17 F_{LPCC} as a function of bath temperature

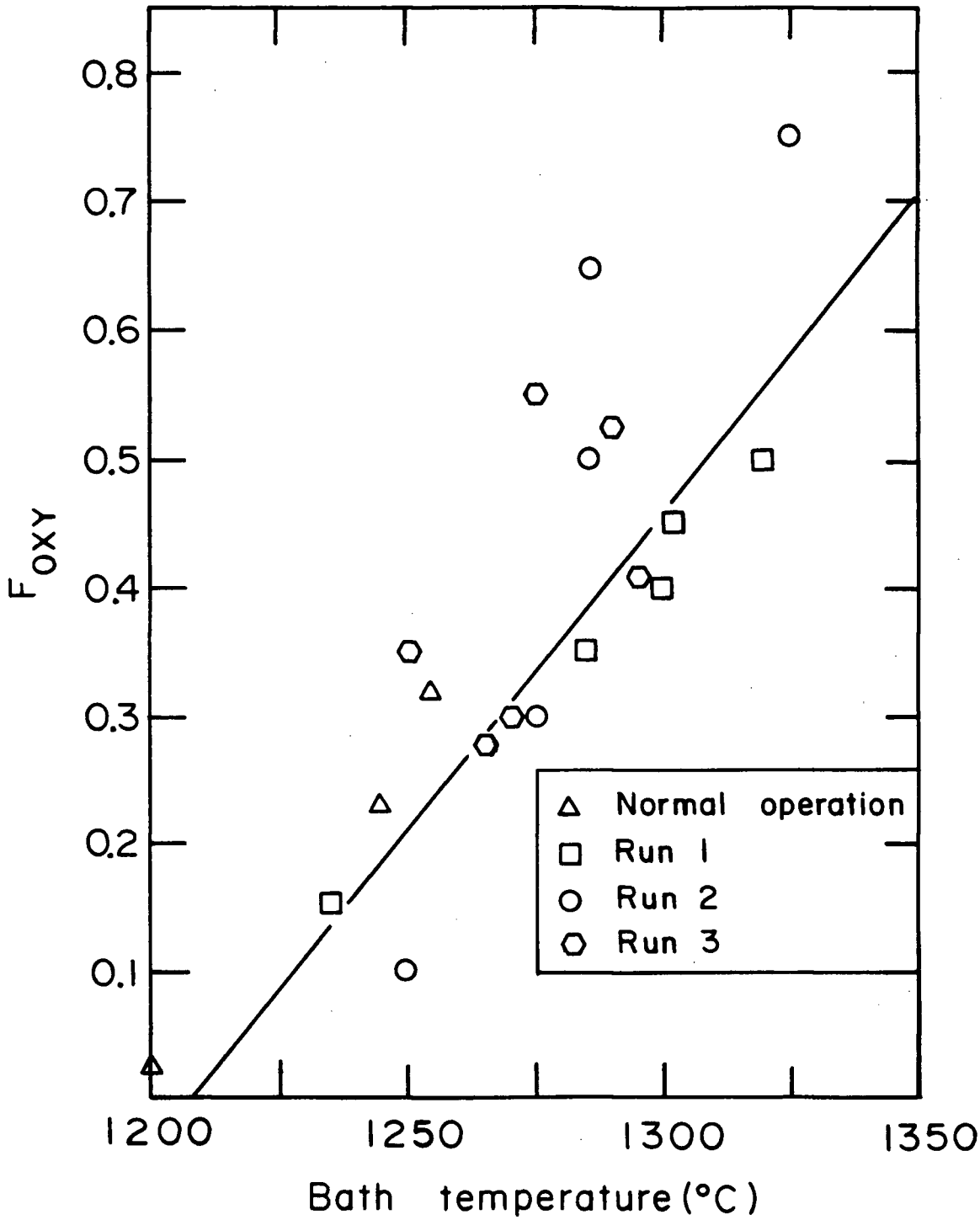

Figure 6.18 F_{oxy} as a function of bath temperature

that the rate of oxidation of ferrous iron (established by F_{oxy}) is sensitive to bath temperature. One possible explanation is that the kinetics of this reaction are sensitive to bath temperature. For example, an increase in bath viscosity resulting from a decrease in bath temperature could cause an increase in the average diameter of the bubbles in the tuyere gas column and, therefore, a reduction in mass-transfer. If this is the case, the kinetics of tuyere gas oxidation of ferrous iron also should be sensitive to bath depth. This trend was observed in the original investigation of the process by Richard et al.[1a,b] Unfortunately, there is a lack of enough experimental data to either confirm or refute their findings.

Having completed a discussion of the model analysis of the high-pressure trials data, it is now possible to assess the influence of high-pressure injection on coal entrainment - the essence of this study.

6.2.2.2 Fit to High-Pressure Operation: Entrainment Factors

Predictions for the high-pressure coal entrainment factors indicate a significant improvement in entrainment, see Table 6.2. Predicted values for F_{HPCE} are 0.75, 0.70 and 0.90 for Runs 1,2 and 3 respectively. It is felt that these valves are reasonable since predictions for fuming rates during those periods of uniform high-pressure injection agree well with furnace behaviour. The value for Run 1, however, is suspect in light of

the addition of a term to account for the melting of zinc-rich material. The difference in the values predicted for Runs 2 and 3 is believed to be due to a combination of the greater bath depth (mass) and the lower high-pressure coal rate in Run 3. It is reasoned that this combination acted to reduce the portion of high-pressure coal stripping through the bath unconsumed.

CHAPTER VII

SENSITIVITY ANALYSIS

For reasons stated previously, it was necessary to modify the Richards[1a] kinetic model to include the reduction and removal of lead prior to the model being fitted to the industrial data from the high-pressure trials. This modification has necessitated the use of parameters whose values can only be estimated. Consequently, it was necessary to establish the sensitivity of the model to these parameters. In addition, the sensitivity analysis was necessary to aid in identifying any potentially significant kinetic phenomena within the process.

To carry out the sensitivity analysis, operational data from the normal low-pressure run previously analyzed in Chapter VI was used as a standard. The data from this run are presented in Table 7.1

7.1 Sensitivity Analysis: Results

The sensitivity of the original model to parameters central to the kinetic conception of the process has been demonstrated previously.[1a,b] Therefore, the sensitivity analysis of the modified model focussed only on the parameters related to the kinetics of lead reduction and removal from the bath. These

TABLE 7.1

Standard Conditions for Sensitivity Analysis

Operating Parameters:

F_{LPCE} = 0.23 - 0.37

F_{LPCC} = 0.40 - 0.65

F_{OXY} = 0.03 - 0.32

F_{PBL} = 0.10

r_p^{Pb} = 1×10^{-3} m

Furnace Dimensions:

L = 8.00 m W = 3.10 m

Injection Dynamics:

Slag Circulation Velocity	= 3.0 m/s
No. Tuyeres	= 74
Bubble Frequency	= 6 s^{-1}
Tuyere Coluan Vord Fr.	= 0.600

Boudouard Reaction:

A_o = 3.13×10^6 $kPa^{-1}S^{-1}$

E_a = 196200 kJ $kg.mole^{-1}$

Char-steam Reaction:

A_o = 1.0×10^6 $kPa^{-1}S^{-1}$

E_a = 183739 kJ $kg.mole^{-1}$

Slag Data:

Initial Composition

15.0% Zn

1.9% Pb

21.5% Fe^{2+}

7.0% Fe^{3+}

11.7% CaO

23.2% SiO_2

* 4.0% Al_2O_3

* 1.0% S

Initial Temperature = 1250°C

Initial Weight = 50,000 kg.

Porosity = 30%

Density Liquid Slag = 3600 $kg.m^{-3}$

Density Solid Slag = 3900 $kg.m^{-3}$

D_{FEO} / $D_{FE_2O_3}$ = 10.0

Coal Data:

Assay (wt.%)	50% Fixed Carbon
	25% Volatiles
	1% Moisture
Volatile Comp. (wt.%)	50% Fixed Carbon
	20% Hydrogen
	10% Oxygen

Furnace Operating Conditions (see Appendix I - Normal Operation)

parameters are: the initial fraction of lead as metal, F_{PBL}, the radius of the metallic lead prill, r_p^{Pb} and the magnitude of the diffusivity of PbO in the slag relative to that of ZnO, D_{ZnO}/D_{PbO} However, in light of the question raised in Chapter VI, the analysis has been expanded to include other parameters:

[i] the circulation velocity of the slag, V_{slag}

[ii] the fraction of remaining oxygen consumed by ferrous iron oxidation, F_{oxy},

[iii] the activity coefficient of Fe_2O_3 in the slag, $\gamma_{Fe_2O_3}$, and,

[iv] the magnitude of the diffusivity of Fe_2O_3 to FeO, ZnO and PbO (D_{FeO} / $D_{Fe_2O_3}$).

7.1.1 Results and Discussion

The sensitivity of the model to F_{PBL} is illustrated in Figs.7.1 - 7.3. A decrease in F_{PBL} from the standard value of 0.5 to 0.1 has no obvious effect on the predicted lead profile, see Fig 7.2. No obvious effect also was observed on the bath temperature profile, not shown. There was however, a noticeable influence on both the zinc and ferrous iron profiles, see Figs. 7.1 and 7.3. A decrease in F_{PBL} brought about a slight decrease in the initial zinc fuming rate and simultaneously a slight decrease in the initial rate of generation of ferrous iron. The effect is opposite for an increase in F_{PBL} to 0.9. It is worth

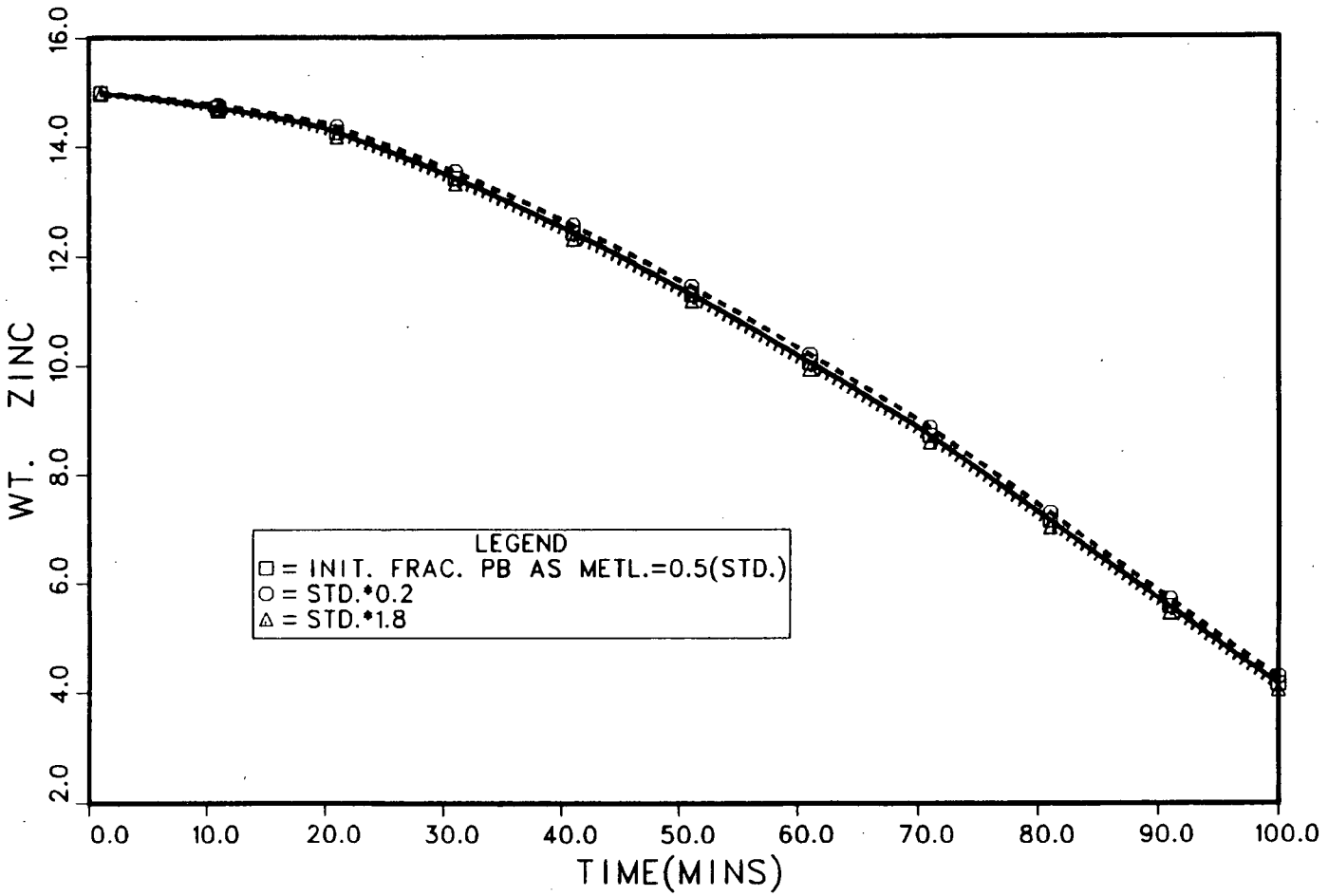

Figure 7.1 The effect of F_{pBL} on the predicted Zn profile

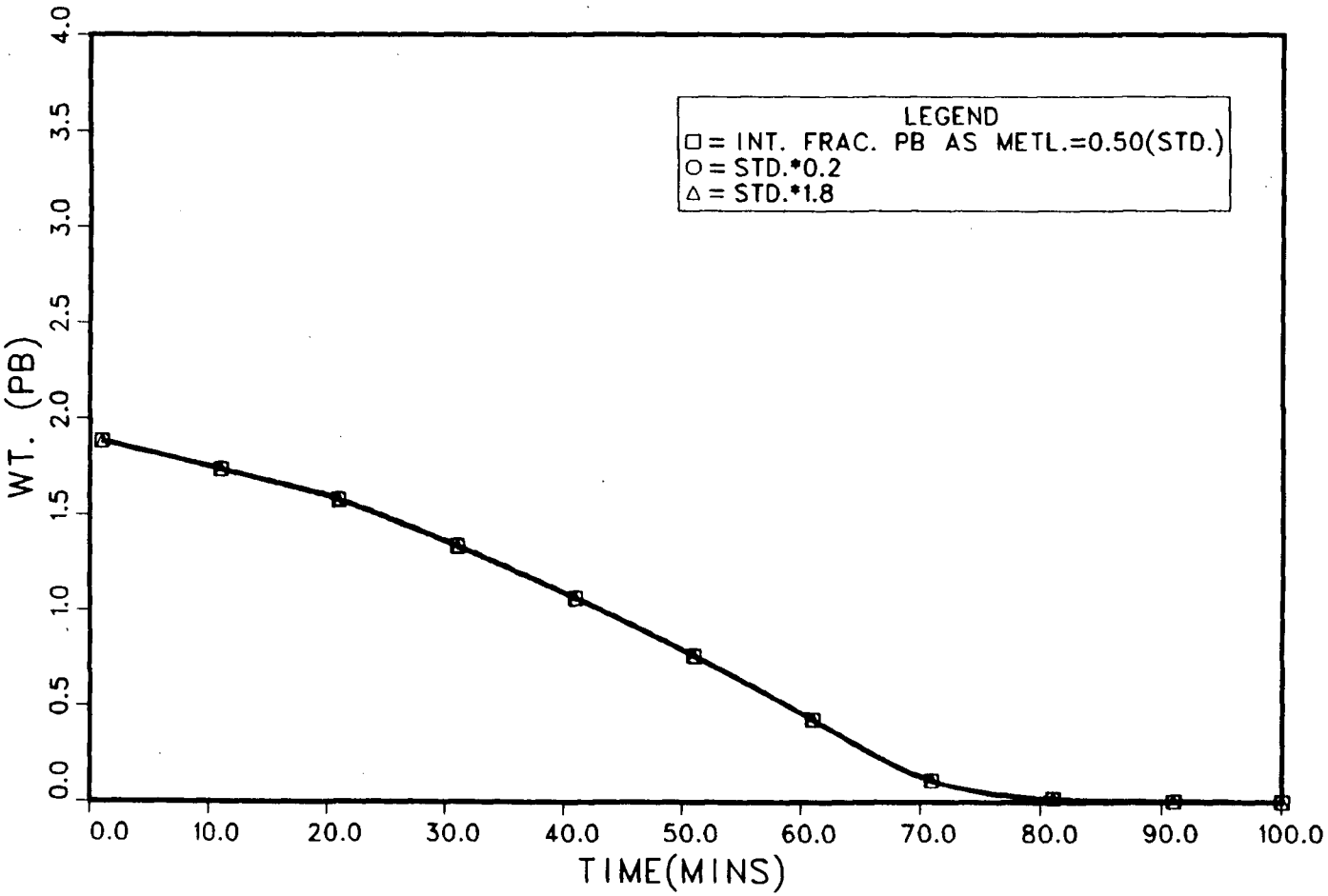

Figure 7.2 The effect of F_{PBL} on the predicted Pb profile

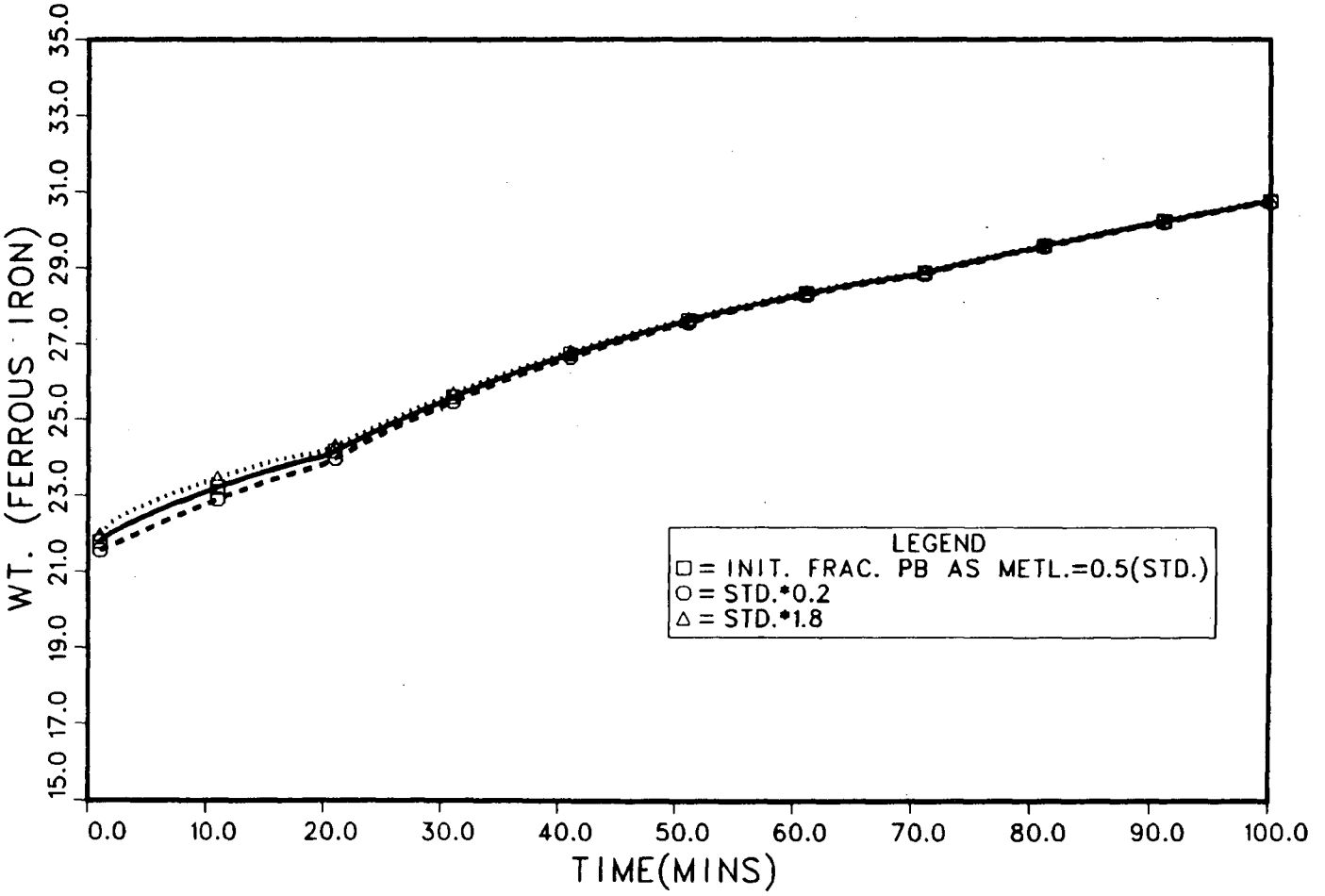

Figure 7.3 The effect of F_{PBL} on the predicted Fe^{2+} profile

noting that the influence on the concentration of ferrous iron is only short term. This behaviour is not unexpected since the model should tend to move toward an equilibrium amount of metallic lead in the furnace for a given slag concentration and set of operating conditions. For example, if the initial value selected for F_{PBL} is high, the rate of oxidation of metallic lead will be elevated relative to the rate of reduction and, therefore, the rate of generation of ferrous iron via oxidation of the lead prill also will be elevated. Since this will result in a short term rapid decrease in the amount of metallic lead, the increase in the ferrous iron generation rate should only be short lived.

It is interesting to note that the zinc and ferrous iron profiles for F_{PBL} = 0.1 and 0.9 bound that for F_{PBL} = 0.5. This indicates that F_{PBL} = 0.5 is closer to the equilibrium amount of liquid lead.

Model sensitivity to r_p^{Pb} is illustrated in Figs. 7.4 - 7.6. Both the lead and ferrous iron profiles show a moderate sensitivity to this parameter, Figs. 7.5 and 7.6, respectively. In the case of the model predictions for lead removal, there is a marked decrease in the removal rate at bath lead contents below approximately 0.75 wt% for a factor of ten increase in r_p^{Pb}. The ferrous iron profiles indicate an initial decrease in the rate of generation for an increase in r^{Pb}. The long term effect,

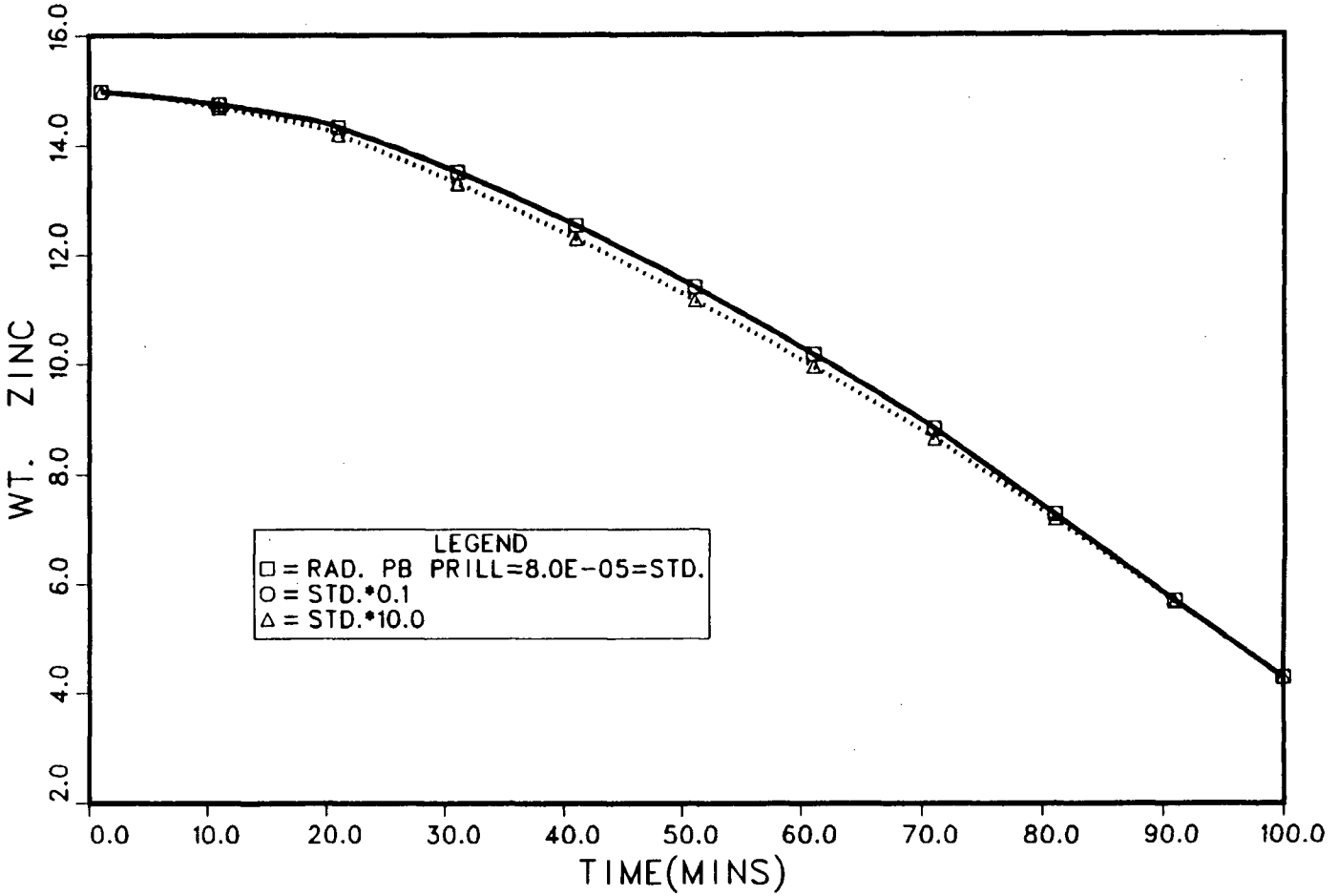

Figure 7.4 The effect of r_p^{Pb} on the predicted Zn profile

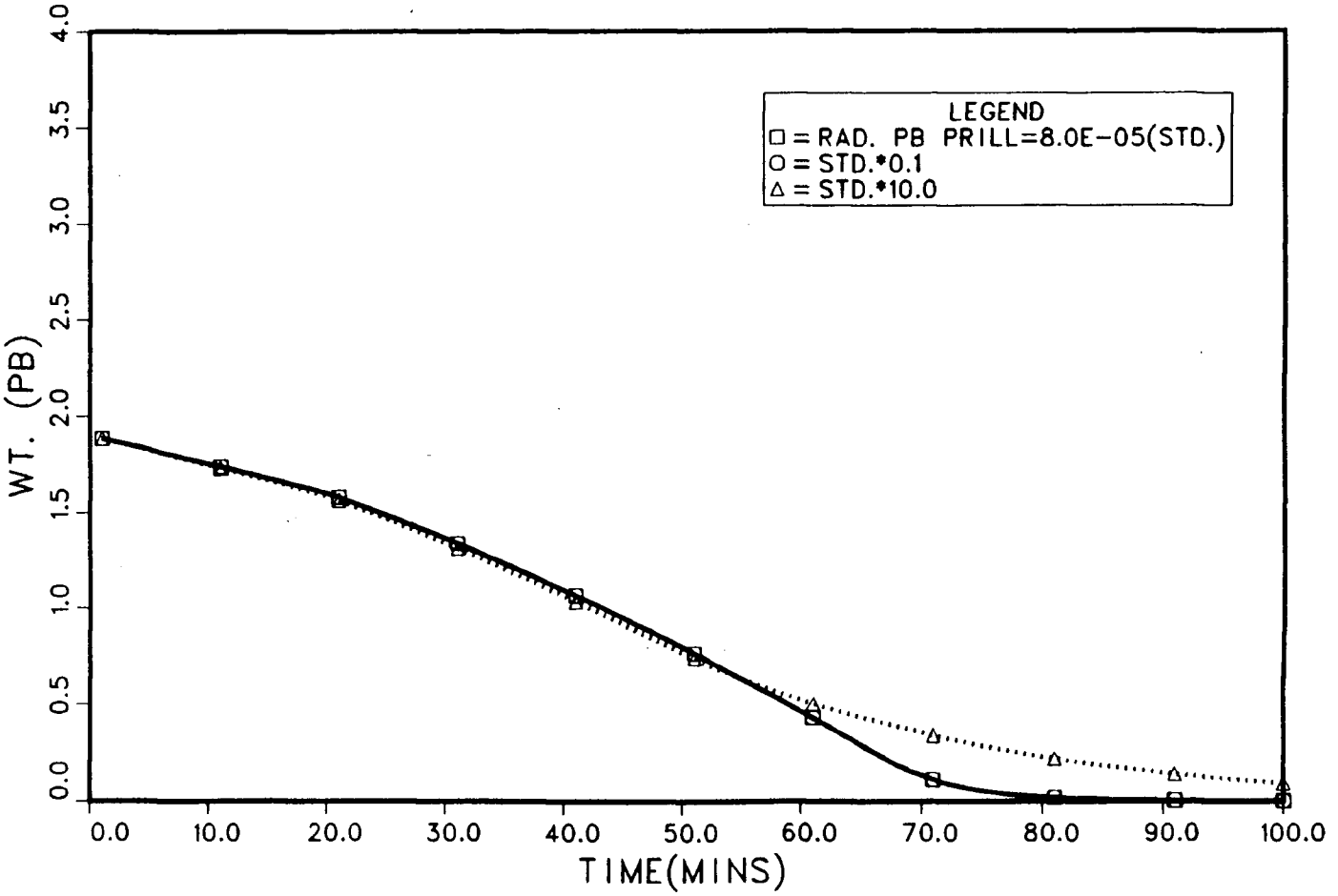

Figure 7.5 The effect of r_p^{Pb} on the predicted Pb profile

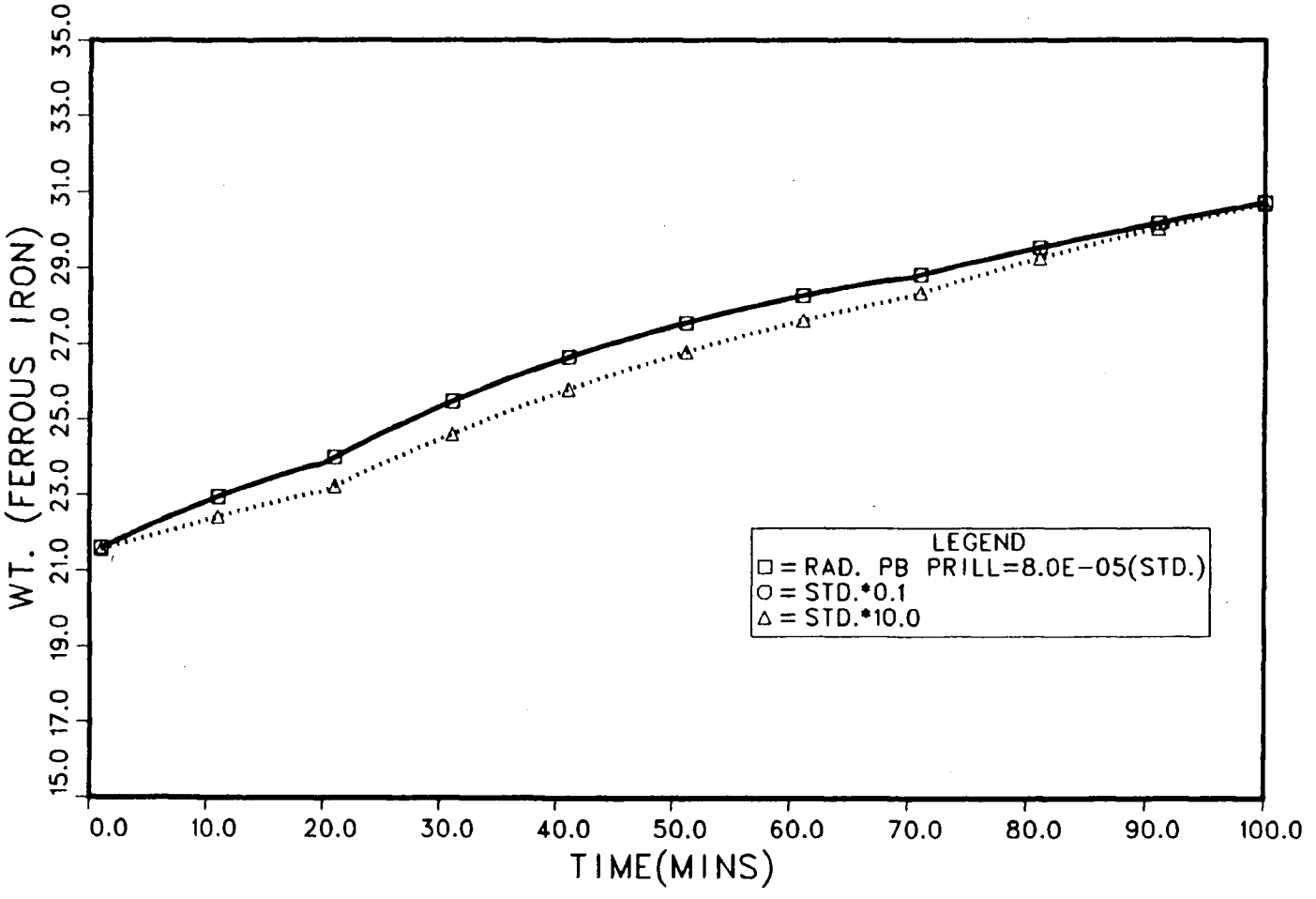

Figure 7.6 The effect of r_p^{Pb} on the predicted Fe^{2+} profile

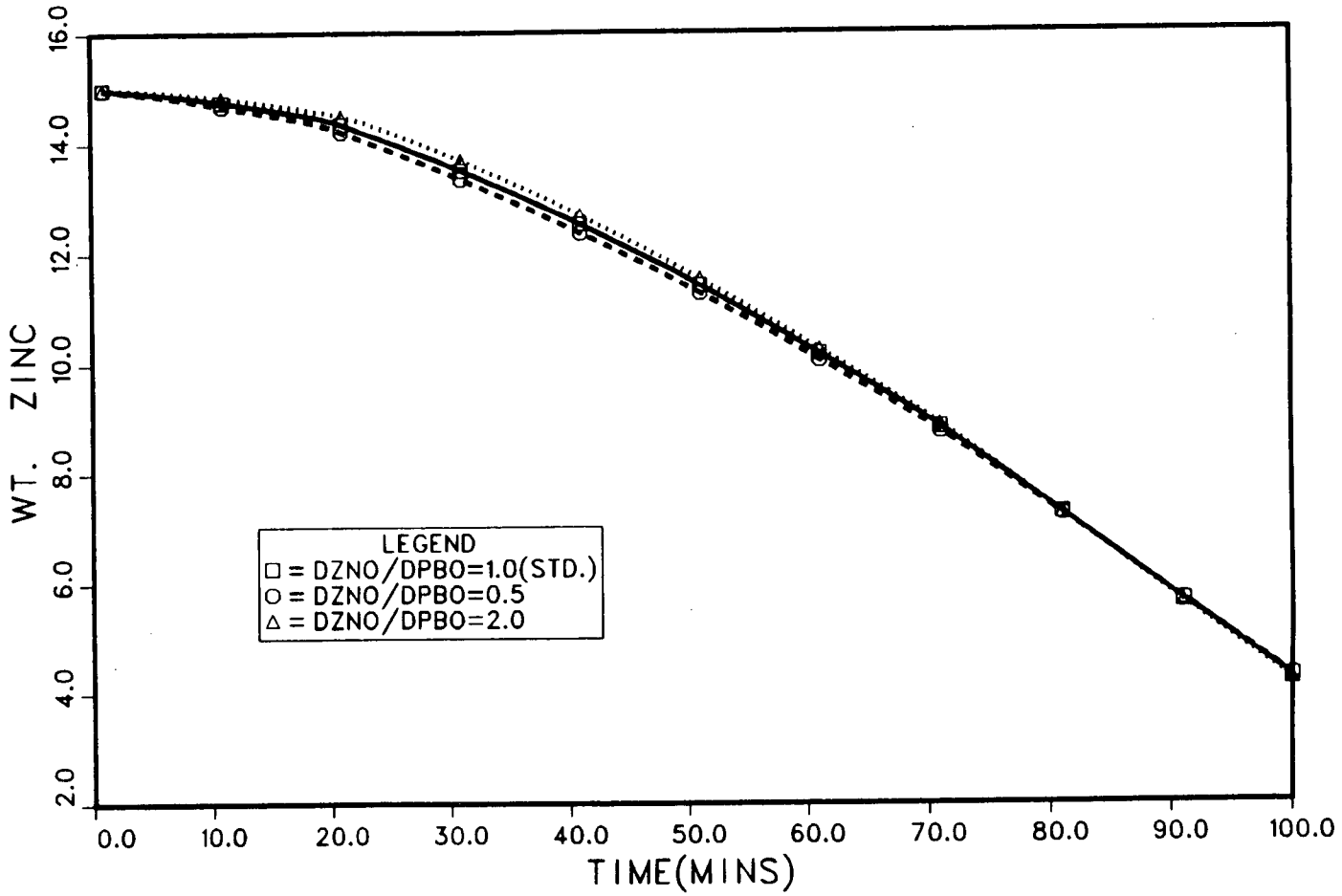

Figure 7.7 The effect of D_{ZNO}/D_{PBO} on the predicted Zn profile

however, is only minimal. The zinc profiles, Fig. 7.4, indicate little sensitivity to r_p^{Pb}. Temperature sensitivity also was investigated (not shown) and was found to be minimal. It is worth noting that in all three cases, zinc, lead and ferrous iron, there is no effect observed for a decrease in r_p^{Pb}.

The sensitivity of the model to the relative magnitude of D_{PBO} is shown in Figs. 7.7 - 7.10. The zinc, lead and temperature profiles are relatively insensitive to D_{ZNO}/D_{PBO} (D_{ZNO}) constant, see Figs. 7.7, 7.8 and 7.10, respectively. For example, a factor of four change in D_{PBO} results in only a 0.5 wt% change in bath zinc concentration. The ferrous iron profile, Fig. 7.9 shows a moderate sensitivity to D_{PBO}. An increase in D_{ZNO}/D_{PBO} results in an increase in the predicted ferrous iron generation rate.

As mentioned previously, the questions raised in Chapter VI have necessitated an investigation of the models sensitivity to several parameters not directly associated with lead reduction. Model sensitivity to these parameters is described below.

One of the more obvious changes brought about by the inclusion of lead reduction was a substantial increase in slag circulation velocity - from 1m/sec previously assumed by Richards[1a] to 3m/sec in the present model. Model sensitivity to

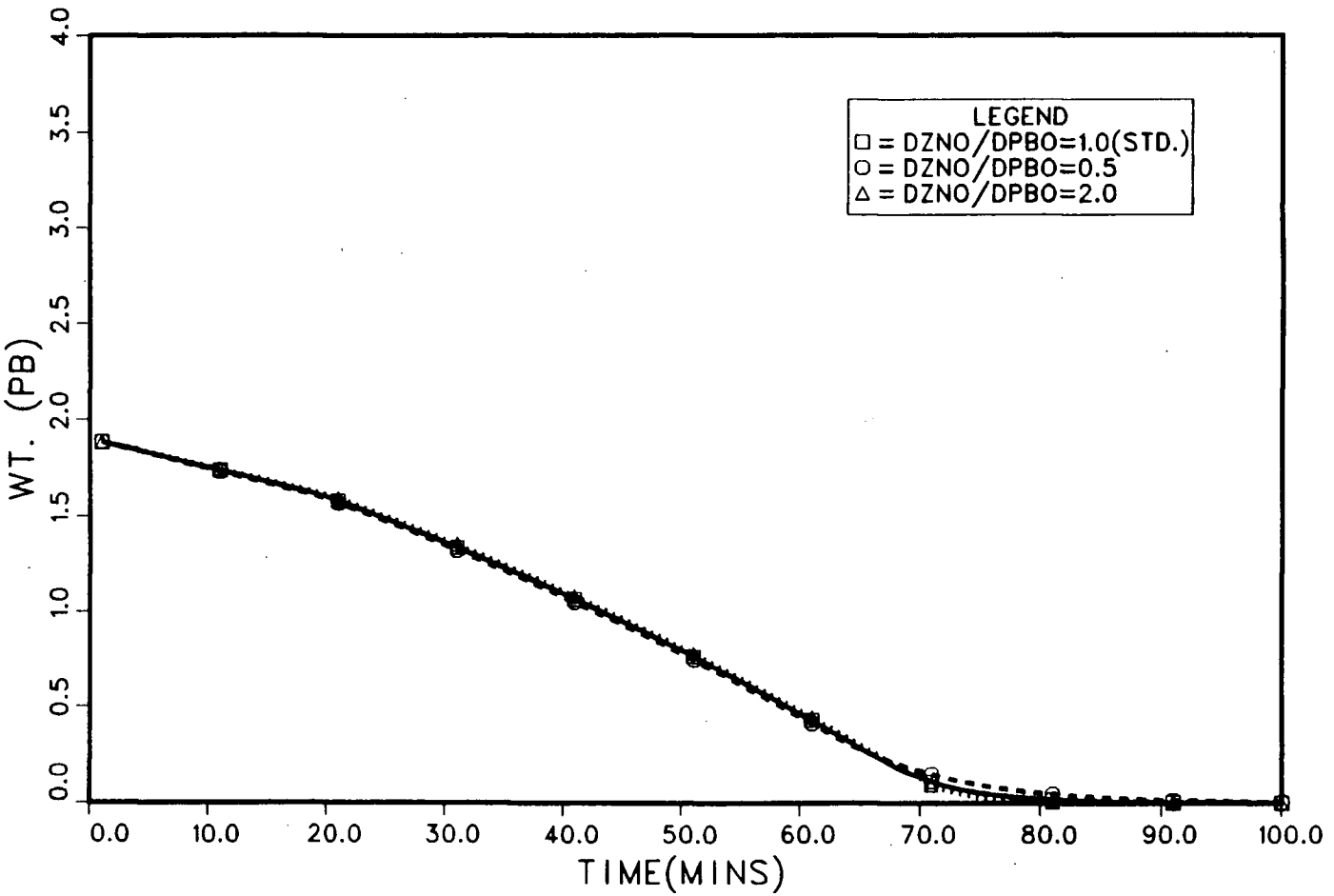

Figure 7.8 The effect of D_{ZNO} /D_{PBO} on the predicted Pb profile

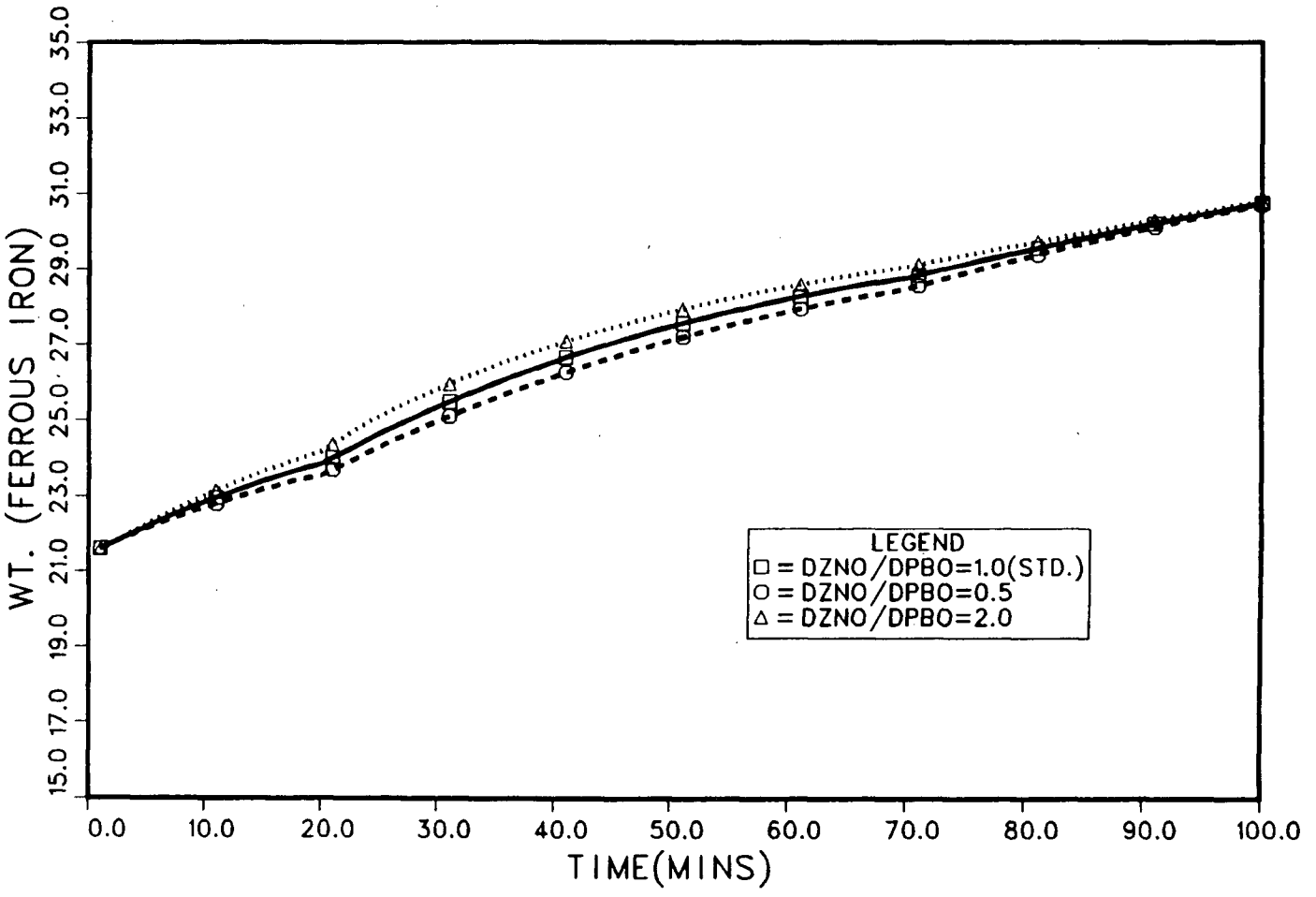

Figure 7.9 The effect of D_{ZNO}/D_{PBO} on the predicted Fe^{2+} profile

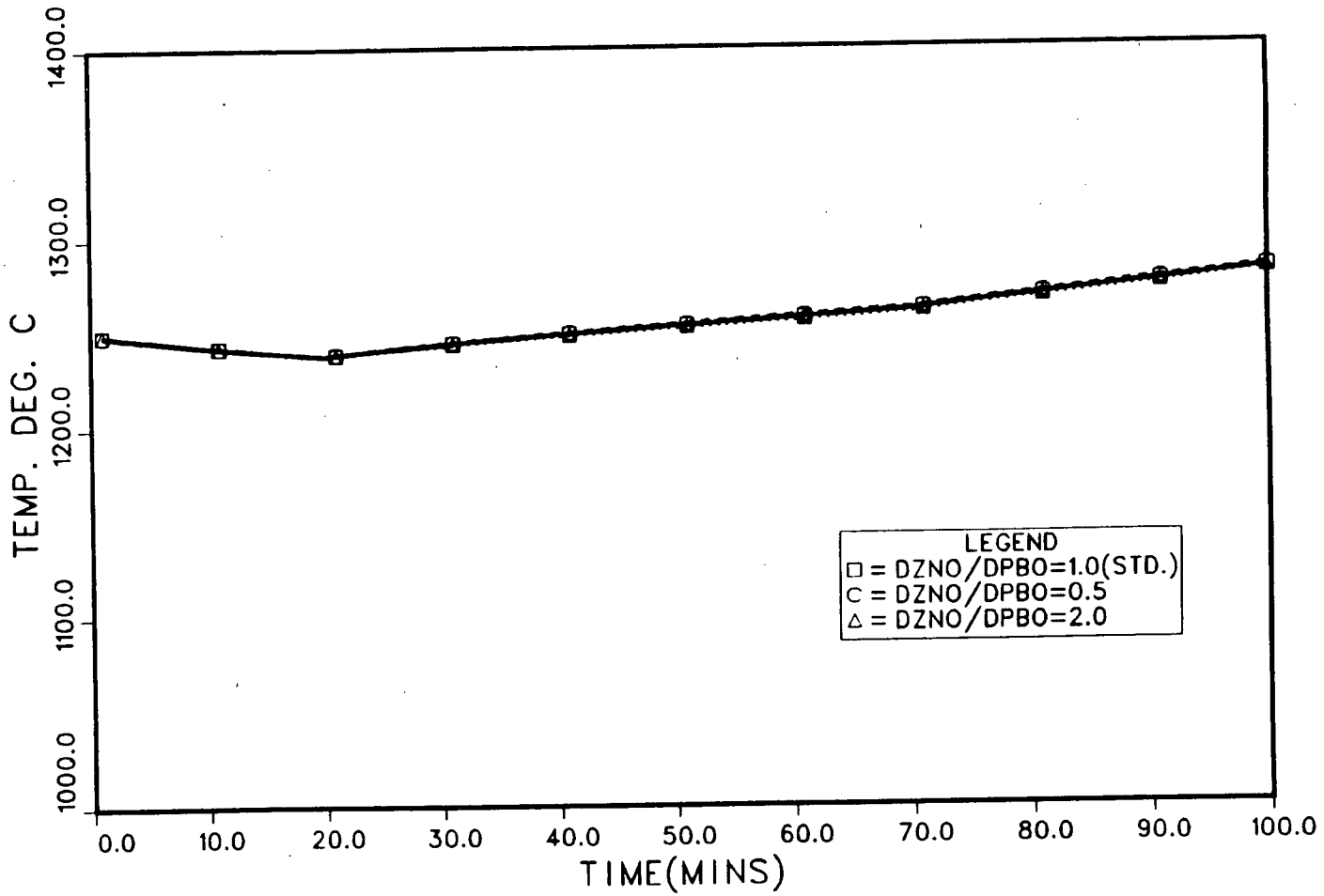

Figure 7.10 The effect of D_{ZNO} /D_{PBO} on the predicted temperature profile

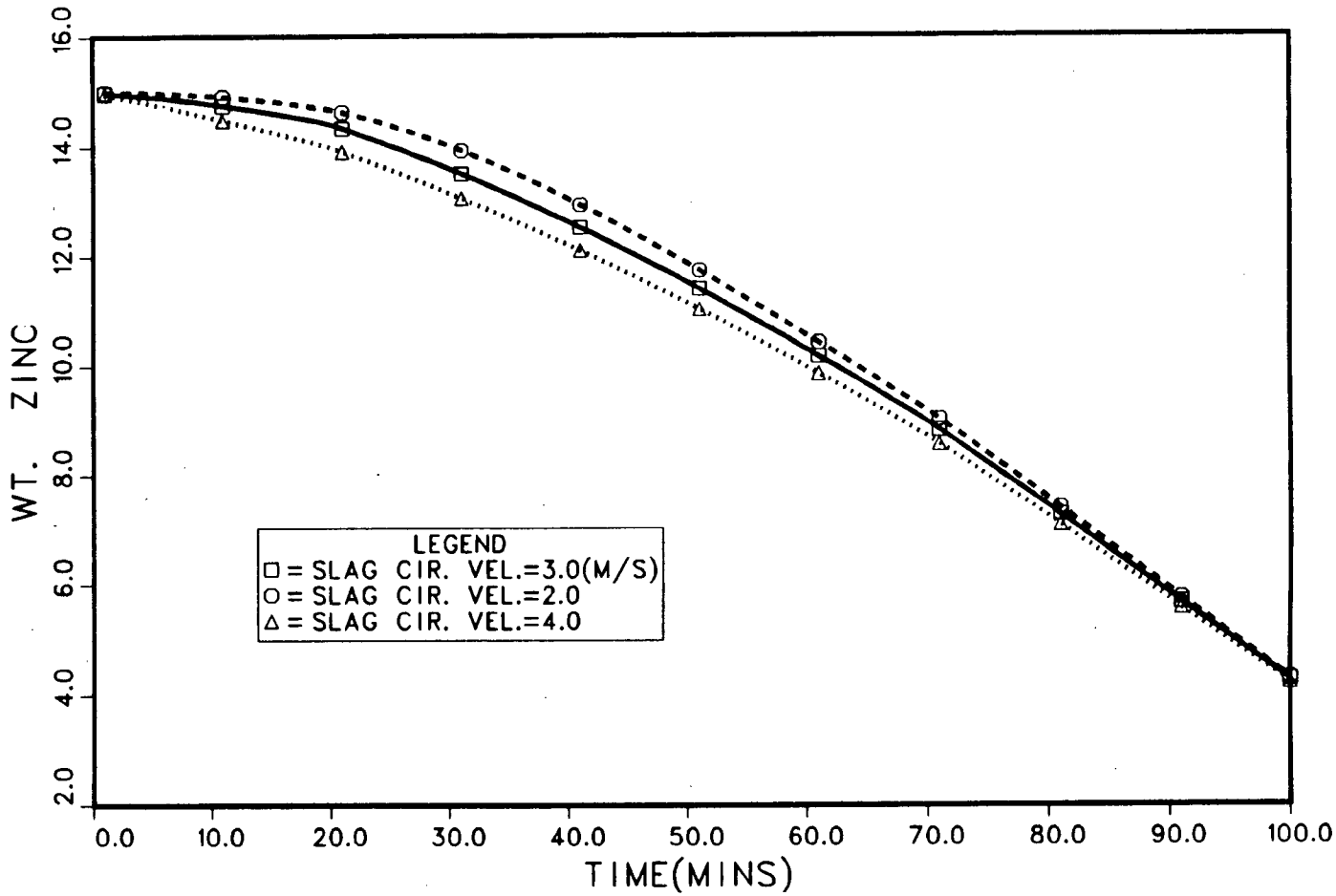

Figure 7.11 The effect of V_{slag} on the predicted Zn profile

the parameter is illustrated in Figs. 7.11-7.14. It should be mentioned that, within the context of the model, slag circulation velocity is effectively a measure of char particle residence time in the bath.

With this in mind, the zinc profile, Fig. 7.11, can be seen to be moderately sensitive to this parameter. There is a significant decrease in the zinc fuming rate, 0 - 20 mins elapsed time, for a 1m/sec decrease in V_{slag}. It should be noted that the effect of a 2m/sec variation in V_{slag} becomes minimal for elapsed times greater than approximately 80 mins. Therefore, for predictions of overall furnace cycle times the effect should be minimal.

Ferrous iron predictions, see Fig. 7.12, are considerably more sensitive to V_{slag} than predictions for zinc concentration in the bath. The rate of generation of ferrous iron is reduced by an increase in slag circulation velocity. This behaviour is opposite to that of zinc. The lead and temperature profiles, Figs. 7.13 and 7.14, respectively, show no obvious sensitivity to the slag circulation velocity.

Model sensitivity to F_{oxy} is illustrated in Figs. 7.15-7.18. The profiles of zinc, lead, ferrous iron and temperature all show a high degree of sensitivity to F_{oxy}. The sensitivity of lead is less, approximately 0.5 wt%, and opposite. An increase in F_{oxy}

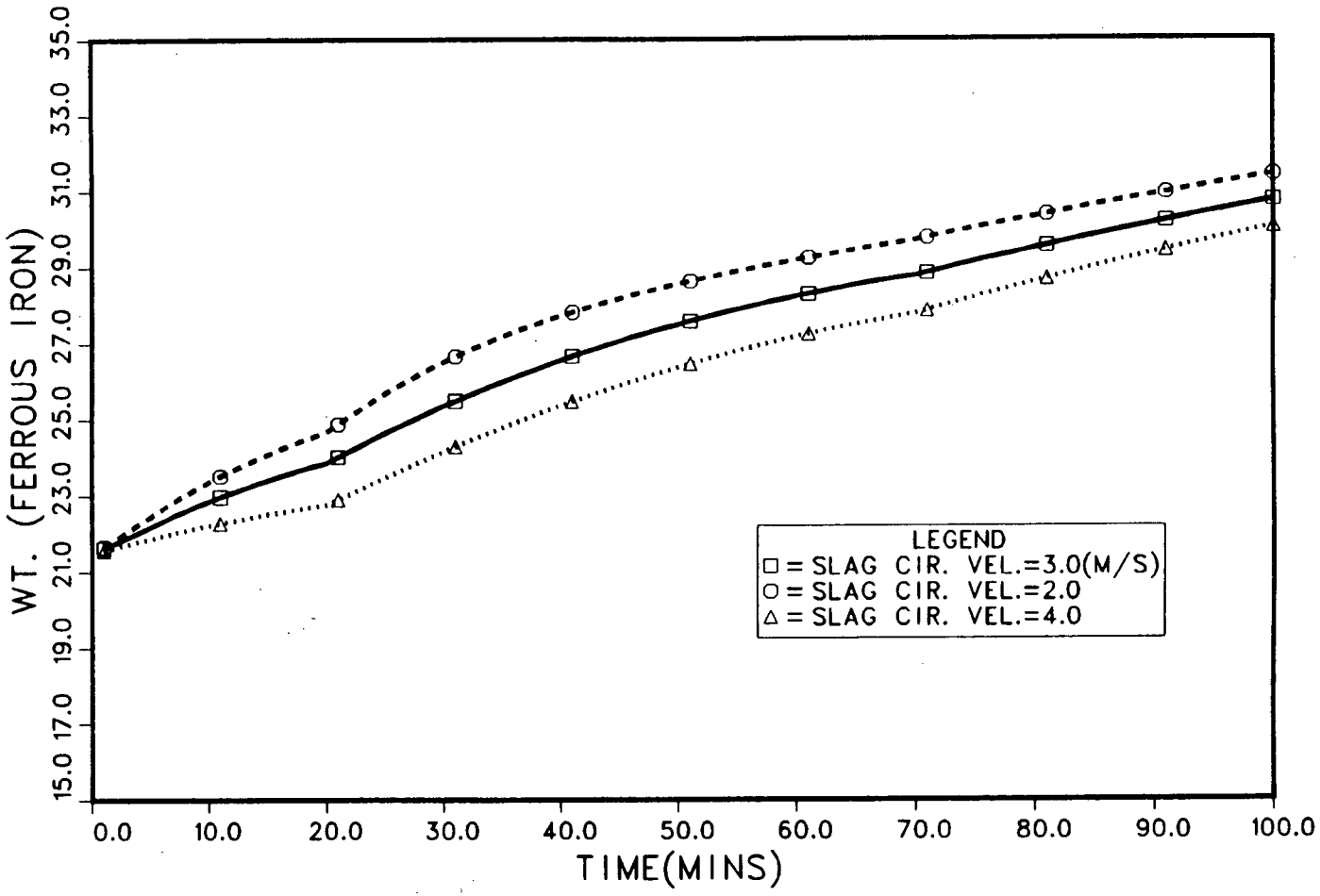

Figure 7.12 The effect of V_{slag} on the predicted Fe^{2+} profile

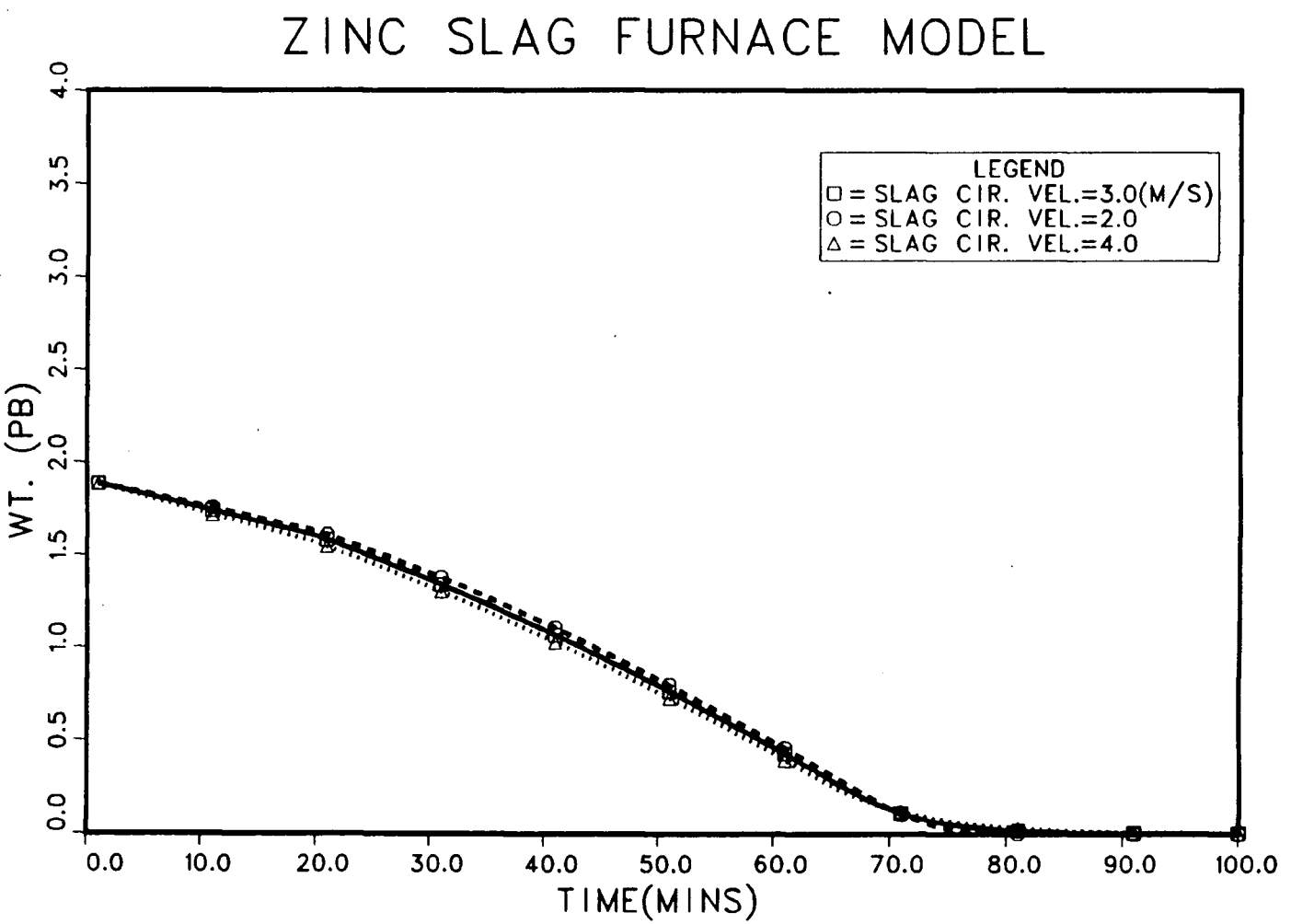

Figure 7.13 The effect of V_{slag} on the predicted Pb profile

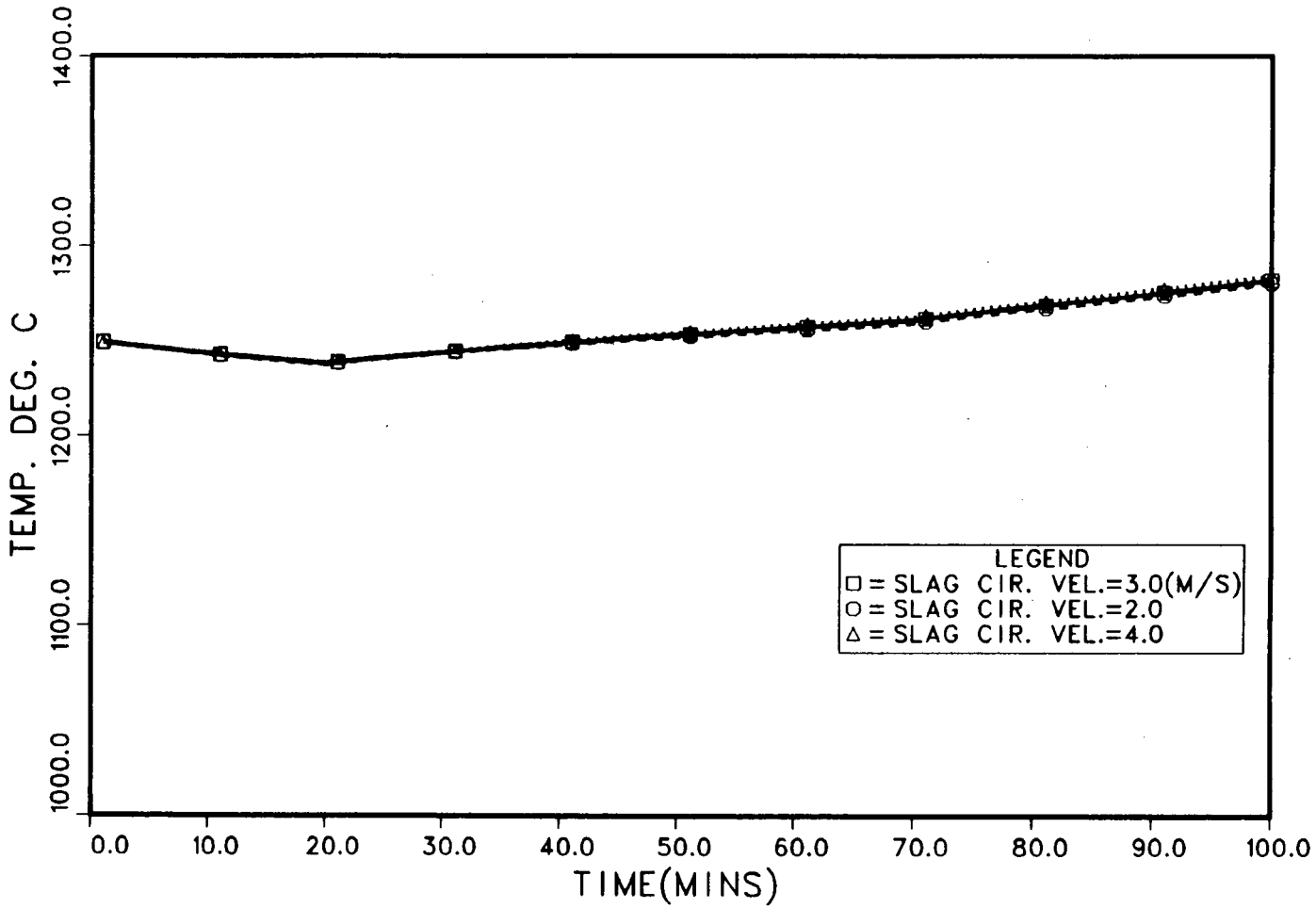

Figure 7.14 The effect of V_{slag} on the predicted temperature profile

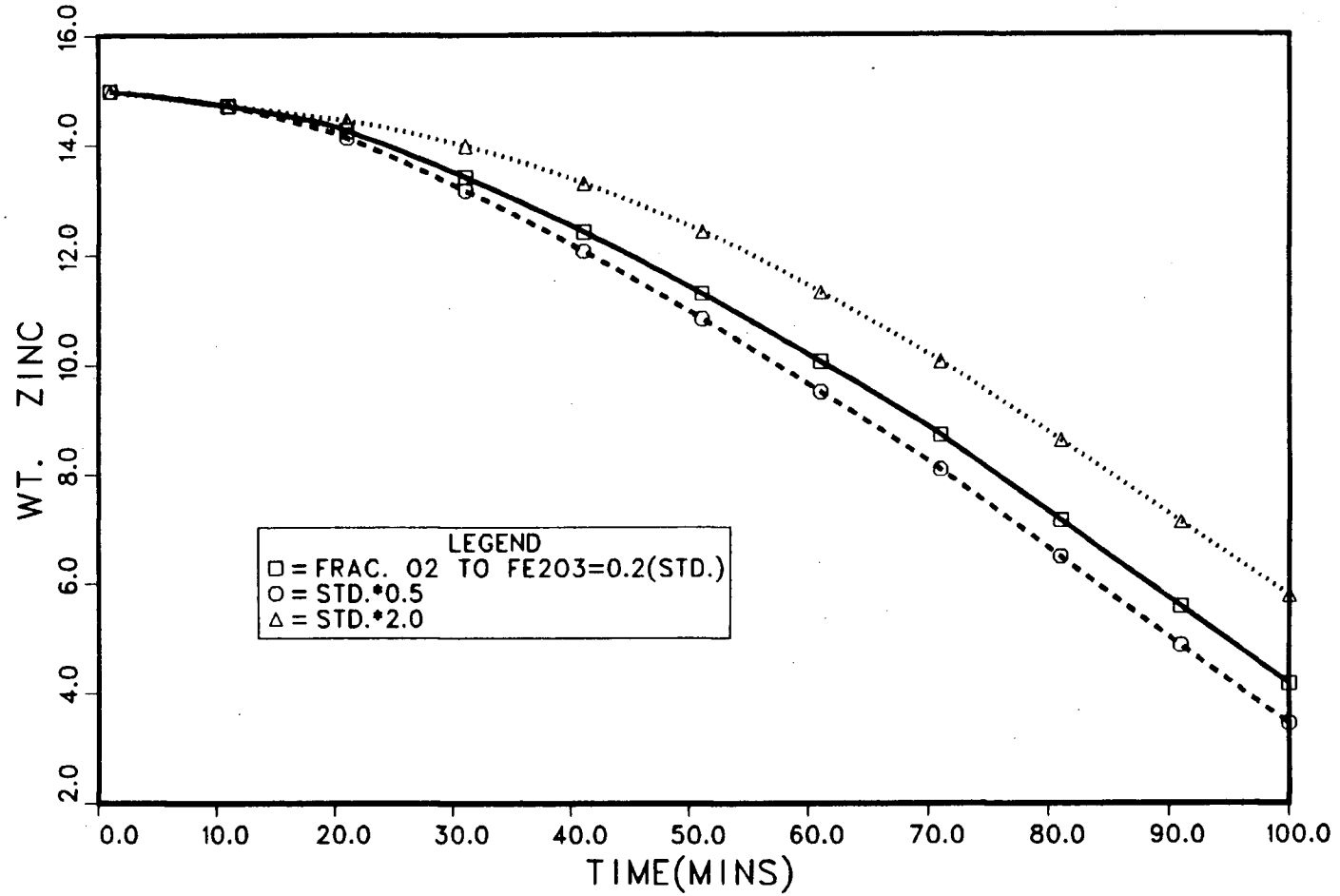

Figure 7.15 The effect of F_{oxy} on the predicted Zn profile

results in an increase in the fuming rate of Pb, see Fig. 7.16. An increase in F_{oxy} also gives rise to a significant decrease in the predicted ferrous iron concentration, and an increase in the predicted bath temperature, see Figs. 7.17 and 7.18, respectively.

Model sensitivity to the slag activity coefficient of Fe_2O_3 is illustrated in Figs. 7.19 and 7.20. As can be seen, there is little or no obvious effect on the zinc or ferrous iron profiles, see Figs. 7.19 and 7.20 respectively. The sensitivity of lead and temperature predictions to Fe_2O_3 , were also investigated (not shown) and found to be minimal.

Finally, the sensitivity of the model to the relative magnitude of $D_{Fe_2O_3}$ was investigated. The results are illustrated in Figs. 7.21-7.24. Both the predicted zinc and ferrous iron profiles show a moderate sensitivity. In the case of the zinc profiles, Fig. 7.21, a factor of four increase in $D_{Fe_2O_3}$ results in a 1 wt% decrease in predicted bath concentration at about 35 minutes elapsed time. At 100 minutes elapsed time the variation is down to 0.5 wt%. In the case of ferrous iron, decreasing $D_{Fe_2O_3}$ by a factor of four results in a 2 wt decrease in the ferrous iron concentration, see Fig 7.23. The predicted lead profile, Fig. 7.22, can be seen to be relatively insensitive, and the temperature profile, Fig. 7.24, completely insensitive to $D_{Fe_2O_3}$.

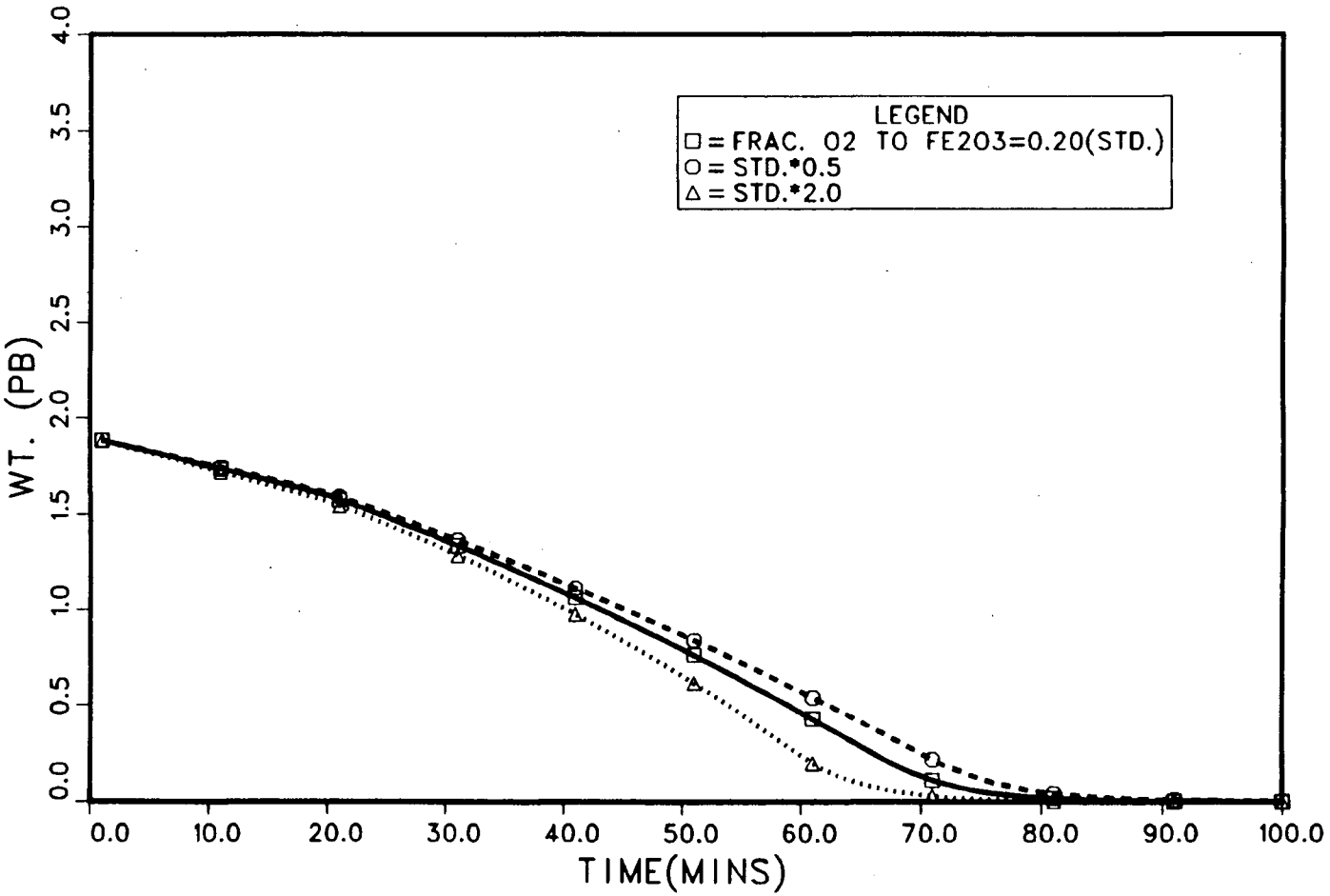

Figure 7.16 The effect of F_{oxy} on the predicted Pb profile

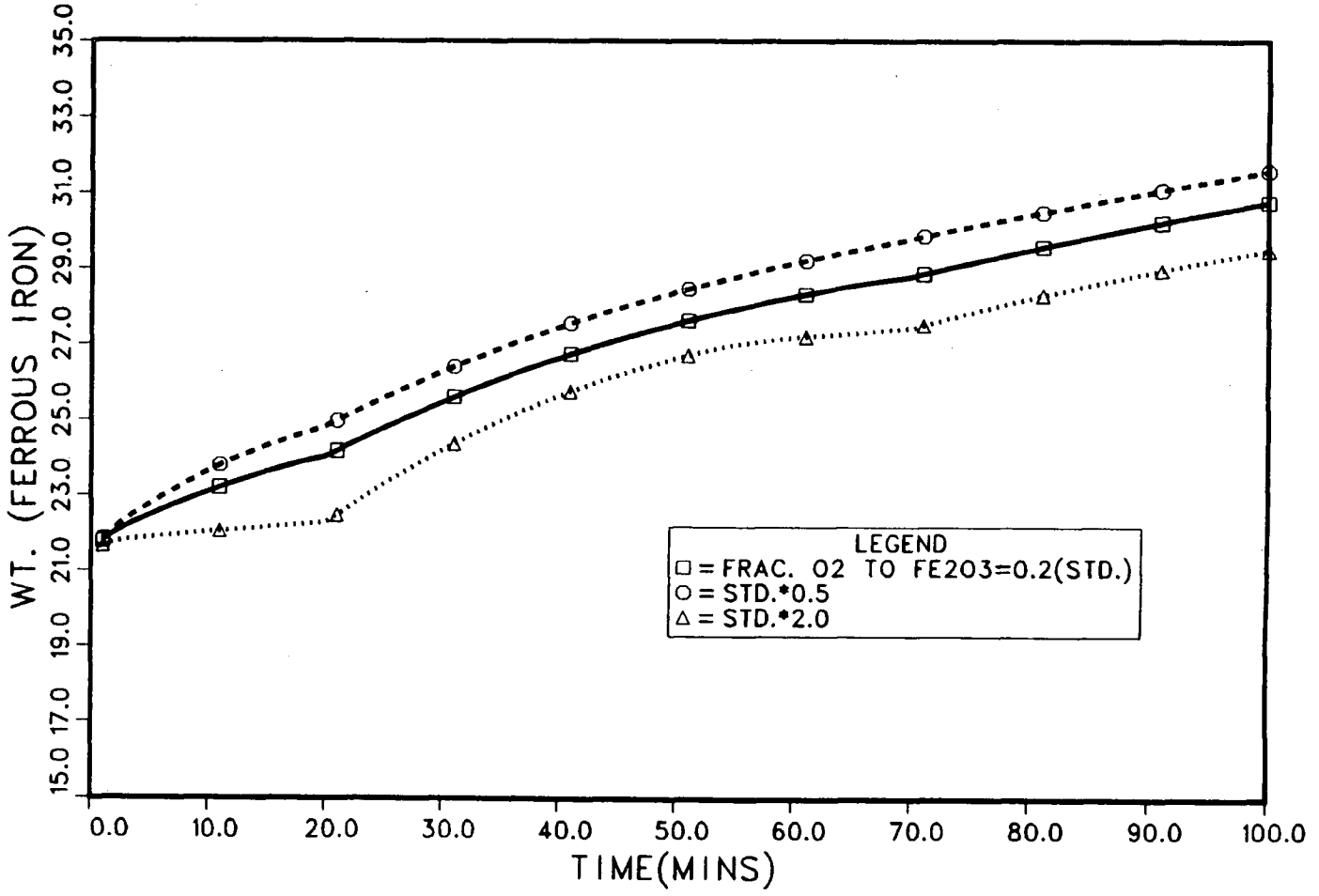

Figure 7.17 The effect of F_{oxy} on the predicted Fe^{2+} profile

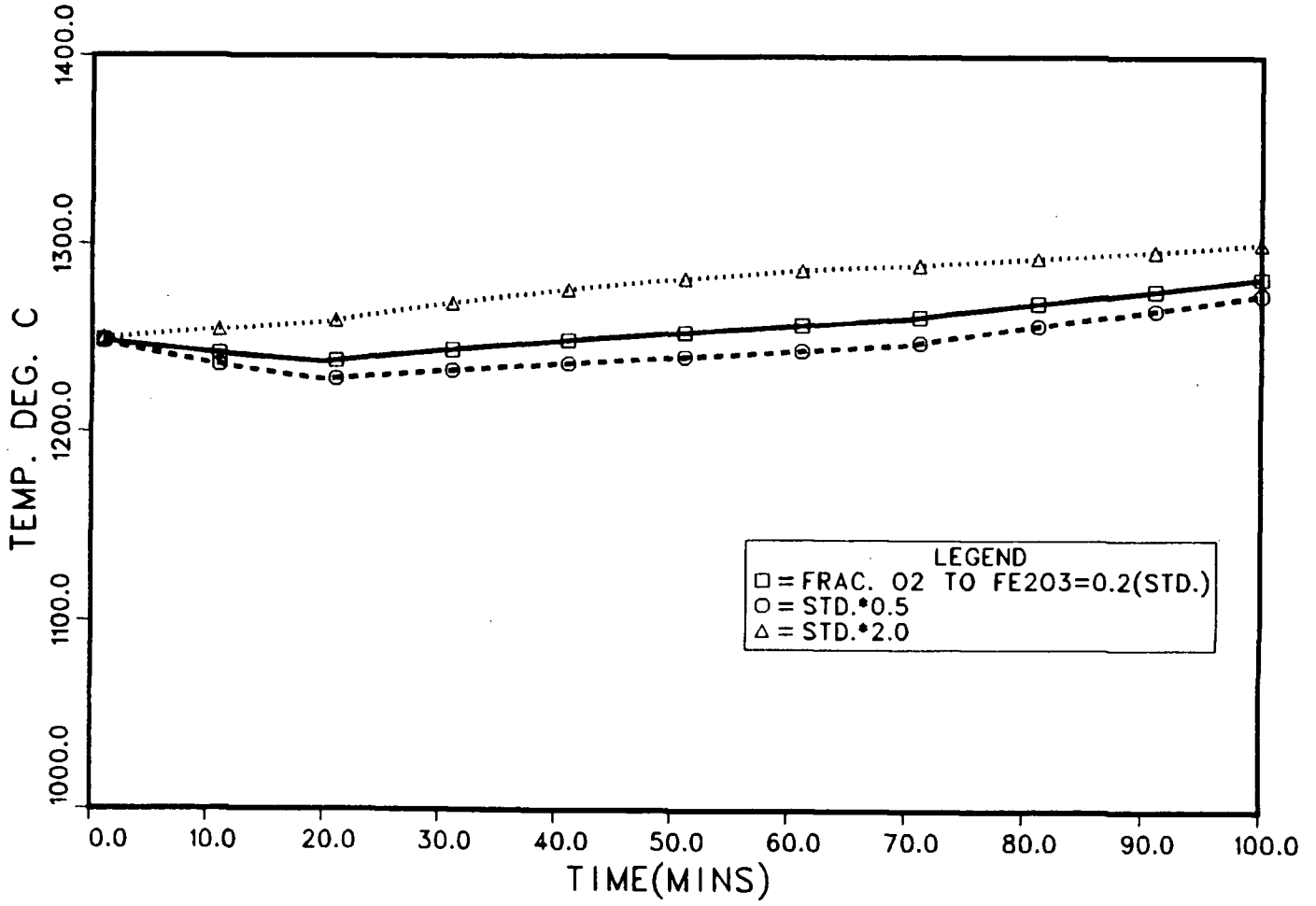

Figure 7.18 The effect of F_{oxy} on the predicted temperature profile

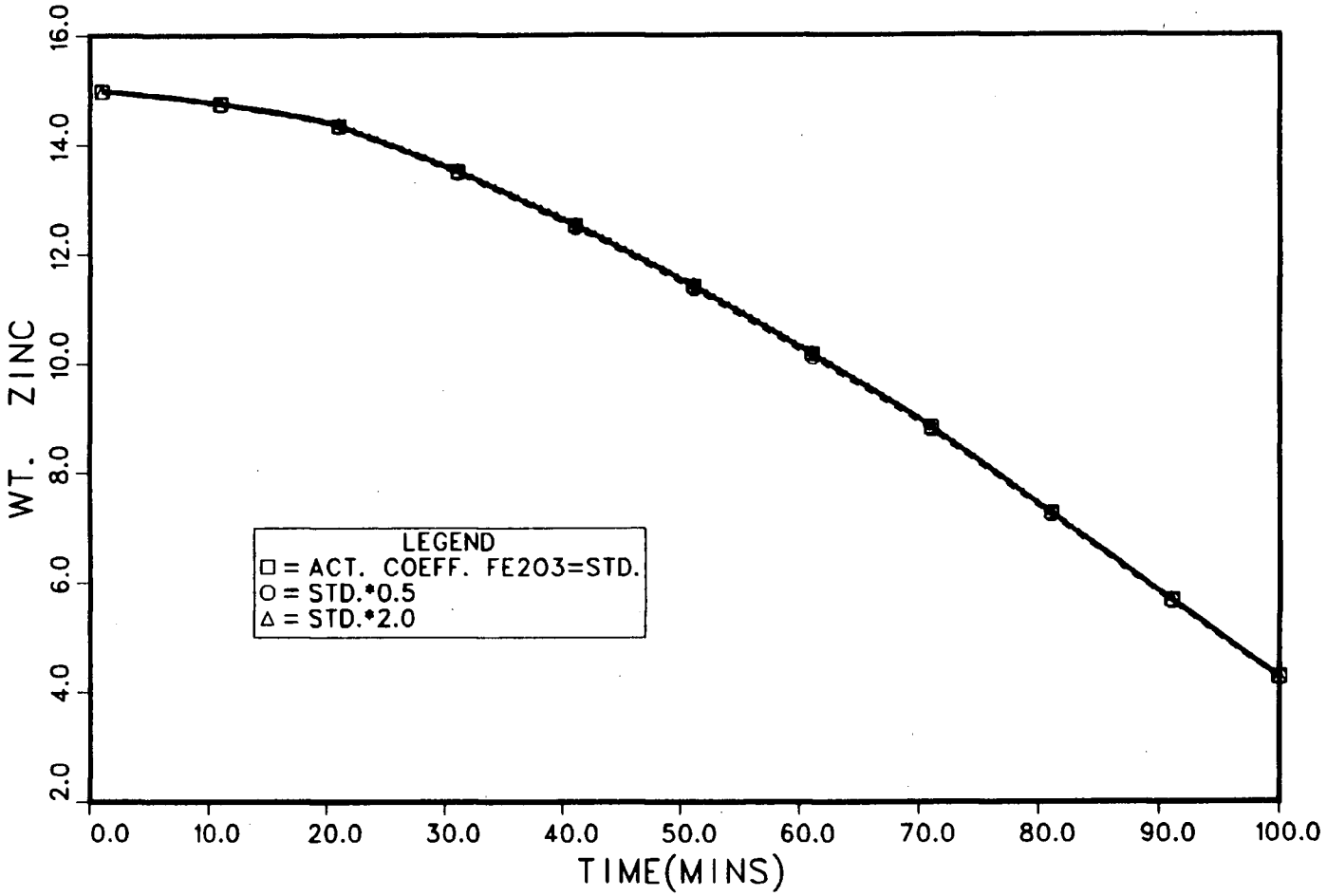

Figure 7.19 The effect of $\gamma_{Fe_2O_3}$ on the predicted Zn profile

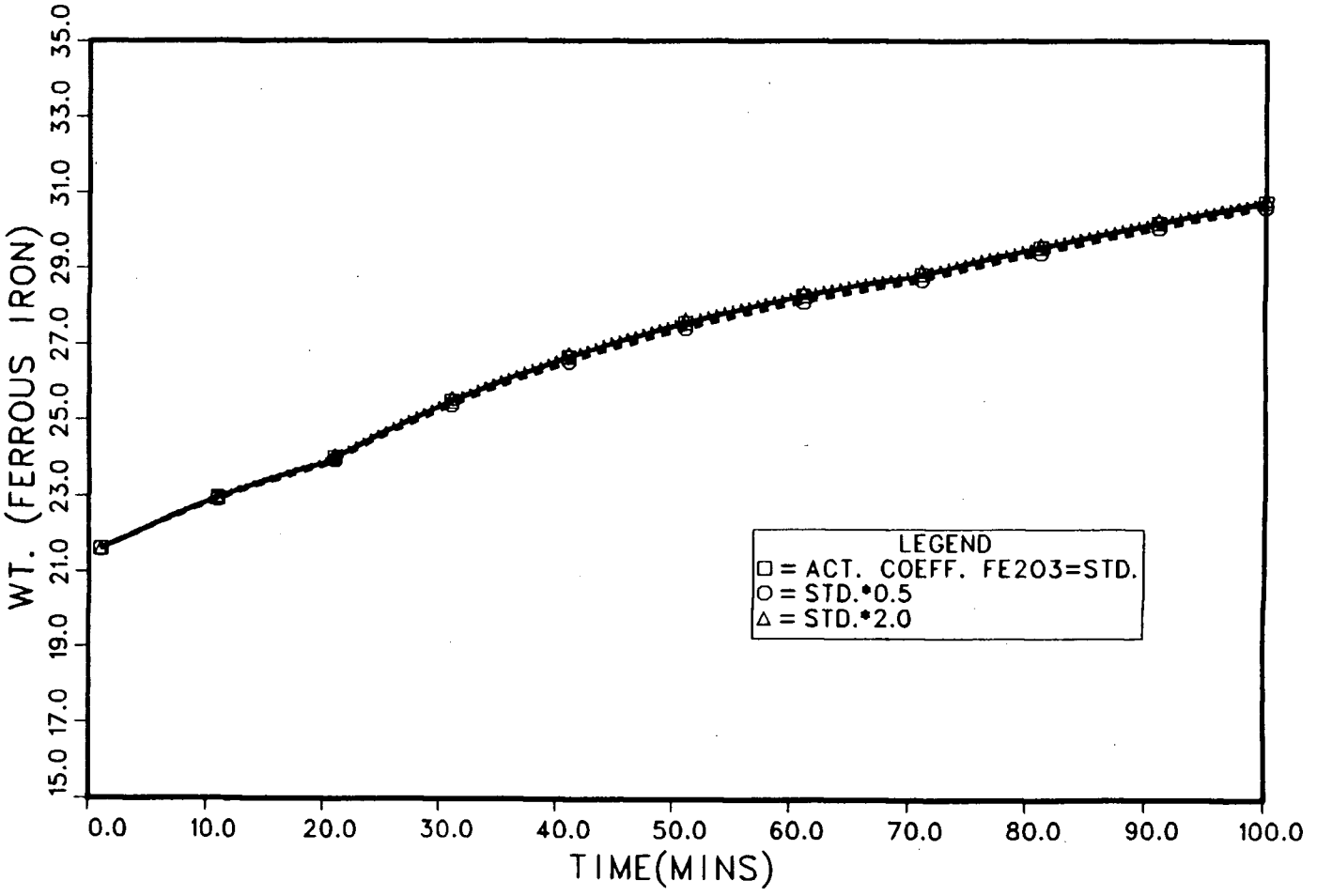

Figure 7.20 The effect of $\gamma_{Fe_2O_3}$ on the predicted Fe^{2+} profile

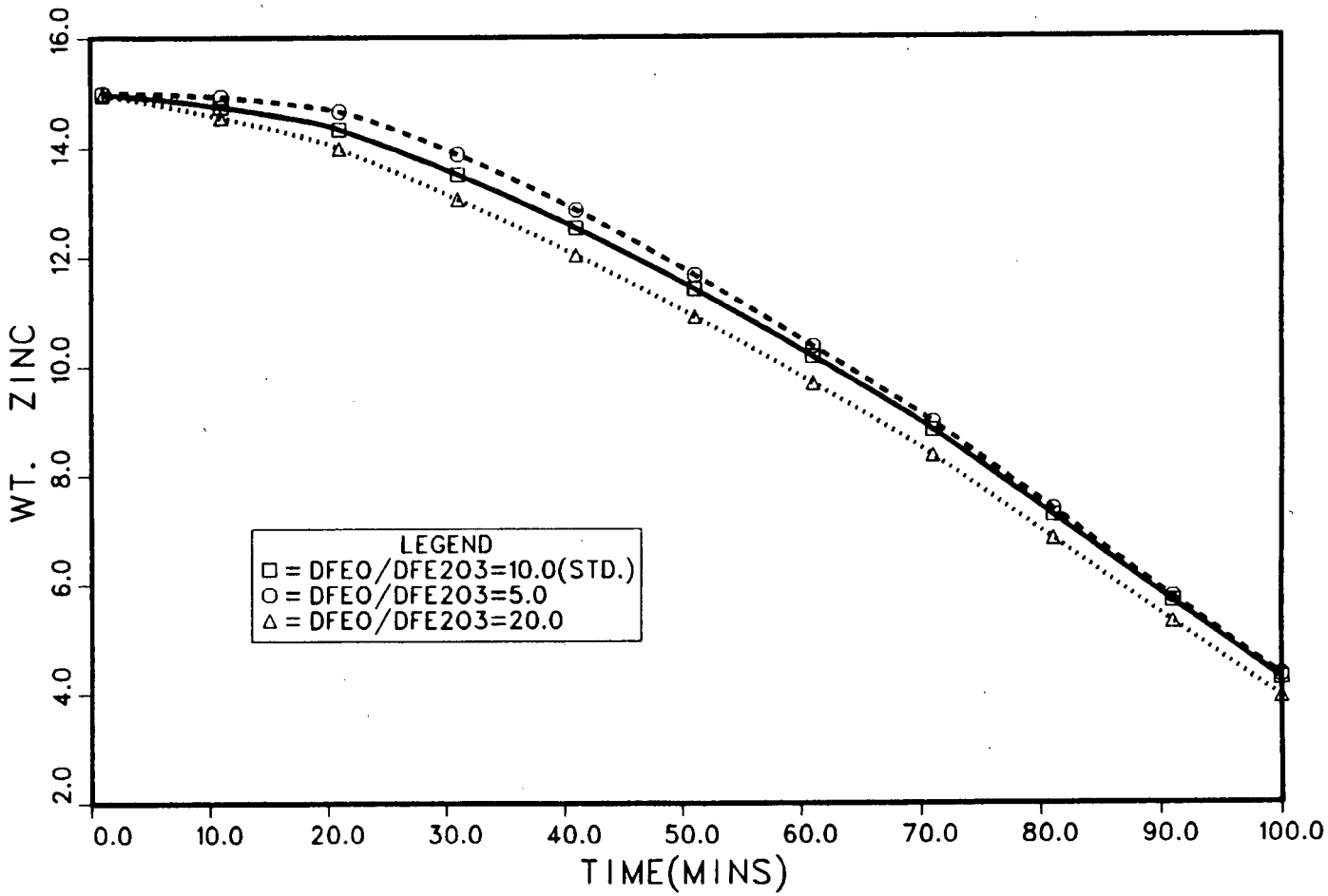

Figure 7.21 The effect of D_{Feo} $/D_{Fe_2O_3}$ on the predicted Zn profile

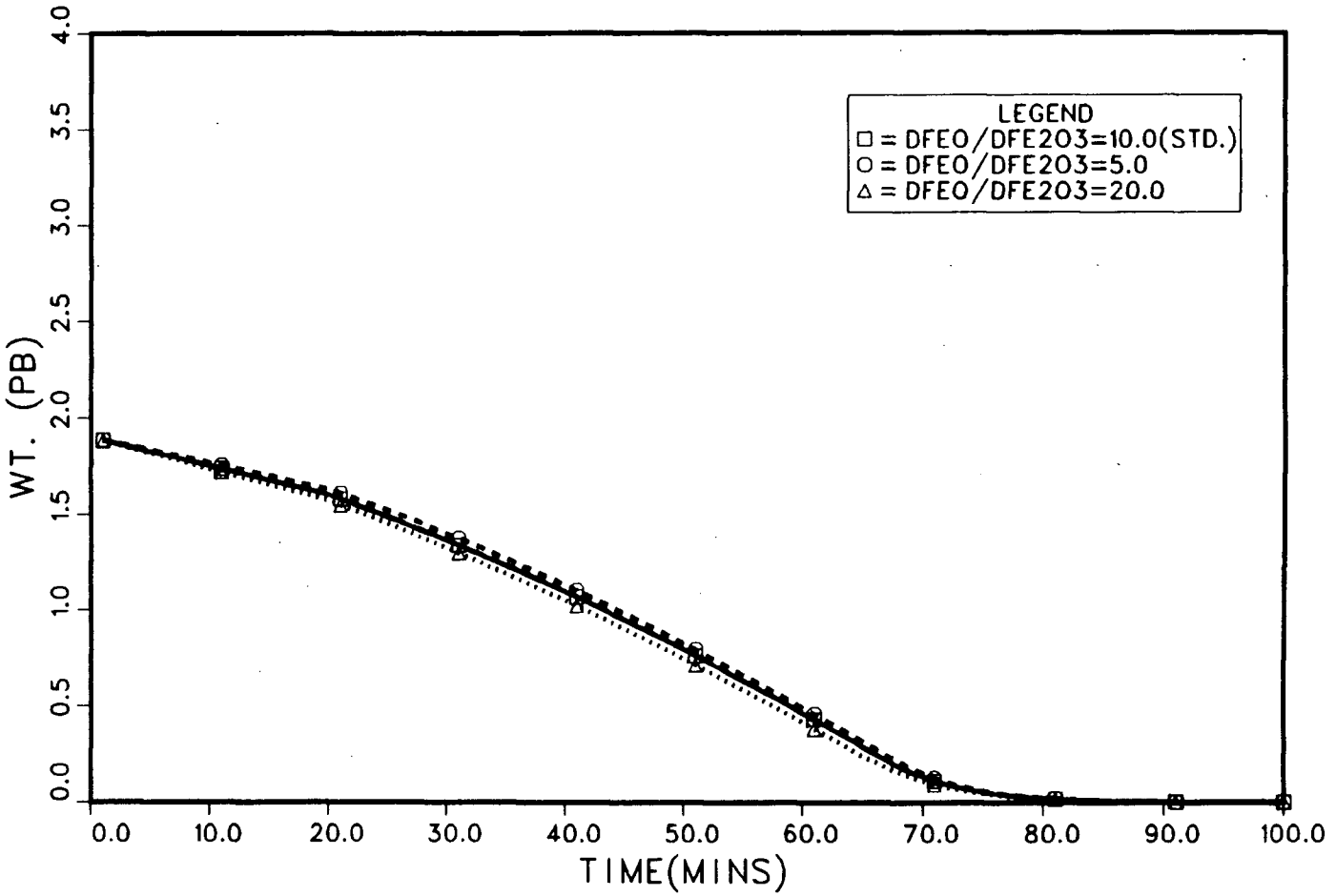

Figure 7.22 The effect of D_{Feo} /$D_{Fe_2O_3}$ on the predicted Pb profile

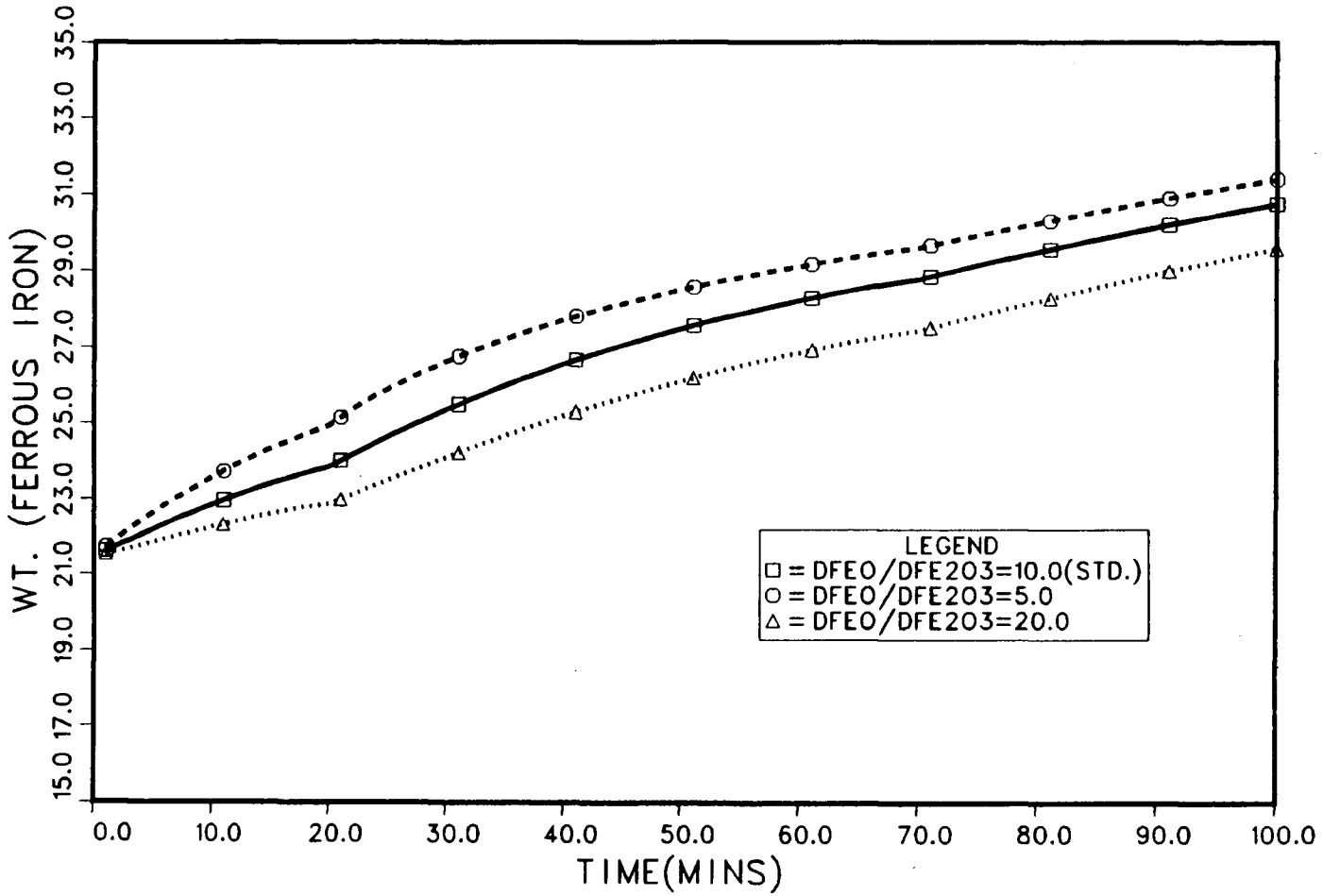

Figure 7.23 The effect of D_{FeO} /$D_{Fe_2O_3}$ on the predicted Fe^{2+} profile

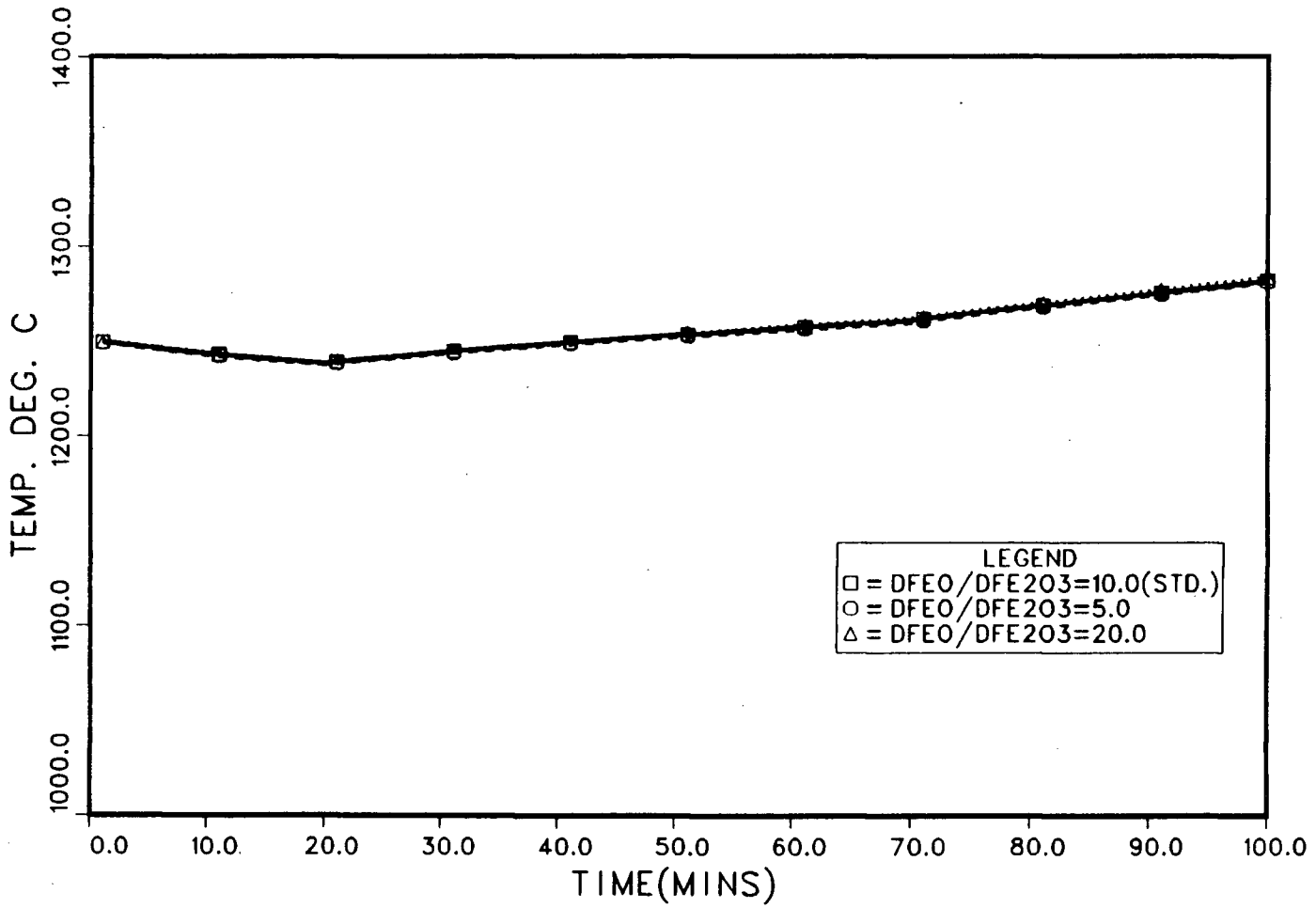

Figure 7.24 The effect of $D_{FeO}/D_{Fe_2O_3}$ on the predicted temperature profile

Having presented the results of the sensitivity analysis, it is worthwhile to assess the influence that the inclusion of lead reduction has had on the prediction of process kinetics before proceeding with a discussion of the results.

7.1.1.1 The Influence of Lead on Kinetics

As described previously, within the overall furnace model, there are two distinct kinetic models which involve lead: the char particle-slag reaction model, and the lead prill-slag reaction model. Therefore, to assess the influence of lead in the overall model, the effect of lead on kinetics of the two reaction models first must be established.

7.1.1.1.1 The Kinetics of the Char Particle - Slag Model

At the initialization of char particle - secondary bubble reaction with the slag, the rates of Boudouard and char-steam reactions are at a maximum. If the combined rates of reaction are sufficiently high so as to fix the secondary bubble oxygen potential, then reduction of ZnO, PbO and Fe_2O_3 will proceed at a rate limited by mass-transfer of these species in the slag. The relative rates of mass-transfer or reduction will be dependent on the particular oxides mobility and thermodynamic stability in the slag.

As reaction proceeds and carbon within the coal char is consumed, the combined rate of Boudouard and char-steam reactions begin to slow. Eventually a point is reached where these reactions can no longer "keep up" with the rate at which reduction is occurring, and therefore, the oxygen potential begins to rise. This results in a decrease in the rates of reduction and a shift in kinetic control to the combined rate of the Boudouard and char-steam reactions. As the oxygen potential continues to rise, a point is reacted eventually where the reduction of ZnO is no longer thermodynamically possible. From this time on, the metallic zinc vapour effectively becomes the source of reductant and is re-oxidized back into the slag. Kinetic control is shifted back to slag diffusion as both PbO and Fe_2O_3 continue to be reduced. As still longer reaction times (slag residence times) the reduction of PbO also is no longer possible. From this time on, the last stages of reaction proceed with the back oxidation of metal zinc and lead, and the reduction of Fe_2O_3 until, if residence time permits, equilibrium with the slag in eventually achieved. It is worth noting that the extent of char particle-secondary bubble reaction with the slag, and therefore, the amount of zinc and lead predicted to be reduced are solely dependent on the residence time of the char particle in the slag for a given set of reaction kinetics.

In summary, from this description, the influence of PbO on the kinetics of the char particle/sag model are clear. In

essence, PbO competes for reductant with both ZnO and Fe_2O_3, and in so doing, effectively decreases the amount of each reduced for a given char-particle slag residence time.

7.1.1.1.12 The Kinetics of Lead Prill Oxidation

In comparison, the kinetics of lead prill oxidation are relatively straight forward. The rate of back oxidation of lead is solely dependent on the mass-transfer rates of Fe_2O_3, PbO and FeO (Fe_2O_3 to the prill-slag interface and PbO and FeO away from the interface). The relative rates of mass-transfer are dependent on several quantities including the relative mobility and thermodynamic stability of the particular oxide. The overall mass transfer rate will be a function of the radius of the lead prill.

Having completed both a sensitivity analysis and a description of reaction kinetics, it is now possible to discuss model sensitivity.

7.2 Sensitivity Analysis: Discussion

The model has been shown to be relatively insensitive to those parameters used in the formulation of lead reduction and removal within the model. Therefore, the values used for r_p^{Pb} F_{PBL} and D_{PBO} in the model may be assumed to be reasonable approximations.

It is interesting to note that industrial lead profiles for the normal low-pressure run and three high-pressure runs, see Figs. 6.4, 6.8, 6.12, and 6.16, respectively, more closely resemble the profile predicted with the model using the larger lead prill size (r_p^{PB} = 80 E - 04 M), See Fig. 7.2. This would seem to indicated that there is some kinetic phenomenon which limits the rate of lead elimination at lower bath lead levels. Within the model, this behaviour is a result of decreasing the rate of oxidation of the lead prill (increasing r_p^{Pb}) to such an extent that it eventually becomes the rate limiting step in the removal of lead. Virtually all the oxidic lead is reduced to metallic lead within the furnace and, hence, must await re-oxidation in order to be re-reduced and removed from the bath. If this is in fact the case, it points to the need for proper reactor design in order to remove the lead in liquid form, eg. collection on the bottom, and avoid the recycling of liquid lead and waste of reductant.

One of the more troublesome questions raised in Chapter VI is the justification for increasing slag circulation velocity from 1m/sec, assumed in Richards[1a] original model, to 3m/sec in the modified model. From the preceding discussion on the kinetics of the char particle reaction system, the reason for the increase becomes clear - it is necessary to reduce the char

particle residence time to offset the ability of lead to displace zinc from the secondary bubble. It remains however, to justify the value of 3m/sec. Unfortunately, there is no direct method of doing this. Therefore, there is little alternative other than to adopt an indirect approach.

Starting with the heat balance, it is clear from the sensitivity analysis and previous work of Richards[1a] that the model temperature profile is only sensitive to two parameters- F_{LPCC} and F_{oxy}. On this basis, the values used for F_{oxy} and F_{LPCC} must at least be close to correct. By necessity, it follows that the rate of reduction of Fe_2O_3 must also be correct since the ferrous and ferric iron profiles exhibit a reasonable fit. To fit the remaining zinc profile, it simply becomes a question of obtaining a correct zinc reduction rate relative to the reduction rates of Fe_2O_3 and PbO, within the model, for a given set of kinetic and thermodynamic data. The only means of doing this is through adjustment of the coal particle residence time or slag circulation velocity. To reiterate, to fit all three profiles - temperature, zinc and ferrous iron - the relative rates of reduction must be correct. Additional support for this argument comes from the fact that all of the runs can be fit with a constant slag circulation velocity once the correct velocity has been found. This was also the case with the original Richards[1a] model.

Finally, the question raised in Chapter VI with respect to the apparent temperature dependence of F_{oxy} can be addressed. Based on the sensitivity of the model to Fe_2O_3, it is unjustifiable to assume that the observed effect is associated with incorrect thermodynamic data.

7.3 Sensitivity Analysis: Summary

To summarize, the modified model is at least as valid as the original Richards model. A general lack of sensitivity to F_{PBL}, r_p^{Pb} and D_{ZNO}/D_{PBO} indicates that the values used in the model are reasonable approximations. The fact that the kinetics based models have been fitted to a wide range of operating conditions including high-pressure coal injection builds support for their general validity.

CHAPTER VIII

SUMMARY AND CONCLUSIONS

8.1 Summary

The results of three runs with a single high-pressure injector on the Cominco No. 2 zinc fuming furnace has demonstrated that substantial improvements in both fuming rate and efficiency can be achieved with high-pressure injection. This is in direct contradiction to the predictions of the equilibrium based models.

The mathematical model by Richards et al[1a,b] has been modified to include the reduction and removal of lead from the slag bath. A model of direct "lead prill" - slag reaction has been developed assuming mass transfer control in the slag phase. This model has been incorporated into the overall furnace model. Fitting of this model to the industrial high-pressure trial data has confirmed that substantial improvements in coal entrainment were achieved with high-pressure injection. Roughly 80% of the high-pressure coal was predicted to have been entrained in the slag. The cycle behaviour of metallic lead in the bath points to the need for proper reactor design.

8.2 Suggestions for Further Work

A total of three runs with a single injector represents only a preliminary study of high-pressure coal injection. In order to better probe the limits of high-pressure injection in the zinc slag fuming process further industrial tests are needed, including:

(a) more single injector trials - varying low and high-pressure coal rates and high-pressure coal to air loading;

(b) a series of multi-injector trials, and;

(c) a series of trials with high-pressure injection of water/coal and oil/coal slurries.

REFERENCES

1 a) Richards, "Kinetics of the zinc Slag Fuming Process", Ph.D. Thesis, U.B.C., 1983.

1 b) Richards, Brimacombe and Toop, "Kinetics of the Zinc Slag Fuming Process: Part I, II and III", Met. Trans. B, Vol. 16B, Sept. 1985, pp 513-549

2) G. Courtney, "The Recovery of Zinc and Lead Blast-Furnace Slags", Proc. Australas. I.M.M., N.S., No. 38, 1920, pp. 75-84

3) A. Laist, "Fuming Off Zinc from Lead Slags at East Helena", Eng. Mining J., 128, 1929, p.325

4) D.R. Blaskett, "Effects of Preheat Blast on Fuel Consumption in a Slag Fuming Operation" in Ninth Commonealth Mining and Metallurgical Congress 1969, Vol 3, Mineral Processing and Extractive Metallurgy, M.J. Jones, ed., I.M.M., London, 1970, pp. 879-889

5) G. Abrashev, "Slag Fuming by the Use of Liquid Fuel" in Advances in Extractive Metallurgy and Refining, M.J. Jones, ed., Instn. Mining Met., London, 1972, pp. 317-326

6) A.I. Evdokimenko, R. Zh. Khobdabergenov, A.P. Sosnin, S.P. Golger, and N.A. Kolesnikov, "The Start and Assimilation of Slag Fuming Using Natural Gas", Soviet J. of Non-Ferrous Metals, 18 (11), Nov. 1977, pp. 62-65

7) Milton N. Kraus, "Pneumatic Conveying of Bulk Materials", 2nd ed., New York, McGraw Hill Chemical Eng., 1980

8) N.A. Stoess, "Pneumatic Conveying" 2nd ed., N.Y. Wiley Co. 1983

9) "Flow of High Bulk Density Mixtures"

10) G. Dockzen, Cominco Ltd., Trail, B.C., private communication

11) "Coal Injection into Blast Furnaces" in Steelresearch 84/85, British Steel Corporation, Sept., 1985

12) R.R. McNaughton, "Slag Treatment for the Recovery of Lead and Zinc at Trail, British Columbia", Trans. AIME, 121, 1936, pp. 721-736

13) P.C. Fedderson, J.B. Schuettenhelm, H.E. Lee, D.R. Gittinger, and G.W. Dunn, "Design and Operation of the Bunker Hill Slag-treatment Plant",

14) H.H. Kellogg, "A New Look at Slag Fuming", Eng. Mining J., 158 (3), 1957, pp. 90-92

15) R.C. Bell, G.H. Turner, and E. Peters, "Fuming of Zinc from Lead Blast Furnace Slag", J. Metals, March 1955, (TMS AIME, 203, pp. 472-477

16) H.H. Kellogg, "A Computer Model of the Slag Fuming Process for Recovery of Zinc Oxide", Trans. Met. Soc. AIME, 239, 1967, pp. 1439-1449.

17) R.J. Grant and L.J. Barnett, "Development and Application of the Computer Model of the Slag Fuming Process at Port Pirie", in South Australia Conference 1975, Australas, I.M.M., Melbourne, 1975, pp. 247-265

18) T.A.A. Quarm, "The Slag Fuming Process", Mining Magazine, 113 (2), 1965, pp. 114-123

19) T.A.A. Quarm, "Slag Fuming - kinetic or thermodynamic", Eng. Mining J., 169(1), 1968, pp. 92-93

20) T.A.A. Quarm, "Physical Chemistry and Pyrometallurgy", Trans. I.M.M., 89, 1980, pp. C139-C144

21) O.A. Sumdstrom, "The Slag Fuming Plant at the Ronnskar Works of the boliden Aktiebolag, Skellefteham, Sweden", J. Metals, 1969 (TMS AIME, 217), pp. 15-21

22) V.A. Ivanov, A.M. Intykbaev, V.S. Korbator and L.I. Varnakov, "Investigation of the Fuming Process by means of Regression Models", Izv. Vyssh. Uchebn. Zaved. Tsvetn. Metals., 1977, pp. 154-156

23) R.F. Blanks, "A Cyclone Furnace for Slag Fuming", Proc. Australas. I.M.M., No. 210, 1964, pp. 71-86

24) R.F. Blanks, "Development of a Cyclone Furnace Process for Slag Fuming", in Advances in Extractive Metallurgy, Symposium, 1967, Instn. Min. Metall., London, 1968, pp. 224-244

25) A.P. Sychev, M.A. Lyamina, I.M. Cherednek, V.M. Fedotov, and Yu.I. Sannikov, "Role of Carbon - Gasification Reaction in the Reaction of Liquid Slags", Russian Metallurgy, (5), 1976, pp. 16-20

26) Yu.I. Sannikov, Yu.M. Abdeyev, and S.P. Makarevick, "Kinetics of the Reaction Between Liquid Zinciferous Slags and Carbon", Russian Metallurgy, (4), 1973, pp. 42-45

27) Yu.I.Sannikov, "Kinetics of Carbon Reduction of Zinc Slags", Russian Metallurgy, (6), 1969, pp. 20-25

28) V.N. Boronenkov, O.A. Esin, and S.A. Lyamkin, "Kinetics of the Reduction of Metal Oxides in Liquid Slags by Solid Carbon", Russian Metallurgy, (1), 1972, pp. 17-23

29) V.M. Chumarev, and T.F.Vlasova, "Reduction of Zinc Oxide in Oxide Melts by Carbon", Russian Metallurgy, (5), 1969 pp. 17-20

30) M.A. Glinkov, A.V. Cirechko, J.N. Nevedomskaya, V.V. Kobakhidze and V.P. Bystrov, "A Study of the Role of Hydrodynamic Factors in the Operating of Fuming Furnaces", Soviet J. Non-Ferrous Metals, 12 ( ), 1971, pp. 16-19

31) J.G. Malone, J.M. Floyd, W.T. Denholm, "Mechanisms of Reductions of Liquid Slag by Carbon", Procedings C.I.M. conf., Aug.18-21, Van., B.C.

32) G.G. Richards, "High-Pressure Coal Injection Proposals", Unpublished

33) D.P. Agarnal and D.R. Gaskell, "The Self-Diffusion of Iron in Fe_2SiO_4 and caFe SiO_4 Melts", Met. Trans. B, 6B, 1975, pp. 263-267

34) F.D. Skinner and L.D. Smoot, "Heterogeneous Reactions of Char and Carbon", in Pulverized Coal Combustion and Gasification, L.D. Smoot and D.T. Pratt, eds., Plenum Press, New York, 1979, pp. 149-167

35) R. Clift, J.R. Grace, and M.E. Weber, Bubbles Drops and Particles, Academic Press, New York, 1978

36) E.T. Turkdogan, Physical Chemistry of High Temperature Technology, Academic Press, New York, 1980

37) C. Bodsworth, "The Activity of Ferrous Oxide in Silicate Melts", J. Iron Steel Inst., 193, 1959, pp. 13-24

38) R. Altman, G. Stavrospoulos, K. Parameswaran, R.P. Goel, "Viscosity Measurements of Industrial Blast Furnace Slags", Physical Chemistry of Extractive Metallurgy, Y. Kudryk and Y.K. Rao, ed., Proc.Conf. AIME, Feb. 24-28, 1985, New York, N.Y.

39) A.J. Taskinen et at, "Thermodynamics of Slags in Direct Lead Smelting", 2nd International Symposium on Metallurgical Slags and Fluxes, H.A. Fine, D.R. Gaskell, ed., AIME, Nov. 11-14, 1984, Lk. Tahoc, Nev., pp. 741-756

40) R.A. Reyes and D.R. Gaskell, "The Thermodynamic Activity of ZnO in Silicate Melts", Met.Trans.B., Vol 14B, Dec., 1985, pp. 725-731

41) M. Timucin, A.E. Morris, "Phase Equilbria and Thermodynamic Studies in the System $CaO-FeO-Fe_2O_3-SiO_2$", Metl.Trans., Vol.1, Nov., 1970, pp. 3193-3201

42) O. Kubaschewski and C.B. Alcock, Metallurgical Thermochemistry, 5ed., Pergamon, New York, 1979

43) K. Azuma, S. Goto, and A. Ogawa, "Thermodynamic Studies on Zinc Oxide Slags", J.Fac.Eng.Univ.Tokyo, Ser.A, 5(1), 1967, pp. 54-55

44) R.P. Goel, H.H. Kellogg, and L. Larrain: Metall. Trans. B, Vol. 11B, March 1980, pp. 107-17.

APPENDIX 1

FUMING SAMPLING DATA

Normal Operation

Bath Weight: 50,000 kg.
Coal Composition: Weight Fraction
Fixed Carbon: 0.500 Volatiles: 0.250 Moisture: 0.01

Coal Volatiles: Weight Fraction
Carbon: 0.500 Hydrogen: 0.200 Oxygen: 0.100 Nitrogen: 0.0

Time (min)	Temp (°C)	Zn %	Pb %	Fe^{2+} %	Fe^{3+} %	CaO %	SiO_2 %	Al_2O_3 %	S %	Primary Blast NM^3 min	Secondary Blast NM^3 min	Coal rate lbs min	H.P - Coal rate lbs min
0.0	1250	15.0	1.90	21.5	7.0	11.7	23.2	4.0	0.1	40	330	104	0
10.0	1254	14.7	1.50	22.7	6.1	11.3	22.9						
20.0	1260	14.1	1.12	23.7	5.3	11.6	23.0					140	
30.0	1250	13.2	0.80	24.6	4.7	11.9	23.1						
40.0	1246	12.4	0.53	25.4	4.3	12.0	23.4						
50.0	1243	11.5	0.43	26.1	4.0	12.1	23.7						
60.0	1240	10.3	0.30	26.8	3.7	12.5	24.3	*E	*E				
70.0	1237	9.5	0.23	27.8	3.4	12.4	24.9	S	S			154	
80.0	1228	8.4	0.16	28.7	3.0	12.5	25.2	T	T				
90.0	1214	7.4	0.10	29.2	2.7	12.6	25.5	I	I				
100.0	1201	6.5	0.10	29.8	2.5	12.6	25.5	M	M				
110.0	1195	5.7		30.4	2.3	12.7	25.4	A	A				
120.0	1191	4.9		30.9	2.0	12.9	25.9	T	T				
130.0	1190	4.3		31.4	1.7	13.1	26.4	E	E				
140.0	1190	3.7		31.7	1.5	13.2	26.7						

Run 1

Bath Composition: 50909 kg.

Coal Composition: Weight Fraction
Fixed Carbon: 0.500 Volatiles: 0.250 Moisture: 0.01

Coal Volatiles: Weight Fraction
Carbon: 0.500 Hydrogen: 0.200 Oxygen: 0.100 Nitrogen: 0.0

Time (min)	Temp (°C)	Zn %	Pb %	Fe^{2+} %	Fe^{3+} %	CaO %	SiO_2 %	Al_2O_3 %	S %	Primary Blast NM^3 min	Secondary Blast NM^3 min	Coal rate lbs min	H.P.-Coal rate lbs min
0.0	1330	8.7	0.21	28.7	3.1	12.8	25.0	4.0	0.1	40.0	330	150	0
5.0	1325	8.3	0.12	28.0	3.6	13.0	26.0			40.0			
10.0	1320	*7.6-7.9	0.12	29.0	3.0	13.0	26.0						
15.0	1305	7.2	0.09	28.6	3.4	12.0	26.2						16
17.0												120	16
20.0	1300	6.8	0.08	27.7	4.3	13.0	26.6					120	20
25.0	1300	*6.3-6.5	0.07	28.4	3.6	13.1	27.0	*E	*E			135	26
30.0	1280	6.1	0.05	28.2	4.0	13.2	27.2	S	S			120	
35.0	1260	5.3	0.04	29.5	3.0	13.3	27.6	T	T				
40.0	1255	*4.8-4.9	0.03	29.6	2.7	13.5	28.4	I	I				
45.0	1250	4.4	0.02	29.6	2.9	13.6	28.6	M	M				
50.0	1240	3.9	0.02	30.6	2.4	13.4	27.8	A	A				
55.0	1230	*3.5-3.5	0.02	31.6	1.0	13.6	29.1	T	T				
60.0	1225	3.1	0.02	30.7	2.0	13.7	29.5	E	E				
65.0	1225	3.0	0.07	30.1	2.7	13.7	29.5	1	1				

*note: the two numbers represent the results of the double sampling procedure (procedure is explained in text)

Run 2

Bath Weight: 52727 kg.

Coal Composition: Weight Fraction
Fixed Carbon: 0.500 Volatiles: 0.250 Moisture: 0.01

Coal Volatiles: Weight Fraction
Carbon: 0.500 Hydrogen: 0.200 Oxygen: 0.100 Nitrogen: 0.0

Time (min)	Temp (°C)	Zn %	Pb %	Fe_2^+ %	Fe^{3+} %	CaO %	SiO_2 %	Al_2O_3 %	S %	Primary Blast Nm^3 min	Secondary Blast Nm^3 min	Coal rate lbs min	H.P.- Coal rate lbs min
0.0	1275	16.0	0.95	21.1	6.9	11.7	23.2	4.0	0.4	40	400	105	0
5.0											330		
10.0	1310	15.7	0.90	19.2	8.8	11.3	23.9					135	
15.0	1325	15.4	0.85	21.1	7.1	11.6	23.0						
20.0	1325	15.2	0.80	21.6	6.8	11.9	23.1						
25.0	1310	14.8	0.75	23.4	5.3	12.0	23.4					105	40
30.0	1290	14.2	0.60	23.8	5.0	12.1	23.7						
35.0	1285	13.6	0.50	25.4	4.0	12.5	24.3						
40.0	1285	13.0	0.40	25.2	4.3	12.4	24.9						
45.0	1285	12.4	0.35	25.7	4.1	12.5	25.2	"E	"E				
50.0	1275	11.7	0.30	26.2	4.8	12.6	25.5	S	S				
55.0	1265	11.0	0.21	26.2	4.0	12.6	25.5	T	T				
60.0	1265	10.5	0.25	26.6	3.9	12.6	25.4	I	I			120	20
65.0	1270	9.8	0.15	27.1	3.9	12.7	25.9	M	M				
70.0	1275	9.3	0.13	28.0	3.0	12.7	26.4	A	A			135	0
75.0	1270	8.6	0.10	28.2	3.1	12.9	26.7	T	T				
80.0	1255	7.6	0.12	28.4	3.4	13.1	27.0	E	E				
85.0	1240	6.9	0.03	29.4	2.2	13.2	27.2						

Run 3

Bath Weight: 58182 kg.

Coal Composition: Weight Fraction
Fixed Carbon: 0.500 Volatiles: 0.250 Moisture: 0.01

Coal Volatiles: Weight Fraction
Carbon: 0.500 Hydrogen: 0.200 Oxygen: 0.100 Nitrogen: 0.0

Time (min)	Temp (°C)	Zn %	Pb %	Fe^{2+} %	Fe^{3+} %	CaO %	SiO_2 %	Al_2O_3 %	S %	Primary Blast Nm^3 min	Secondary Blast Nm^3 min	Coal rate lbs min	H.P.-Coal rate lbs min
0.0	1265	13.5	3.30	21.9	6.8	10.6	23.1	4.0	.01	40	330	105	0
5.0	1270	13.4	3.10	21.1	7.8	10.6	23.2			40	330	105	0
10.0	1272	13.2	2.90	21.2	7.8	10.7	23.3						
15.0	1275	13.0	2.70	21.6	7.8	10.7	23.3						
20.0	1280	12.9	2.70	20.3	8.8	10.8	23.3						
25.0	1290	12.5	2.50	22.1	7.6	10.8	23.2					120	
30.0	1300	12.4	2.10	24.2	5.9	10.8	23.6					120	35
35.0	1290	11.8	1.70	24.9	5.4	11.1	24.0					120	
38.0												105	
40.0	1275	11.0	1.20	26.5	4.3	11.3	24.4						
45.0	1265	10.5	1.00	26.1	4.9	11.5	25.0	"E	"E				
50.0	1255	10.0	0.85	26.7	4.6	11.6	25.5	S	S				
55.0	1252	9.3	0.62	28.1	3.6	11.8	26.0	T	T				
60.0	1250	8.4	0.40	28.0	3.8	11.9	26.4	I	I				
65.0	1255	7.9	0.33	28.5	3.5	12.0	26.9	M	M				
70.0	1255	7.1	0.25	28.4	3.7	12.1	27.4	A	A				
72.0								T	T				0
75.0	1255	6.8	0.21	28.5	3.9	12.15	27.6	E	E				
76.0												120	
80.0	1260	6.3	0.15	29.6	3.0	12.2	27.7					120	
81.0												135	
85.0	1260	5.7	0.12	29.8	3.2	12.2	27.8					135	